ESCUELA TÉCNICA SUPERIOR DE INGENIEROS INDUSTRIALES Y DE TELECOMUNICACIÓN

UNIVERSIDAD DE CANTABRIA

Trabajo de Fin de Máster

Diseño y análisis de un Oscilador 2-Push en banda X, basado en CSRRs

(Design and analysis of an X-Band 2-Push Oscillator based on CSRRs)

Para acceder al Título de

Máster en Tecnologías de la Información y Comunicaciones en Redes Móviles (TICRM)

Autor: José Luis Flores

Junio - 2013

TÍTULO	Diseño y análisis de un Oscilador 2-Push en banda X, basado en CSRRs			
AUTOR	José Luis Flores Martin			
DIRECTOR	Franco Ramirez Terán			
TITULACIÓN	MÁSTER TICRM	FECHA	Junio-2013	TOMO I DE I

Resumen

En el contexto de la aplicación de las técnicas de análisis no lineal a sistemas de osciladores acoplados, y aprovechando el potencial demostrado para obtener resonadores con un alto factor de calidad y reducidas dimensiones, de las estructuras de anillos resonantes utilizadas como partículas de base en el diseño de metamateriales; se ha decidido diseñar osciladores de tipo *push-push* (dos osciladores acoplados y sincronizados en oposición de fase) que incluyen resonadores basados en anillos CSRR – *Complementary Split Ring Resonator*, y resonadores clásicos basados en línea micrsotrip. Ambas estructuras han sido comparadas, demostrando el potencial del diseño con CSRRs para reducir el ruido de fase.

Una dificultad importante de este diseño es garantizar el modo de oscilación deseado (osciladores en oposición de fase, ó modo impar). Además de la caracterización y modelización de los anillos CSRR, y el ajuste de los modelos de transistor para una correcta reproducción del ruido de fase.

Hasta la fecha no tenemos constancia de la publicación de ningún oscilador tipo N-push que emplee anillos CSRR como resonadores en su red de acoplo.

Synopsis

In the framework of the application of nonlinear analysis techniques to coupled oscillator systems, and taking advantage of the demonstrated capability to obtain high Q resonators with reduced dimensions by employing resonant rings of the type used as basic particles in metamaterials for microwave applications; it was decided to design push-push oscillators (two oscillators coupled together and synchronized, operating out of phase) including Complementary Split Ring Resonators (CSRR) as well as classic resonators based on microstrip line stubs. Both approaches have been compared, showing the CSRR potential to reduce phase noise.

An important difficulty of this design is to guarantee the desired oscillation mode of the sub-oscillators (out-of-phase or odd mode). Also the characterization and modelling of the CSRRs and the fitting of transistor models to correctly reproduce phase noise.

To date we do not know of any published work on N-push type oscillators using CSRRs as resonators in their coupling network.
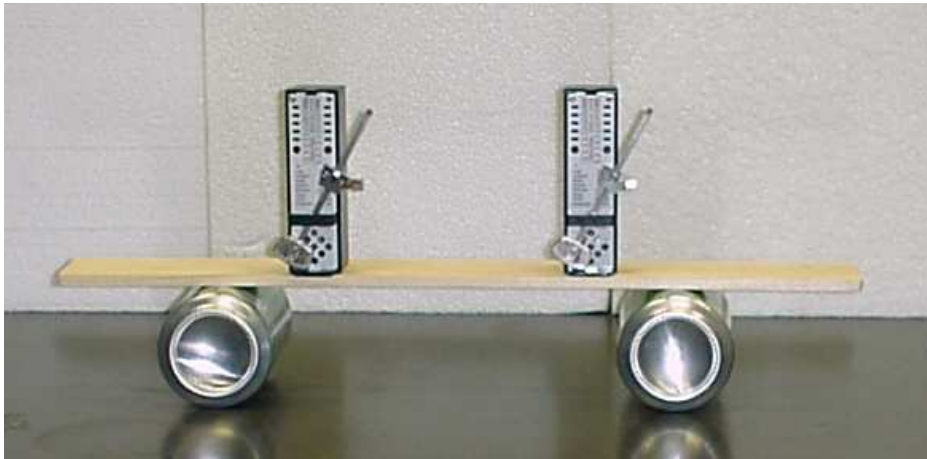
"*Synchronization is a common phenomenon in physical and biological systems. When two or more metronomes are placed on a freely moving base, the small motion of the base couples the pendulums causing synchronization. The synchronization is generally in-phase, with antiphase synchronization occurring only under special conditions.*"

James Pantaleone, *Synchronization of metronomes*. Am. J. Phys., Vol. 70, No. 10, October 2002

Preface

The present work is the conclusion of a 2-year long dedication to a Master`s Thesis in which I have concentrated on the study of nonlinear phenomena affecting the behaviour of microwave circuits, and the reproduction of those phenomena on simulation tools.

I arrived at the beginning of this Master with a cumulated work experience of 15 years in Industry and Research Institutions such as ESA/ESTEC, Alcatel Space or Philips Microwave Laboratories (now OMMIC), where I got strong simulation skills through an intensive MMIC design activity during the first half of my career in The Netherlands and France.

The following years passed at Companies in the military RF and wireless communications sectors in Spain, where I appreciated a very different approach to design; basically constrained by a lack of accurate nonlinear models for pcb and a limited use of the powerful simulation tools at hand. Nevertheless the increasing complexity and density of the pcb circuits in present communications systems made the design problem very close to the handling limitations encountered with monolithic functions, in terms of difficulty –almost impossibility- to implement any changes after the board had been manufactured, and the need for test boards to evaluate specific parts of the design which could not be tested on the main circuit.

I understood that the design approach needed to be modified substantially, as the lack of robust first pass designs was affecting product competitiveness, according to the management.

As a consequence I undertook initiatives for a more efficient cooperation with Academia, and to promote dedicated projects within Industry, to search for solutions to common problems appearing repetitively in different front-end designs (such as matching, filtering, spurious avoidance, stability...). I did my best to attend those targets during the wealthy years where public funding for R&D activities was available to Companies, and in this context I made proposals for cooperation with research institutions such as the DICOM – where I have performed this Master's work at the University of Cantabria (UC), and the CIMITEC –a center specializing in metamaterials research at the Autonomous University of Barcelona (UAB).

When the economic recession and the consequent cut off of the public funding to my Company placed me in the job search market, I decided to go into a Master's Program with the double objective of refreshing and updating my past design experience, and becoming highly experienced in nonlinear microwave circuit simulation and design.

I have followed this Master in the distance as I resided in Granada, at more than 900 km from Santander, in the opposite side of the Country. This fact has had some implications on the approach to work that I have followed, mainly due to practical limitations related to economics and geographical mobility. For that reason I concentrated much more on

the theoretical and simulation aspects than in actually obtaining a specific result from the evaluation boards designed.

Under the supervision of Dr. Franco Ramirez, from the GIMSR – Microwave & Radiocommunications Systems Group (DICOM/UC), I have learned the guts of the time and frequency domain tools used in microwave circuit analysis, together with some powerful simulation strategies that allow for the prediction of phenomena which can not be detected using the basic techniques known to the average industry engineer.

As part of my work at the GIMSR, I have implemented the Auxiliary Generator (AG) Analysis in AWR's Microwave Office, which to my knowledge is a first; as it was only implemented in Agilent's ADS by the Group (who developed the technique), and as a result the AWR Company invited me to make two public presentations on this subject at a joint AWR-Rohde & Schwarz seminar in Madrid (Oct. 4th, 2012) and the last Conference Meeting of the ARMMS RF & Microwave Society (Apr. 22-23, 2013. Steventon, UK). A paper was submitted to the ARMMS Conf., which I co-authored with Prof. Almudena Suárez, head of the GMSR and author of the AG technique.

I chose to undertake the design of Coupled Oscillators and Metamaterial based Planar Resonators to implement a 2-push structure in which to test two of the techniques I had discovered during my previous industrial experience, and which I found promising enough to deserve a prospective analysis in view of their potential application to improve RF performance and Company know-how, while at the same time using only components and materials not affected by export restrictions. This had made the subject of a proposal for cooperation between my previous Company and the DICOM, back on July 2009, signed by myself and Prof. Almudena Suárez. But it had no continuation.

In the present work two 2-Push Coupled Oscillators have been designed. They share the same active networks and differ only in the resonators used. One incorporates a classic Transmission Line Resonator, while the other uses Metamaterial based Planar Resonators. The theories concerning the particularities and potential benefits from the Coupled Oscillator Systems and the Metamaterial based Planar Resonators are presented and discussed for the purpose of this project. The design of the 2-push structures is commented and the simulation results are shown, with a detailed description of the techniques used for their analysis.

José Luis Flores

June, 2013

visit my web page
www.muwavetech.com

Index

Acknowledgements

Objectives and Accomplishments of this work

The main objectives of this work have been to design 2-push oscillator structures using metamaterial based resonators which at the same time act as coupling networks to achieve a desired mode of oscillation, and to compare the achieved performance – mainly in terms of phase noise, with that of an identical 2-push using classical stub resonators in the coupling network.

This has required the mastering of complex nonlinear analysis techniques; a deep understanding of them has been essential to accomplish the numerous simulations required to obtain the simulated results.

We have considered fully planar implementations because they benefit from the minimum component count and are the easiest to manufacture, which is very practical for production oriented designs. An additional advantage of this approach is that the initial extra difficulty in designing, modelling and simulating the resonator networks translates into a proprietary know-how that is critical in every competitive activity. And furthermore, the design process is flexible because the resonator performance is controlled by the designer and the procurement of very specific high performance components is avoided – they are often subject to export restrictions which limit the commercialisation of the end product.

Among the contributions of this work are:

- o   Improving current CSRR models to fit EM data so that they can be used as inter-oscillator coupling networks.

- o   Showing a step-by-step design process for the 2-push structures with an in-depth explanation on every aspect of the simulations performed.

- o   Comparison of the phase noise performance achieved with a CSRR based resonator with respect to a classical microstrip line stub resonator in a 2-push.

- o   Fitting of an Angelov HEMT model to simulate Flicker and Shot noise effects on phase noise, which were not correctly reproduced with the available Agilent EEHMT1 model for the transistors used in this project.

- o   And finally, an in-depth literature survey was performed on every published article using resonator + power combiner networks in N-push oscillators and resonators made of metamaterial particles. There are only a few groups doing research on these topics and we have selected their most relevant works.

Additionally, the Auxiliary Generator technique has been implemented for the first time into the AWR/Microwave Office simulator and an article was written describing its usefulness in nonlinear analysis, broadening the results from Harmonic Balance simulations. This article made the subject of two invitations by the AWR Company to participate at an AWR seminar in Madrid and at the 2013 spring meeting of the ARMMS RF & Microwave Society in Oxfordshire (UK).

1 The role of Oscillators in Communications Systems

Oscillator circuits at RF and microwave frequencies have many applications. They can be used as clocks in frequency synthesizers and in navigation satellite systems for global positioning such as GPS or Galileo, to generate interfering carriers in wireless conformance test equipment, as CW generators in Radar or in microwave laboratory test equipment such as signal generators and network analyzers.

Oscillators are used in communications systems in conjunction with mixers to perform the frequency conversion of microwave signals. The convolution between a non modulated high frequency oscillation and a modulated carrier is a natural phenomenon which takes place when both signals are combined in a nonlinear system, such as a mixer. The result of that convolution is that the modulation information is transferred to the mixing products between the two original carriers; the most important products being the sum and difference of frequencies, which respectively produce the *up* conversion or the *down* conversion of the modulated signal.

In real systems, oscillators are always modulated in phase and amplitude by the natural fluctuations affecting the currents and voltages in electronic circuits. These fluctuations have different origins; the most common being the thermal agitation of free charge carriers, imperfections in the semiconductor crystals, the granular nature of electricity, or the generation-recombination processes and trapping. Noise is the term given to those fluctuations and it is usually of much lower amplitude than the average value of the parameters. Oscillator noise forms sidebands of energy around the carrier power spectrum.

Due to the saturation of conversion gain in mixers with Local Oscillator power, the amplitude fluctuations of the oscillator do not degrade considerably the modulation information on the converted carrier; the major cause for amplitude degradation being the gain compression taking place in the amplifier chain, which affects the modulated carrier. This is particularly an issue in transmitter applications. The major impact of oscillator noise is on the phase information of modulated carriers.

Phase and amplitude are the principal parameters used to transmit information in present digital communication systems showing high spectral efficiency (information rate that can be transmitted over a given bandwidth). Binary data is packed in groups of "n" bits which are associated to a 2^n point constellation in a complex I-Q plane (i.e. QPSK, 16-QAM, 64-QAM...). Each point or *symbol* in the constellation defines a vector with unique amplitude and phase values. These vectors can be streamed to modulate in amplitude and phase a single RF carrier which is then amplified and transmitted trough free air or guided. They can also modulate different sub-carriers (one each vector) which are then combined through an Inverse Fourier Transform operation to form the modulation signal that is applied to an RF carrier and transmitted; this is the working principle of the OFDM (Orthogonal Frequency-Division Multiplexing) digital modulation schemes used by the actual radio standards such as WLAN, WiMAX or LTE. Using a large number of narrow data sub-carriers reduces the amount of crosstalk in signal transmissions.

In all cases we have vectors defining points in a constellation. As the number of symbols increase, more data is transmitted in a given bandwidth, but the resulting constellation becomes denser and less robust against detection errors produced by phase and amplitude perturbations on its points. During the transmission and reception processes, the symbols of the constellation are affected by amplitude and phase errors. The error vector is the difference between actual and ideal symbol locations. The power from the error vectors is averaged and normalized to the signal power giving a magnitude called EVM or Error Vector Magnitude. The EVM is a measure of how far the points in a constellation are from their ideal locations and provides a comprehensive measure of the quality of a radio receiver or transmitter for use in digital communications.

Oscillator phase noise is a major contributor to the phase error in the symbol locations and its reduction is one of the principal parameters of an oscillator specification.

Active devices influence phase noise; depending on the carrier transport mode the current flow will be more or less affected by defects and traps close to interfaces in the semiconductor, which seem to be the cause of Flicker *1/f* noise. In FET devices the electrons travel along an interface and so are more strongly affected by *1/f* noise, while in bipolar transistors the electrons cross the interfaces in a perpendicular direction, being less affected. This low-frequency noise from the device modulates the signal's phase to create noise sidebands with an f^{-3} characteristic near the carrier.

The resonator is an essential part of an oscillator and determines the phase noise and frequency stability. In the words of an important oscillator manufacturer[1] "*A wide range of military, industrial, medical, test and measurement markets demand very stable frequency sources with enhanced phase noise performance and low thermal drift. A popular solution in the range of 3-18 GHz frequency spectrum is the dielectric resonator oscillator (DRO), recognized for its superiority in ultimate noise floor and spectrum purity when compared to other competing solutions such as multiplied lower frequency fundamental sources*".

I will treat the problem with multiplied sources in the next chapter; they use resonators at a lower frequency in order to get high Q values and obtain low phase noise, but they are not the only means of producing a high frequency oscillation form a lower frequency fundamental. Coupled oscillators do not present the problems of the frequency multipliers and can be made to work in a mode that combines a harmonic at the output and rejects the fundamental and other frequencies.

The purpose of the present work is the design of a structure made of two single oscillators coupled together and sharing a common resonator. Two versions of the structure have been designed differing on the resonator used. We have selected planar resonators which can be printed or etched in the substrate; this has the advantage of an easy implementation as it does not require any specific mounting technique, like DRO's. In terms of the same manufacturer[1] "*DRO's tend to be prone to vibration noise since the dielectric resonator itself cannot be secured mechanically. Therefore vibrations must effectively be damped by other means before they reach the dielectric*

---

[1] Synergy Microwave Corp. Product Feature "*Ultra-Low Noise Dielectric Resonator Oscillator*", published in Microwave Journal, Dec. 2012

resonator, and a rugged construction is needed to minimize vibration noise and microphonic effects to prevent unwanted modulation".

Our resonators are based on sub-wavelength particles used for metamaterial design. They offer lower losses and higher Q factor as compared to classic printed structures on PCB. Their design is not an easy task due to the lack of commercial synthesis tools at this writing. The use of EM simulation is mandatory and the extraction of equivalent circuit models is required to perform the simulation of the oscillator circuits. But in return, our designs are flexible, easy to manufacture and incorporate *know-how*. This is an important aspect for a competitive product as it can not be easily reproduced by anyone having access to the same components (which are all cheap and commercially available).

2   Coupled Oscillator Systems: The 2-Push architecture

2.1 Operation principle

A high frequency signal can be generated from an oscillator operating at its fundamental or a harmonic frequency. As the oscillator frequency increases the Q factor, device gain and phase noise are degraded (for a same technology). The frequency doubler and other means of up-conversion may provide a practical and quick solution to generate high frequency signals from oscillators operating at lower frequencies, but they introduce distortions and have poor phase noise performance. One alternative approach to overcome this limitation is the coupled 2-Push oscillator topology.

A 2-Push or push–push oscillator is a frequency doubling structure that consists of two identical sub-oscillators coupled together in out-of-phase operation, so only the second harmonic is combined at the output load. Fig.1 shows the block diagram of a classical push-push topology.
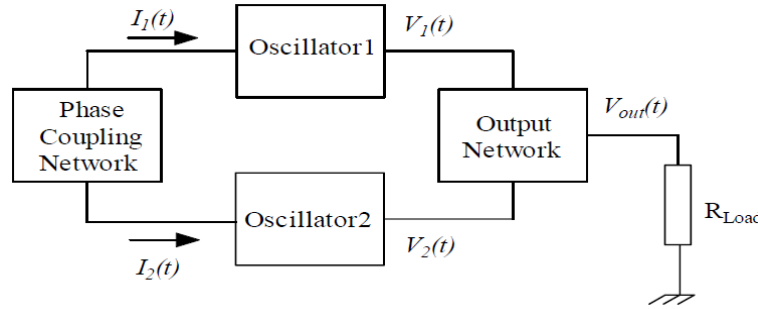
Fig.1.   Block diagram of 2-Push/Push-Push topology [1].

By combining the two sub-oscillator outputs, the fundamental and odd frequency components are cancelled out, and the second and even harmonic components are enhanced and added constructively when the two sub-oscillators produce the same frequency and operate with a phase difference of 180º. Equations (1)-(3) represent the possible output signals from these circuits.

$$(1) \quad V_1(t) = \sum_n a_n e^{jn\omega_o t} = a_0 + a_1 e^{j\omega_o t} + a_2 e^{j2\omega_o t} + a_3 e^{j3\omega_o t} + ...$$

$$(2) \quad V_2^{odd}(t) = \sum_n a_n e^{jn(\omega_o t - \Delta\varphi)}\bigg|_{\Delta\varphi=\pi} = a_0 - a_1 e^{j\omega_o t} + a_2 e^{j2\omega_o t} - a_3 e^{j3\omega_o t} + ...$$

$$(3) \quad V_2^{even}(t) = \sum_n a_n e^{jn(\omega_o t - \Delta\varphi)}\bigg|_{\Delta\varphi=0} = a_0 + a_1 e^{j\omega_o t} + a_2 e^{j2\omega_o t} + a_3 e^{j3\omega_o t} + ...$$

Thus, provided that the phase difference between the sub-oscillators outputs is $\Delta\varphi = \pi$, we will have a cancellation of the odd harmonics from $V_1(t)$ and $V_2(t)$ with the even

harmonics being enhanced. Both even ($\Delta\varphi = 0$) and odd ($\Delta\varphi = \pi$) solutions always co-exist in the 2-push structure, so a proper design of the coupling network (resonator) must guarantee the stability of the desired odd mode and make unstable the even mode. As unstable modes are not physically observable [2], only the odd mode will contribute to the output waveform and, provided that the structure is well balanced (symmetrical) high rejection levels will be observed at the undesired fundamental and harmonics. If the sub-oscillators were uncoupled, then $\Delta\varphi$ could have any value between 0-2π and would not be constant with time due to random noise and parametric drifts affecting the oscillator's phase. The correct mode of operation is observed when the two sub-oscillators synchronize with each other and have opposite phase.

As the sub-oscillators operate at half the output frequency, higher resonator Q_r values can be achieved, improving phase noise characteristics. Additionally, due to the limiting mechanisms of active devices under saturation, which transfer power to the harmonics, the output frequency range can be extended beyond the limitation caused by the cut-off frequency of the active devices [3].

In N-push architectures, only the Nth harmonics are combined at the output load by achieving a phase difference of $2\pi/N$ between any two consecutive fundamental signals. Since the resonators in N–push oscillators operate at $1/N$ the design (output) frequency, higher resonator Q_r are achievable. In addition, designing at lower frequencies allows for increased device gains. Because of these advantages, the approach based on the N–push principle has been identified as an attractive method for low phase-noise oscillator design at microwave and millimeter-wave frequencies [4].

2.2 Phase noise performance

An important figure-of-merit in oscillators is phase noise. N-push oscillators operate by the principle of mutual injection in a Coupled Oscillator System through which the sub-circuit oscillators influence each other and synchronize. In this operation mode the noise contributions from all the individual elements are averaged and, if the N oscillators are identical (same noise power spectral density of the noise sources), the total phase noise is improved by a factor of N, in comparison with the single individual uncoupled oscillator.

The resulting phase noise from the N-coupled oscillator, as compared to the single uncoupled oscillator, satisfies [1]:[3, 5-7]

$$(4)\quad \text{£(fo\_Ncoupled)} = \text{£(fo\_Single)} - 10\log(N)$$

From (4), push-push or 2-push oscillator structures can reduce up to 3 dB the phase noise with respect to a multiplier/doubler design, which degrades phase noise by a factor N^2 or $20\cdot\log(N)$.

In an attempt to quantify the relative improvement in phase noise offered by a 2-push with respect to a fundamental oscillator working at the same output frequency, Rohde makes a noise analysis on a typical (fundamental mode) Colpitts oscillator, and concludes that the 2-push structure can reduce the phase noise ideally 9 dB as compared

to the phase noise that would show an oscillator if made to operate at twice its design frequency [1].

In his study, the oscillator's LF (low frequency) noise centered on the carrier f_o is obtained by calculating a "*pushing factor*" which relates the effective oscillator noise (square root of the noise spectral density) to low frequency noise perturbations across the junction capacitance of the transistor (Bipolar C_{be} or FET C_{gs}) which produce a deviation of the oscillator's phase and frequency.

He then derives the pushing factor at the fundamental (operating) frequency f_o and half this value $f_o/2$, assuming the same values at both frequencies, for the resonator's quality factor Q_r and the C(V) characteristic of the junction capacitance. He obtains a factor of about 4 relating the pushing factors at f_o and $f_o/2$, which translates to a **12 dB** degradation of the single sideband (SSB) phase noise at f_o with respect to $f_o/2$, then:

$$(5) \quad £(f2) = £(f1) + 12\log_2(f2/f1)$$

Thus, phase noise would be degraded by 12 dB/octave when tuning a given oscillator at increasing frequencies. This figure could be even larger because the analysis is based on a simplified oscillator model and assumes that the device parasitics, LF noise characteristics of the active device and dynamic load Q_r of the resonator do not vary with frequency, while in practice they would degrade when doubling the frequency.

When two identical oscillator circuits are coupled through an arbitrary coupling network in Push-Push configuration (like in Fig.1), mutual injection occurs (part of each oscillator's signal is injected into the other) and synchronization takes place. The effect of the synchronization is that the uncorrelated noise voltage perturbations at both transistors are averaged, thus if both oscillators are identical a **3 dB** improvement in phase noise is obtained, which is in agreement with (4).

2-Push oscillators are designed to operate at the second harmonic, noted as f_o because it is the output frequency of the structure. With this notation the fundamental from each single oscillator is $f_o/2$. If the coupling network is properly designed, the 2-push structure will be symmetrical and the differential *odd* mode prevails (the common *even* mode being rejected). In that case the $f_o/2$ frequency is rejected, as well as the $(2n+1)\cdot f_o/2$ contributions and only lines at $n\cdot f_o$ are observed in the output spectrum.

The phase noise spectral density at f_o is degraded by 6 dB with respect to $f_o/2$, in virtue of the double frequency. But, as each synchronized sub-oscillator has improved its phase noise by 3 dB, the net result is a degradation of only 3 dB in the phase noise at f_o compared to the phase noise from a single (not synchronized) oscillator at $f_o/2$. In general, the N-push structures degrade phase noise by a factor of only **10·log(N)** as compared to the **20log(N)** achieved by frequency multiplication, and their output spectrum is much cleaner thanks to the sub-harmonic cancellations produced by the symmetrical structure.

Now we can calculate the relative improvement in phase noise offered by a 2-push with respect to a fundamental oscillator working at the same output frequency: Starting from the noise spectral density of a single $f_o/2$ oscillator, the 2-push will induce a 3dB degradation on the f_o output carrier noise, but (5) states that a single $f_o/2$ oscillator

would suffer a 12dB phase noise degradation if tuned at f_o. Then the net phase noise improvement is **9 dB**.

Table 1 presents the above mentioned results.

	PN degradation (dB)	**PN degradation (N=2)**
Re-tuning	$12 \cdot \log_2(N)$	+12 dB
Multiplier	$20 \cdot \log(N)$	+6 dB
N-Push	$10 \cdot \log(N)$	+3 dB

Table 1   Phase noise spectral density degradation due to an increase in oscillation frequency from different methods

It is not easy to design the same oscillator to operate at $f_o/2$ and f_o and maintain the same operating parameters of the active device, coupling coefficient, drive level, quality factor, and so on [1]. Oscillators at very different frequencies are not usually made in the same technology, or they will not be similar enough up to the extent of considering both behaving as the same oscillator tuned at two different frequencies. Comparisons become less meaningful as N increases. Also, the previous study assumes identical oscillators in the 2-push, with the same noise spectral density (while in practice they will be affected by the natural statistical variations), and do not considers the 1/f noise contribution from individual oscillators. Nevertheless, two practical results sustain the theoretical considerations made by Rohde:

1. A single 2GHz oscillator has been compared with a 2GHz 2-push having two of this same oscillator coupled and tuned at 1 GHz. The respective phase noise densities measured at 10 KHz offset from the carrier were -105 dBc/Hz (single, uncoupled) and -113 dBc/Hz (2-push, coupled) respectively, thus differing in 8 dB [1]. Package parasitics, dynamic loaded Q, and tolerances of the component values of the two uncoupled individual oscillator circuits are meant to be responsible for this figure not being higher.

2. In [3] a 1-4/4-8 GHz wideband VCO in 2-Push topology is compared to one of its individual 1-4 GHz sub-circuit VCOs. Comparison is performed at their common frequency range of 2-4 GHz. The measured phase noise is better than –115 dBc/Hz @ 100kHz offset for the uncoupled VCO at 4 GHz, and a 5-7 dB improvement is observed on the phase noise of the Push-Push topology over the band. The discrepancy of 2-4 dB is attributed to the package parameters and tolerances of the component values of the two sub-circuits and also to the phase deviations of the coupling network[2] over the tuning range.

In a more recent work [8] the phase noise performance of BJT based direct and push-push VCOs, both using a same type of *microstrip square open loop* resonator, is measured and compared with a new push-push structure that employs an improved *microstrip square open loop multiple SRR* resonator with larger coupling coefficient (and thus higher Q) and rat race coupler instead of a Wilkinson for better power combining efficiency. The measured phase noise in the 5.7 - 5.8 GHz tuning range of the new VCO is -128.33 to -126.00 dBc/Hz at 100 kHz offset, with an output power of

---

[2] In his book [1] Rohde suggests a further improvement of the PN performance in N-Push wideband VCOs by the use of an integrated phase detector to compensate for the phase deviations of the combine network over the VCO tuning range.

+10.5 dBm. The phase noise improvement is 12.17 dB and 3.66 dB as compared with the direct and conventional push-push architectures. Also, the output power is increased by 5.67 dB, and 1.83 dB, respectively.

2.3 The 1/f noise upconversion problem

Choi and Mortazawi [4] suggest that, although the aforementioned advantages can make the push–push have low phase-noise performance as well as an extended frequency range, this oscillator may be vulnerable to a large *1/f* noise upconversion if not carefully designed, because the large second harmonic signals in sub-oscillators may degrade phase noise considerably due to *1/f* noise upconversion.

The low-frequency *1/f* noise plays a dominant role in determining the close to carrier phase-noise performance in oscillators as it is upconverted to the carrier frequency, resulting in a *1/f^3* term.

These authors use Hajimiri's linear time-varying (LTV) theory for phase noise [9, 10] to investigate the effect of oscillator waveform symmetry on the phase noise performance of microwave push–push and triple-push GaAs MESFET oscillators. MESFETs (metal–semiconductor field effect transistors) and HEMTs (high electron-mobility transistors), are known to have high *1/f* noise corner frequencies (up to several MHz), and thus make the low frequency noise upconversion problem particularly important.

Hajimiri describes the perturbation-to-phase conversions in a free running oscillator by analyzing how impulses of noise current injected into a circuit node affect the phase of the oscillator waveform. The phase shift varies depending on the node voltage value at the instant time the impulse of noise current arrives. Amplitude zero crossings of the node voltage will have the greatest phase sensitivity, and maximum amplitude levels will have the lowest phase sensitivity. Thus, waveforms close to square waves will have sensitivities localized to the transitions.
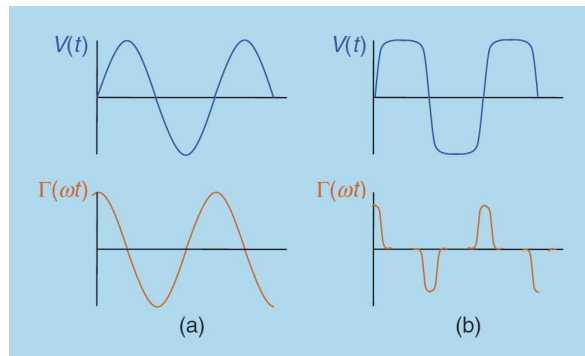

Fig.2.   Hajimiri oscillator waveforms, *V(t)*, and impulse sensitivity functions, $\Gamma(\omega t)$, for (a) a sinusoidal oscillator and (b) a limiting oscillator [11]

He developed the concept of an impulse sensitivity function (ISF), which is a periodic function dependent on the oscillation waveform (see Fig.2), and computed the phase perturbations *φ(t)* due to a noise current injected into a circuit node in terms of the ISF and the maximum charge displacement across the node capacitance. Taking the

autocorrelation of $\varphi(t)$ and Fourier transforming, gives the phase-noise spectral density function $S_\varphi(\omega_m)$ [11]. By doing this Hajimiri establishes a relationship between the device-noise $1/f$ and the phase-noise $1/f^3$ corner frequencies in terms of the direct current (dc) and root mean square (rms) values of the ISF.

Hajimiri's theory states that symmetry in the waveform's rise/fall times and their slopes reduces the value of the ISF's dc value, and this contributes to reducing $1/f$ noise upconversion. On the contrary, asymmetry in the rise/fall times causes $1/f$ noise upconversion to become significantly large [4]. Plots of these ISFs, along with the oscillator waveform, help designers gain insight and make the known importance of waveform symmetry very clear when trying to minimize $1/f$ modulation [11].

According to [4, 12] the requirements for symmetry in the oscillator waveform that lead to zero dc values of the ISF are (1) absence of even harmonic components or (2) equal phase in all the harmonics (even and odd).

Thus, the even harmonics amplitudes should be minimized to improve phase noise performance in the $1/f^3$ region, but this is in contradiction with the operation of 2-push structures which require strong second harmonic power levels in the sub-oscillators for improved dc-to-RF efficiency. The presence of high second harmonics distorts the waveforms of the two sub-oscillators, leading to a considerable asymmetry in their rise and fall times and causing a large $1/f$ noise upconversion which degrades $1/f^3$ phase noise performance. To overcome this problem, Choi and Mortazawi suggest minimizing the phase difference between the fundamental and harmonic components at the device port in push–push oscillators.

Triple-push oscillators do not posses this drawback as they do not use the even harmonic components for the output power; therefore, the second harmonic components can be eliminated in the individual sub-oscillators, thus satisfying the waveform symmetry conditions in the triple-push structure [4].
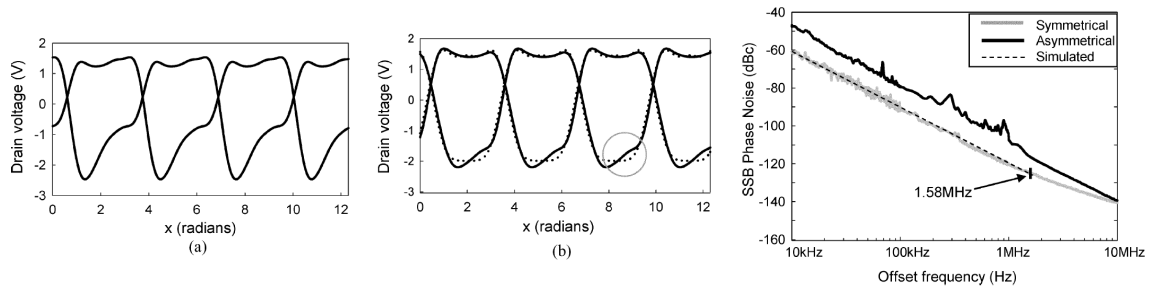

Fig.3.   Simulated asymmetrical (a) and symmetrical (b) voltage waveforms from the sub-oscillators in two push–push versions. Measured phase-noise results showing the different $1/f^3$ corner frequencies obtained. The reactive values of gate and source terminations in the sub-oscillators are optimized to maximize the second harmonic power level and to design symmetrical waveforms [4].

Not mentioned in [4], but a logical consequence from the noise averaging process that takes place in 2-push structures due to the synchronization of the coupled sub-oscillators, is that their resultant phase noise spectral densities are reduced by 3 dB with respect to their uncoupled mode of operation, and this includes the $1/f^3$ region as well. The problem with the 2-push is that the sub-oscillators need to have strong second harmonic components which would not be required if they were meant to operate in

single (uncoupled) mode; this imposes some limitations for the optimization of the sub-oscillators for low phase noise in the $1/f^3$ region.

In order to demonstrate the contribution of oscillator waveform symmetry to reducing $1/f$ noise up-conversion and improving the phase noise in the $1/f^3$ region, the authors implemented two versions of a 2-push structure with different symmetries in the sub-oscillators waveforms and reported a measured phase noise improvement of 12–15-dB from 10 kHz to 1 MHz offset frequencies (see Fig.3). They attribute this result to the different $1/f^3$ corner frequencies obtained; 1.58 MHz in the symmetrical push–push oscillator and 9 MHz in the asymmetrical version.

3 Planar Resonators made from sub-wavelength resonant particles

3.1 Purpose and Requirements of the Resonator circuit

In an array of oscillators coupled together, synchronization is achieved through mutual injection locking. A transmission-line network is designed to provide the appropriate coupling between the oscillators and it can also be used to act as a common resonator and power combiner, thus leading to a very compact design. Fig.4 shows two topologies used in literature to implement 2-push structures.

The resonators developed in this work are used as common resonators and coupling networks in 2-push structures and correspond to the topology of Fig.4 (a).
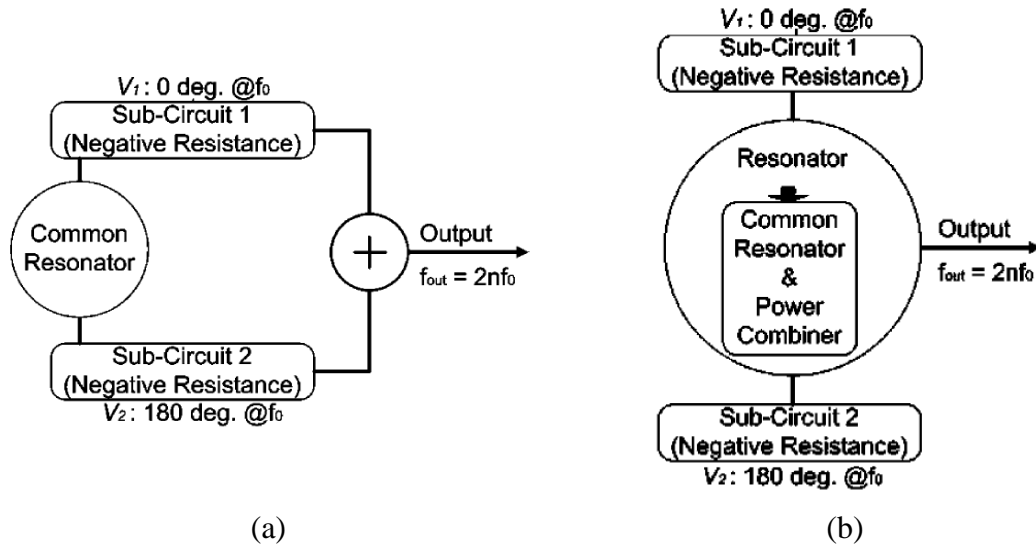

| (a) | (b) |

Fig.4. Circuit structures for a push–push oscillator. (a) Common resonator and coupling network. (b) Simplified structure using a Resonator-Combiner [13].

We started with a simplified topology like the one in Fig.4 (b), but the inclusion of resonant particles in the power combining network made it very difficult to simultaneously achieve the requirements for high-Q resonance at the fundamental frequency f_o (for low phase noise), out-of-phase coupling at f_o (to reject the first harmonic at the output), and in-phase coupling at $2f_o$ for power combining.

Unsatisfactory results were obtained during the lab test of the boards, and it was found that the oscillators were not coupling to each other correctly at the fundamental; as a consequence quasi periodic type solutions were observed. When coupling was achieved through gate bias control in one of the two oscillators, an in-phase or EVEN oscillation mode was observed and the first harmonic was not rejected at the output. The systems also had a solution at $2f_o$, but it was a fundamental oscillation mode from both oscillators and not the result of the combination of two out-of-phase signals, which was the wanted solution. The output level at $2f_o$ was very close to the simulated value (within 2 dB) as the power combiner had been tuned at that frequency.

At this writing we have not found in the literature any coupling + resonant + combine network containing sub-wavelength resonant particles as the ones used in this work, and the same can be said for the coupling + resonant networks that we have finally selected.

The purpose of a common resonator is to make the two active sub-circuits oscillate in accurate and stable out of phase mode at the fundamental frequency f_o, and to achieve low phase noise. The purpose of the power combiner in a push-push is to enhance $2f_o$ and reject f_o and $3f_o$.

Loose coupling of the resonator with the two active sub-circuits results in low phase noise performance, but it can also cause resonance instability; in that case it may be necessary to stabilize the fundamental resonance mode.

3.2 The basic cells

The resonant coupling networks developed in this work are basically made from Split Rings Resonators or SRR, which are planar particles of sub-wavelength size (electrically very small) that are able to inhibit signal propagation in a narrow band in the vicinity of their resonant frequency. They can be printed or etched, depending on the type of transmission line used and ring coupling mode. Some examples of these structures are shown in Fig.5, Fig.6 and Fig.7.

Printed SRRs are magnetically coupled to their host line (Fig.5(b) and Fig.6), while their complementary counterparts (etched CSRRs) resonate through electrical coupling (Fig.5(a) and Fig.7). When a time varying magnetic field is polarized along the SRR axis, current loops are induced in the rings at resonance, creating opposing fields that reflect back the incident waves. A dual electromagnetic behaviour takes place in etched CSRRs according to the duality theorem, so they are excited by a time varying electrical field parallel to the ring axis.

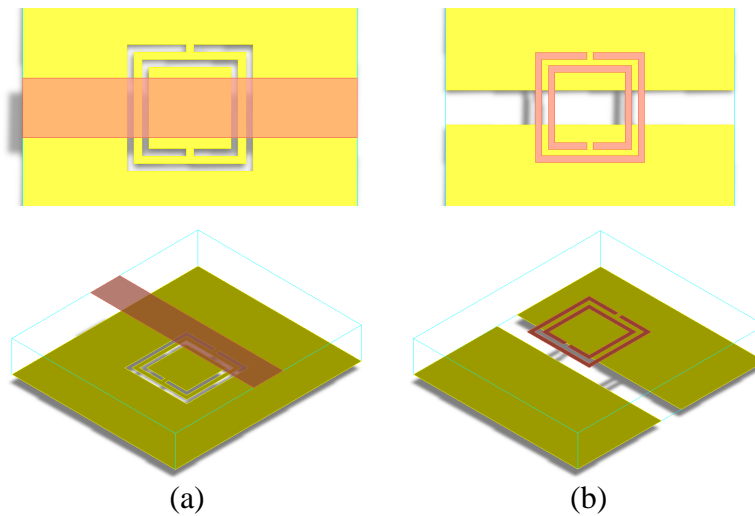(a)   (b)

Fig.5.   (a) Etched SRR (also called Complementary SRR) electrically coupled to a microstrip line.
             (b) Printed SRR magnetically coupled to a slot line

SRRs placed under the gap of CPW structures are preferred on thin dielectric substrates in order to obtain high inductive coupling between line and rings. For the CSRRs etched on the ground plane of microstrip lines, a high-permittivity dielectric substrate enhances the capacitive coupling.

(a)   (b)
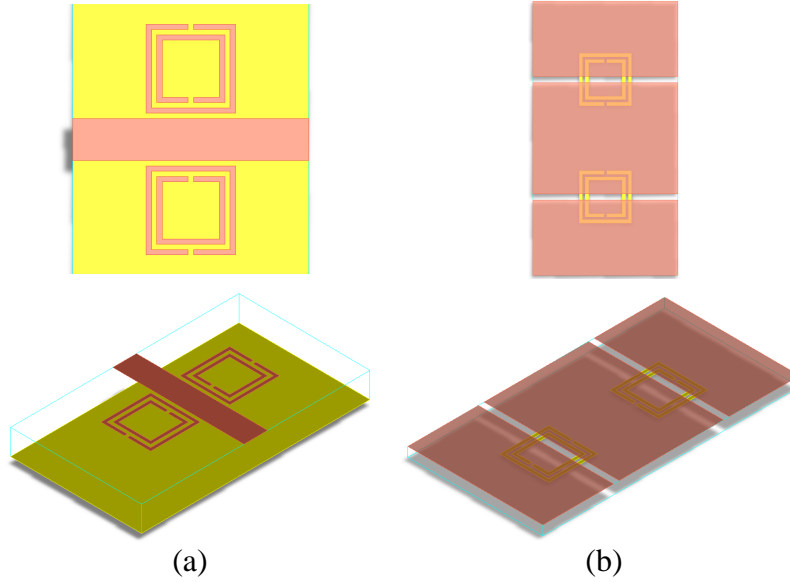
Fig.6.   (a) Printed top-SRRs magnetically coupled to a microstrip line.
                (b) Printed bottom-SRRs magnetically coupled to a coplanar waveguide
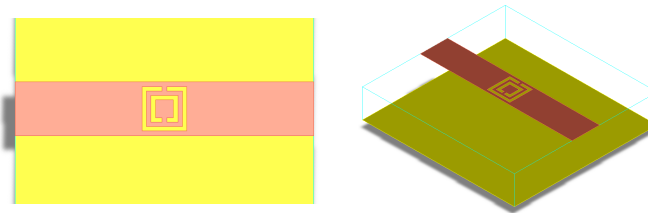

Fig.7.   Complementary SRR etched on the microstrip line.

The current loops induced in a SRR are closed through the distributed capacitance between its concentric rings, thus behaving as an LC resonant tank and so they are modelled [14]. As the equivalent capacitance of the resonator is given by the edge capacitance between concentric rings, the resonant frequency can be made very small by reducing the inter-rings' separation. High levels of miniaturization can thus be achieved for these particles provided that the lateral resolution of the layout generation system (typically a drilling machine or photo/mask etching) is small [15].

Square-shaped SRRs have been magnetically coupled to microstrip transmission lines in order to fabricate efficient stopband structures that exhibit high frequency selectivity with a relatively small number of SRR stages and, therefore, are potential candidates for the synthesis of microwave filters with compact dimensions in planar technology.

These properties can be of interest to the design of planar compact resonators for low phase noise oscillators with high spectral purity and unaffected by mechanical

vibrations. They would then be insensitive to the vibration noise and microphonic effects that produce unwanted modulations in dielectric resonator oscillators (DROs), which are a popular solution for frequency sources in the 3-18 GHz frequency range.

The high frequency selectivity of SRR's is attributed to a sharp transition of the effective permeability μ_{eff} of the media at the resonance frequency, with a change of sign from positive to negative values. The structures fabricated with these particles are named "*single negative metamaterials*". In the case of their dual counterpart, the CSRR, it is the effective permittivity ε_{eff} which becomes negative above the resonance frequency. When both μ_{eff} and ε_{eff} become negative in a limited frequency range (and usually for specific directions of propagation) the structure is called "*left-handed metamaterial*".

3.3 Metamaterials overview

Metamaterials are artificially fabricated periodic (or quasiperiodic) structures that present new electromagnetic properties (in one or several directions) not found in nature. These new electromagnetic properties are observed at macroscopic level as an *emergent property*; that is, they are the result of the interaction of a number of simple entities (basic cells) operating in a common environment, and forming a more complex behaviour as a collective[3].

The electrical response of materials to applied fields is determined by the permittivity (ε) and permeability (μ) which are macroscopic level parameters representing the average response of their atoms. They are called *constitutive parameters* and tell us all we need to know about the system on a length scale much greater than the separation between atoms. Metamaterials carry this idea one step further: the constituent material is structured into basic units or cells and on a length scale much greater than the cell dimensions, properties are again determined by an effective permeability and permittivity, valid on a length scale greater than the size of the constituent units. In the case of electromagnetic radiation this usually means that the cells must be much smaller than the wavelength of radiation [16].

During the last decade, an extensive research activity was focused on the synthesis of metamaterials, which show interesting properties making them very attractive to the design and optimization of microwave devices. They have found applications as Radar-absorbent materials (RAM), frequency selective surfaces (FSS) and polarization conversion systems (PCS).

A particular class of metamaterials, called double-negative or *left-handed media* (LHM), present simultaneously negative values of the electric permittivity and magnetic permeability and were first proposed by Victor Veselago in a theoretical study published in 1968. These materials are reported to have new and exotic electromagnetic properties, such as negative refraction index and phase velocity, reversed Doppler shift, and backward wave propagation.

---

[3] *Emergence*, Wikipedia

But, since such substances do not exist in nature, Veselago's work remained as a scientific curiosity for more than 30 years. It was not until the first left-handed medium was synthesized by David Smith and his team at the University of California San Diego (UCSD) in 2000, that a burst of scientific works on this topic suddenly took place. Envisaged applications in high frequency electronics (filters, antennas ...), nano-optics (subwavelength imaging, data storage...) and RF (magnetic resonance imaging...) also called the attention of electrical engineers[4].

Double-negative media can be implemented with artificial periodic structures composed of sub-wavelength constituent elements that make the structure behave as an effective medium with negative values of permittivity (ε) and permeability (μ) at the frequencies of interest [14].

Smith implemented a periodic composition of printed Split Rings Resonators (SRRs) with intercalated metallic posts between consecutive rings as shown in Fig.8. SRRs had already been proposed by Pendry in 1999 as non-magnetic resonant particles able to provide the media with a negative value of the effective permeability (μ<0). The metallic posts intercalated between consecutive rings provided for the negative permittivity (ε<0) required to achieve left-handedness.
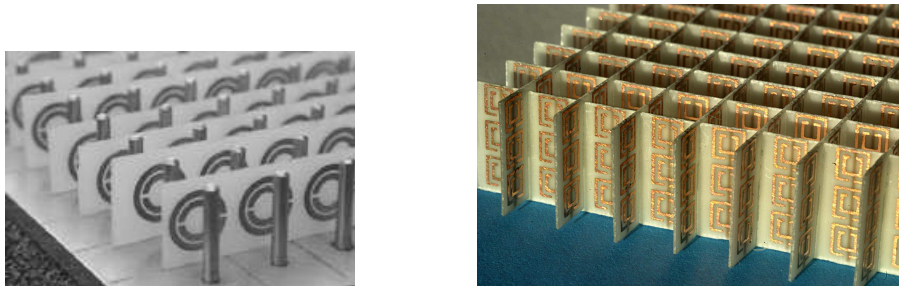

Fig.8.   The first metamaterial synthesized by Smith in 2000 (left) and a fully planar implementation from the same author with the metallic posts printed on the back substrate side (right).

Fig.9.   Vectors in right and left handed materials. In left handed materials the Poynting vector has the opposite sign to the wave vector. The anti-parallel phase and group velocities result in backward-wave propagation.

As a consequence of this double inversion of the material parameters **ε** and **μ**, Veselago found that the energy flow is reversed with respect to the wave vector, that is; rays travel in the opposite direction to waves. As a matter of fact, flipping the sign of both **ε** and **μ** is equivalent in Maxwell's equations to flipping the sign of the magnetic field **H** but keeping the same wave vector **k**. Solutions are exactly the same as those for a

---

[4] From Ricardo Marqués web page at GMUS (Microwaves Group of the University of Seville) http://personal.us.es/marques/

conventional positive system except for this inversion. As shown in Fig.9, vectors **E H k** now obey the left-hand rule, so Veselago referred to these new materials as being *left-handed*. Since the Poynting vector is given by **S** = **E**×**H**, its direction is opposite to **k**.
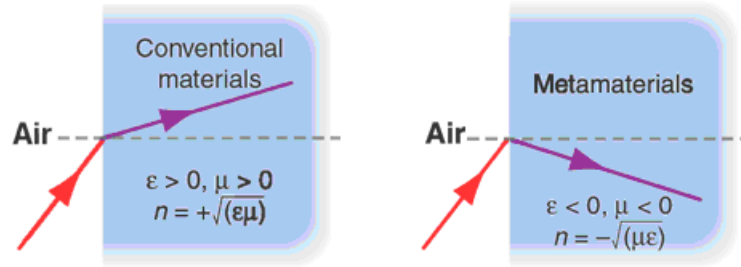
An immediate consequence of this is the inversion of the Snell law at the interface between doubly positive and doubly negative materials; light is bent "the wrong way" making a negative angle relative to the normal (see Fig.10). This was shown to be consistent with a negative refractive index and subsequently verified by simulations and experiments.

Another new property following directly from negative refraction is the ability of the LH materials to focus light, acting like lenses. Light formerly diverging from a point source in a positive medium (i.e. air) is set in reverse at the interface air-LHM, so it converges back to a point and diverges. But the process is reproduced again at the interface LHM-air, so once released from the negative medium the light reaches a focus for a second time. Pendry gives a good explanation of this and other phenomena in [16].

For the purposes of this work, our main interest in SRR's is their small electrical size; Thanks to the high electric coupling between the concentric rings forming the particle, the first resonance can be driven to small values [18]. In fact, a reduced size of the basic cells forming the negative materials is a key factor in obtaining continuous media properties in periodic structures, (the smaller the basic cell size, the better the structure approximates a continuous media). But it is also of great interest for microwave engineering applications, in order to reduce the size of circuits and components. The miniaturization of planar devices using SRR-based metamaterials and similar structures allows for a reduction of losses with increased quality factors in compact resonant structures like the coupling resonant networks that we have developed.

Before continuing with the design of the inter-oscillator coupling resonant networks, which are one of the contributions of this work, it is worth reviewing some of the previous works that have inspired the use of SRR particles as resonators in coupled oscillators design.

A type of one-dimensional metamaterial structure is the Left Handed Transmission Line, which can be implemented by combining SRR's magnetically coupled to a line (μ<0) and metallic grounding wires acting as shunt inductors (ε<0). A microstrip implementation of such line is shown in Fig.11a.

In [14] such type of line is implemented in Coplanar Waveguide technology (CWG) with the SRR's printed in the back substrate side, underneath the slots (where the

magnetic field is maximum), and shunt metallic strips between the central strip and ground planes (Fig.11b).
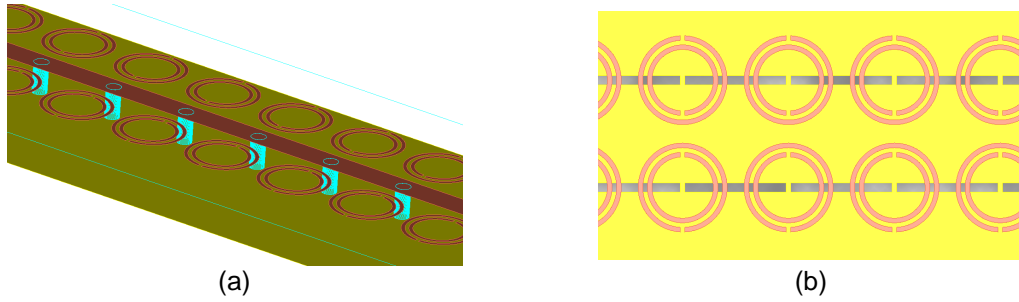

Fig.11.   (a) Microstrip implementation of a LH Transmission Line loaded with SRR's and vias to ground.
            (b) Coplanar Line loaded with SRR's printed on the bottom side and shunt metal strips to ground.

The presence of the rings leads to an effective negative-valued permeability in a narrow band above resonance, where signal propagation is inhibited. By simply adding shunt metallic strips between the central strip and ground planes, the stopband switches to a bandpass characteristic. This effect has been interpreted as due to the coexistence of effective negative permeability and permittivity (the latter introduced by the additional strips).

The same authors also use the SRR's dual counterpart, the Complementary Split Rings Resonator (CSRR), etched in the bottom ground plane of a microstrip. These particles are electrically coupled to the line and provide for a negative value of effective permittivity ($\varepsilon<0$) in a narrow band in the vicinity of their resonant frequency. They are combined with series capacitive gaps in the line which provide for the negative value of the permeability ($\mu<0$) to form a left handed microstrip (Fig.12).
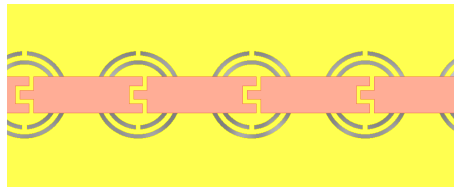

Fig.12.   Left Handed microstrip line loaded with CSRR's etched on the back substrate side and series gaps etched in the conductor strip

It is reported that a CSRR loaded microstrip shows a narrow stopband at approximately the same resonant frequency of an SRR loaded microstrip with identical dimensions of the resonators (Fig.11a without vias). Then, by periodically etching capacitive gaps in the conductor strip, the stopband switches to a passband. This effect is interpreted as due to a left-handed behavior of the CSRR loaded line.

In summary:

o   By properly coupling CSRRs (SRRs) to a microstrip (Coplanar) transmission line, planar structures with effective negative $\boldsymbol{\varepsilon}$ ($\boldsymbol{\mu}$) can be obtained.

o By adding capacitive gaps (shunt strips), effective negative **μ** (**ε**) is introduced and a left-handed behavior is achieved.

o These structures are fully planar (they do not incorporate vias or other non planar inserts) and can be easily fabricated by using standard photo-etching techniques. They can also incorporate modifications of the basic SRR/CSRR geometry.

As we will later see, by introducing some modifications on the basic cell geometry to accommodate varactor diodes, electrical tuning is achieved.

3.4 Basic cell modelling

The basic cells employed in the design of the different resonators used in this work are the single negative CSRR electrically coupled to a microstrip line (Fig.13a) and the double negative or left handed CSRR with a capacitive series gap in the line (Fig.13b). The CSRR provides for a negative effective permittivity (ε<0) above its resonant frequency, while the capacitive series gap introduces the negative value of the effective permeability (μ<0).
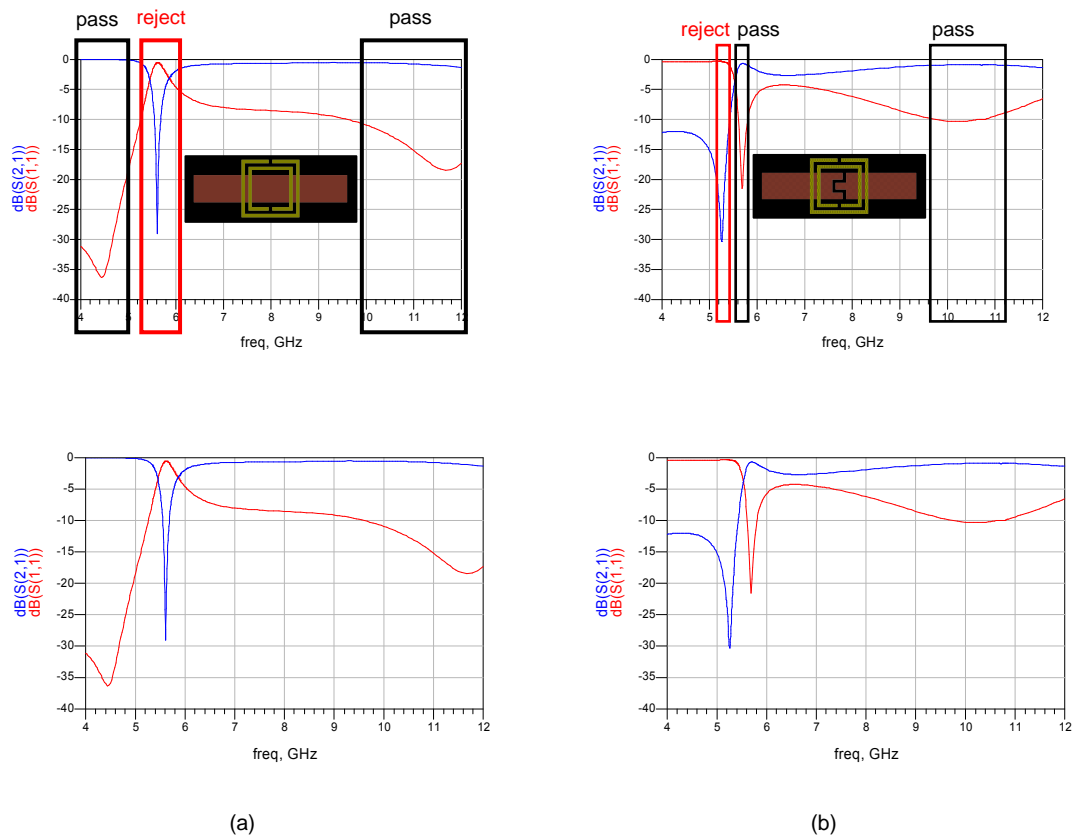

Fig.13.   Single negative (a) and left handed (b) resonant structures based on CSRRs electrically coupled to a microstrip line

Inspired by previous works [14],[18] I have chosen the Rogers RO3010 substrate to implement the resonators, thus taking advantage of the low loss of the material and

high-permittivity to enhance the capacitive coupling between the CSRRs etched on the ground plane and the microstrip lines.

The simulations have been performed with Momentum v350 (ADS2009) and substrate parameters: Er = 10.2, h = 50 mils, Td = 0.0023, t = 35 um, σ = 5.88E7 S/m

We observe that, up to a certain frequency above the CSRR's resonance, both cells show an opposite behavior with respect to each other; the single negative cell acts as a stop-band resonator of high selectivity, while the left-handed one has a band-pass characteristic. Both structures transmit energy in their higher frequency region. These aspects could be exploited to design networks capable to act as reflection resonators at the fundamental frequency of negative resistance oscillators, but transparent to the second harmonic, thus allowing for signal combination in 2-Push structures. We intend to take advantage of the high-Q (selectivity) for improved phase noise and spectral purity (1st harmonic rejection). Cancellation will nevertheless be limited in discrete 2-push structures due to the dispersion of values leading to a lost of symmetry.

We have decided to work with RLC lumped element models because they allow for faster simulations and also ease the time domain integration.
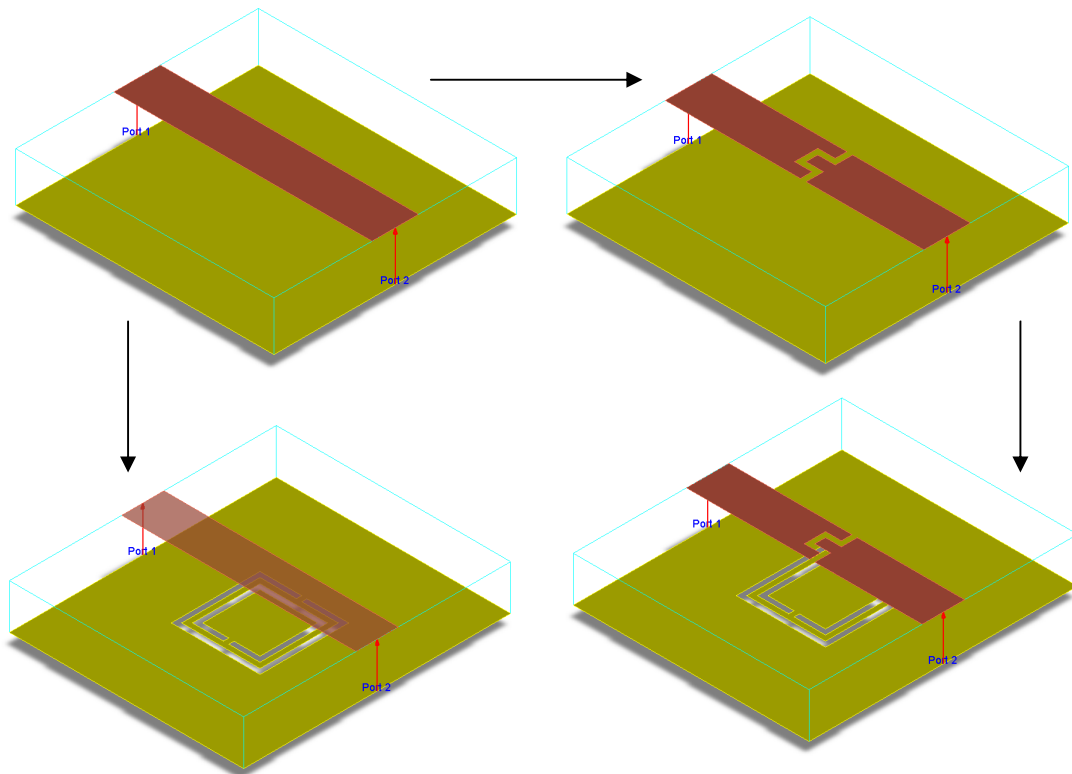

Fig.14.   Modelling process. From left to right and top to bottom: microstrip line, microstrip line with capacitive gap, CSRR coupled to a microstrip line, and CSRR coupled to a microstrip line with capacitive gap

The extraction process of the lumped element models has been performed in several steps: as shown in Fig.14 we first extract the elements of a single microstrip line, based on EM simulated data with Momentum. To this model we added a series capacitor and fit its value using EM simulated data for the series gap transmission line; at this point an overall optimization was performed on the other model elements. Finally we added the

coupling capacitor and resonator as proposed by R. Marqués [18] and optimized their values to fit EM simulated data from the CSRR coupled to a microstrip line with capacitive gap structure. A second overall optimization was again performed on all the model elements. The comparison between EM data and lumped model simulation are shown in Fig.15; the fitting is particularly good in the frequency band where the first and second oscillator harmonics are to be expected.
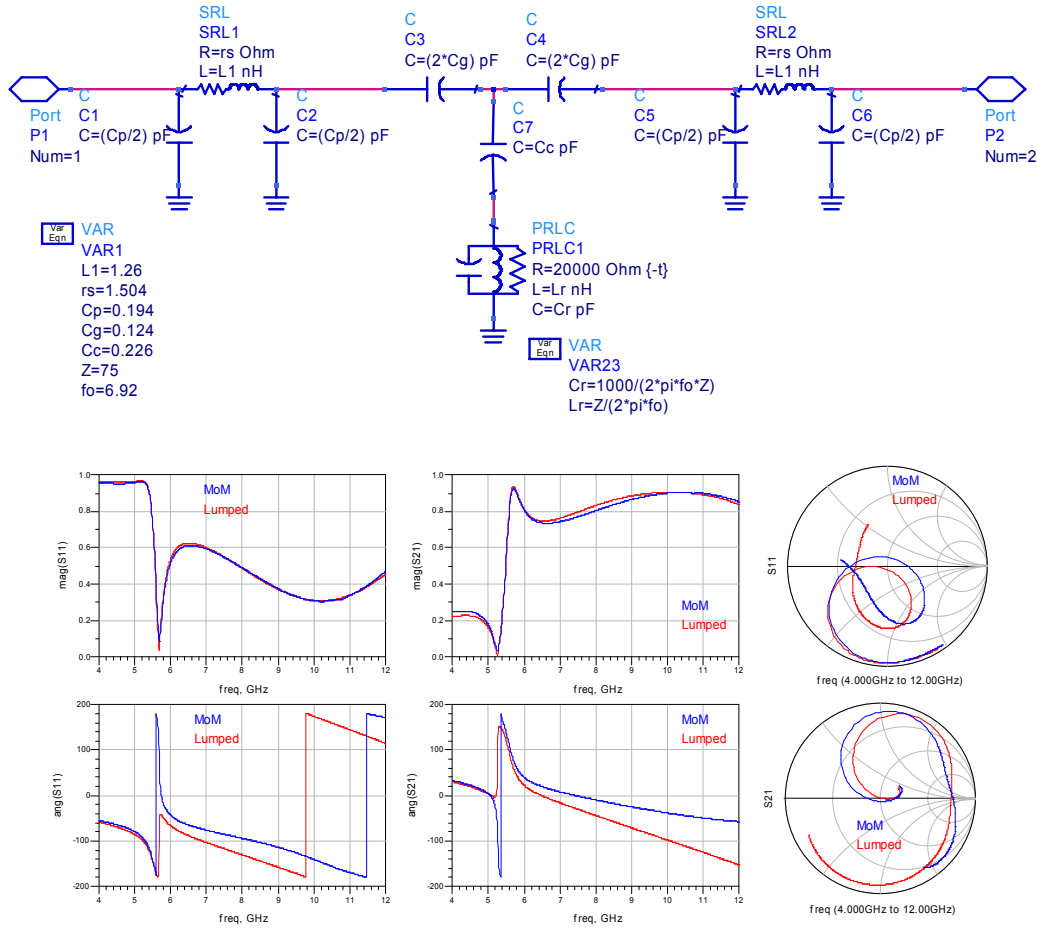

Fig.15.   Model of a CSRR coupled to a microstrip line with capacitive gap

We have included resistive losses and a "pi" network topology to model the access lines to the structure, which are not included in the original model; [18] can easily fit the magnitude of S11 and S21 but this is achieved in detriment of the phase. This is not critical for filter applications which intend to produce a given rejection characteristic, and [18] also includes inter-coupling capacitors to model the effect of having many rings very close to each other along the line, forming a CSRR loaded microstrip line which behaves as a metamaterial in the direction of energy propagation. In that case the phase only affects to the input/output access ports which do not influence the rejection characteristics of the structure because they are 50 ohm matched. But in our application, the phase and magnitude of the parameters are equally important because we intend to use the CSRR structures as common resonators and as inter-oscillator coupling networks, whose phase performance will influence the oscillating mode of the 2-push. Adding resistive and capacitive elements to the access lines produced an additional

degree of freedom which allowed for a better fit of both, the phase and amplitude of the scattering parameters.

The model of the CSRR coupled microstrip line (with no capacitive gap) was achieved by adding the coupling capacitor and resonator proposed by R. Marqués [18] to our single microstrip line model, and fitting the element values using EM simulated data of the CSRR coupled microstrip line. Then an overall optimization was performed on all the model elements. The comparison between EM data and lumped model simulation are shown in Fig.16; the fitting is also very good in the frequency band where the first and second oscillator harmonics are to be expected.
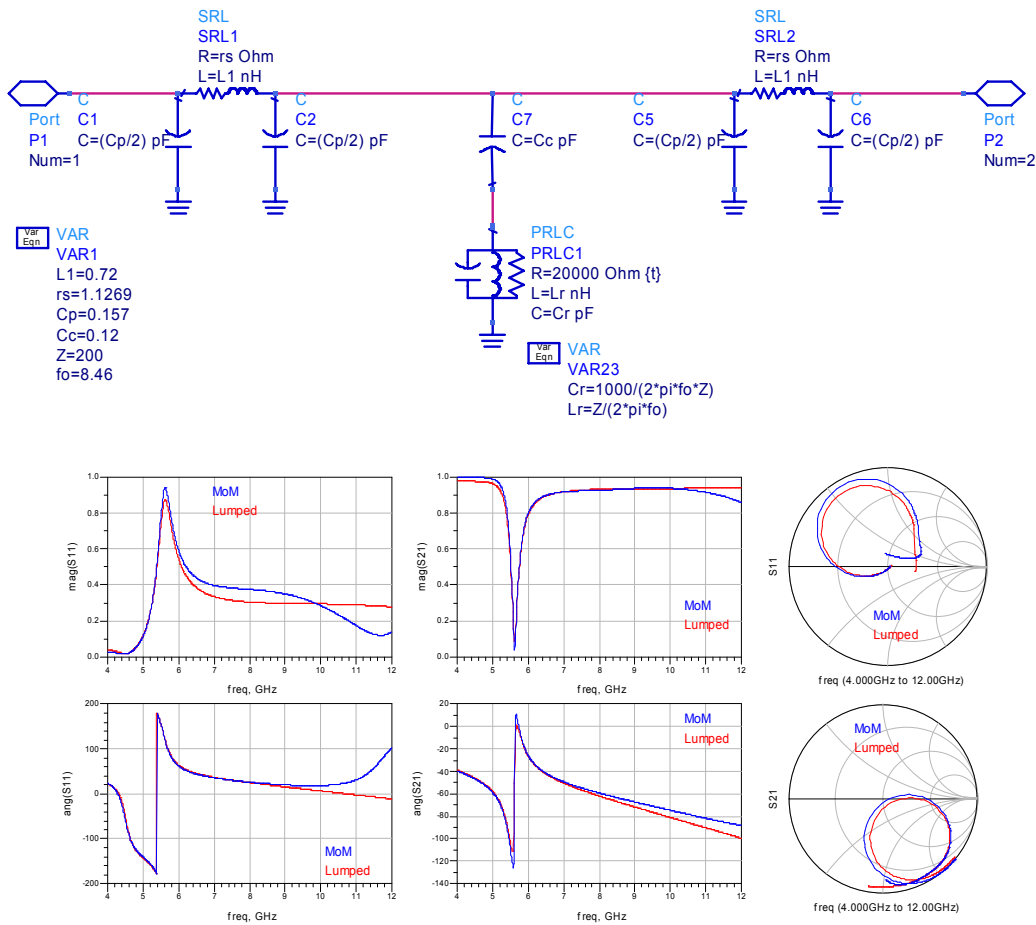

Fig.16.　　　Model of a CSRR coupled to a microstrip line

A resonator-combiner structure was implemented using CSRR's coupled to capacitively loaded microstrip lines using a 50 mils thick Rogers RO3010 substrate (ε_r = 10.2). The layout and photographs of this structure can be seen in Fig.17, and the simulated results (using a lumped element model) are compared to Network Analyzer measurements in Fig.18. A TRL calibration was used to extract the measured data.
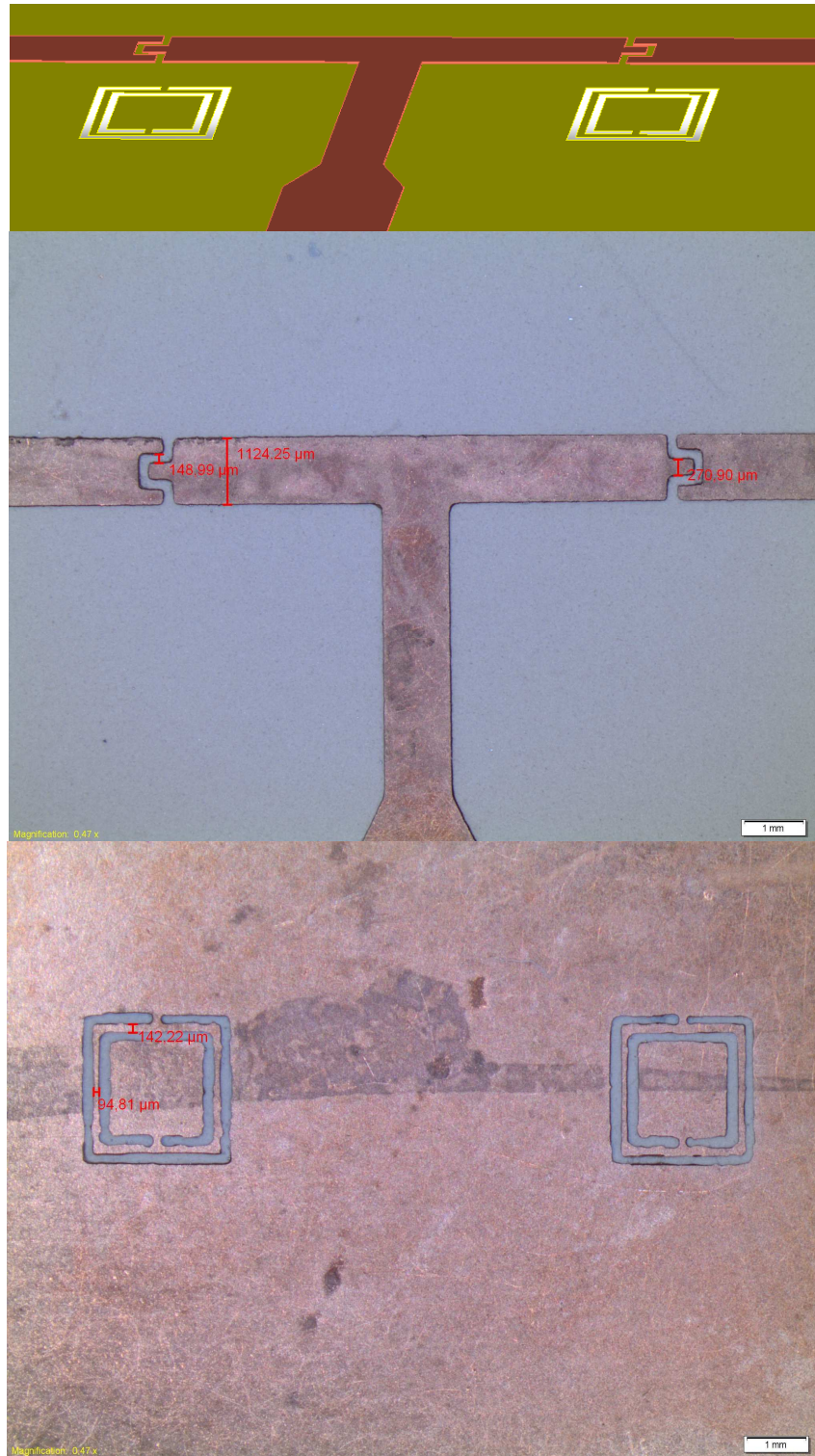
Fig.17.   3D layout and photographs of the resonator coupling network based in CSRRs coupled to capacitively loaded microstrip lines. The CSRR's are etched on the bottom metal.

The transmission data (S12 and S31) shows a very good agreement between model and measurements in Fig.18, while a shift in frequency is observed in the reflection data (S11 and S33). We do not have yet a clear understanding of the possible causes to this difference; more tests should be carried out in order to determine whether the frequency shift is caused by the TRL calibration kit or by the CSRR etching process, as [18] use a mechanical drill while we have used a chemical etching which

produced a lower shape definition. This is in part due to the use of 1 oz. copper lines instead of ½ oz (17 μm) thick, which would have required a lower chemical etching time.
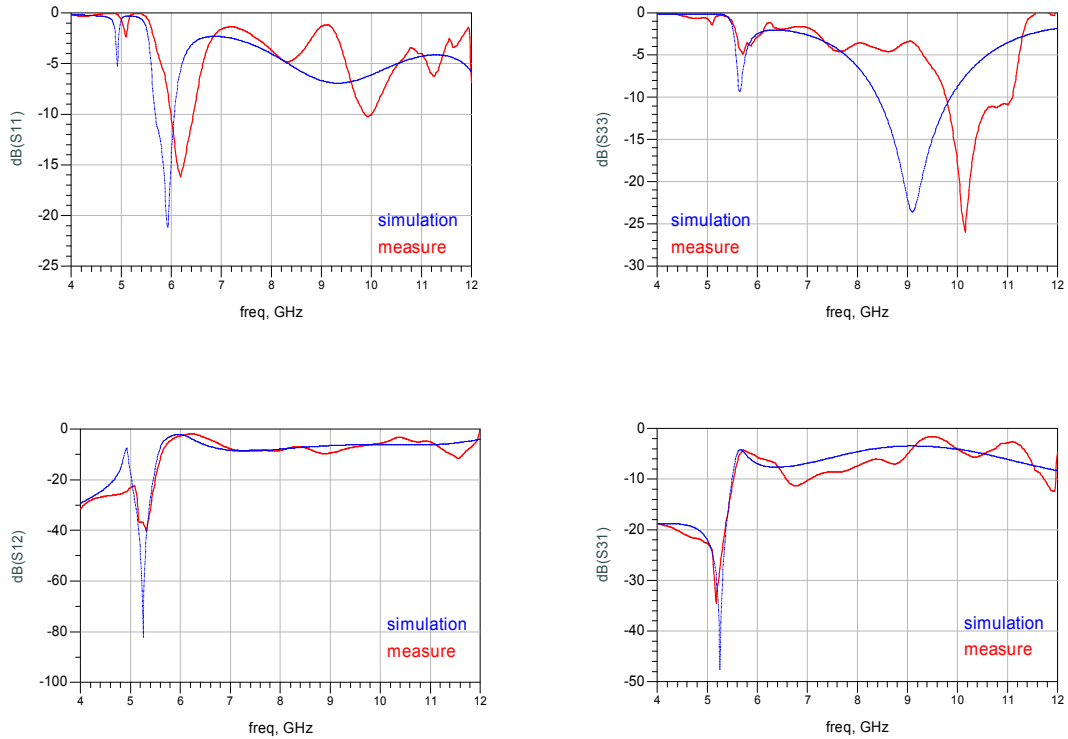

Fig.18.   Comparison of simulated vs. measured results for the resonator coupling network based in CSRRs coupled to capacitively loaded microstrip lines. A TRL calibration has been applied to the measurements.

4 Oscillator Design

An active circuit has been designed to offer negative resistance around 5.4 GHz, from which two fully planar 10.8 GHz coupled oscillators, working in 2-Push mode, have been implemented using different resonators; one of them is based on short circuited microstrip line stubs while the other takes advantage of the improved selectivity of Complementary Split Ring Resonators (CSRR) etched in the back substrate side.

A Rogers RO3010 material with Er = 10.2 and 50 mils thick has been selected as the substrate. This decision was driven by the need to achieve a high electric coupling between the CSRR's and their host microstrip lines.

4.1 Single Oscillator Design

We have started with a series feedback single transistor topology, which can produce negative resistance around the resonances of the source stubs.

The transistor chosen is the NEC's NE3210S01; an AlGaAs/InGaAs pHEMT with mushroom shaped gate fingers for decreased gate resistance and improved power handling. Overall Gate width and Length are 160 μm and ≤ 0.2 μm respectively. This device is quoted to have an *excellent low noise figure and high associated gain*, according to its datasheet information. In fact, Indium content in the channel of a HEMT is associated with low noise and good gain figures. Noise and Gain parameters for using this device as an amplifier are given in the 2-18 GHz range.

A complete list of parameter values for this transistor is available in its datasheet[5], which includes some S-Parameter data measured at typical bias. Some of the figures of interest for our application are listed in the Table 2 below.

		unit	range	typ
IDSS	Saturated Drain Current, V_{DS} = 2V, V_{GS} = 0V	mA	15 / 70	40
V_P	Gate to Source cutoff Voltage, V_{DS} = 2V, I_D = 100 μA	V	-2/-0.2	-0.7
$V_{DS,max}$	Max. Drain to Source Voltage	V	+4	
$I_{GS,max}$	Max. Gate Current	μA	100	
P_T	Total Power Dissipation	mW	165	

Table 2   Some datasheet characteristics of the NE3210S01

The main reason for choosing this transistor was that it is available and widely used in the Department for oscillator design in our frequency range of interest. The chip transistor comes housed in a low cost plastic package.

We know from experience that the datasheet is conservative with respect to the maximum rated VDS bias, and have decided to operate the device at saturated IDS (0 VGS) with 4V drain-to-source voltage, for maximum output level and second harmonic efficiency. This is a common operation point found in the literature survey for similar transistors working in 2-Push mode structures. A discussion on the bias point and model selected is given in Appendix A II.

---

[5] NEC's Super Low Noise HJ FET - NE3210S01. California Eastern Laboratories, 07/01/2004

Fig.19 shows the basic circuit used to find proper Source and Gate stubs and to set an adequate value for the Drain load. At this stage non dispersive and lossless transmission line models are used in order to ease the optimization of the electrical length and line impedances.
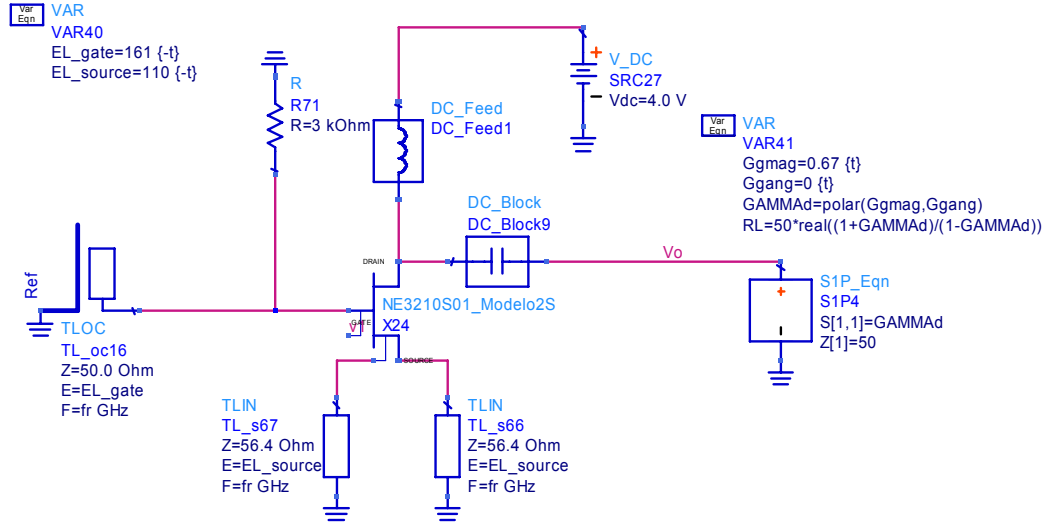

Fig.19.   Circuit used to find the optimum values of the Source/Gate stubs and the drain load, which is a real impedance of 253 ohm.

The Source stubs impedance is determined by the width of the device's source pads and the substrate selected. Their electrical length affects the frequency range in which negative resistance is observed. In fact sub-bands of negative resistance are formed at multiples of the stubs resonance frequency. The optimization of the Drain load impedance is performed to prevent having negative resistance at the harmonic sub-bands. Finally, the Gate stub length fixes the frequency at which the start-up condition is achieved, according to (9)-(11) in section 5.2. A high value resistor is used as a simple means to ground the Gate.

Fig.20 shows the simulated small signal admittance (top left) measured at the internal gate node available in the model used. The imaginary part crosses the zero value (resonance) at 5.4 GHz where the resistive part is negative, thus allowing for excess energy to start oscillations. A time domain analysis is also performed and the output voltage waveforms are obtained, showing the transient response. The frequency spectrum is calculated in the stationary part of the time waveforms.

One implementation of the load impedance using transmission lines and lumped components is presented in Fig.21, where special care has been taken to prevent harmonic resonances from showing negative resistance. From the simulated results in Fig.22 the admittance's imaginary part crosses the zero value at the main resonance with a slope of 16.1 mS/GHz at 6.02 GHz; high slope values are related with low frequency sensitivity to noise fluctuations, and thus a reduced phase noise. The time domain simulation shows spectral lines with amplitude values of +9.78 dBm at 5.4 GHz (fo) and +1.78 dBm at 10.8 GHz (2fo).

The circuit in Fig.21 is the basic topology of the Gate stub resonator oscillator. The same active circuit in implemented in Fig.23 with a CSRR based resonator at the Gate port, showing the simulated results of Fig.24.
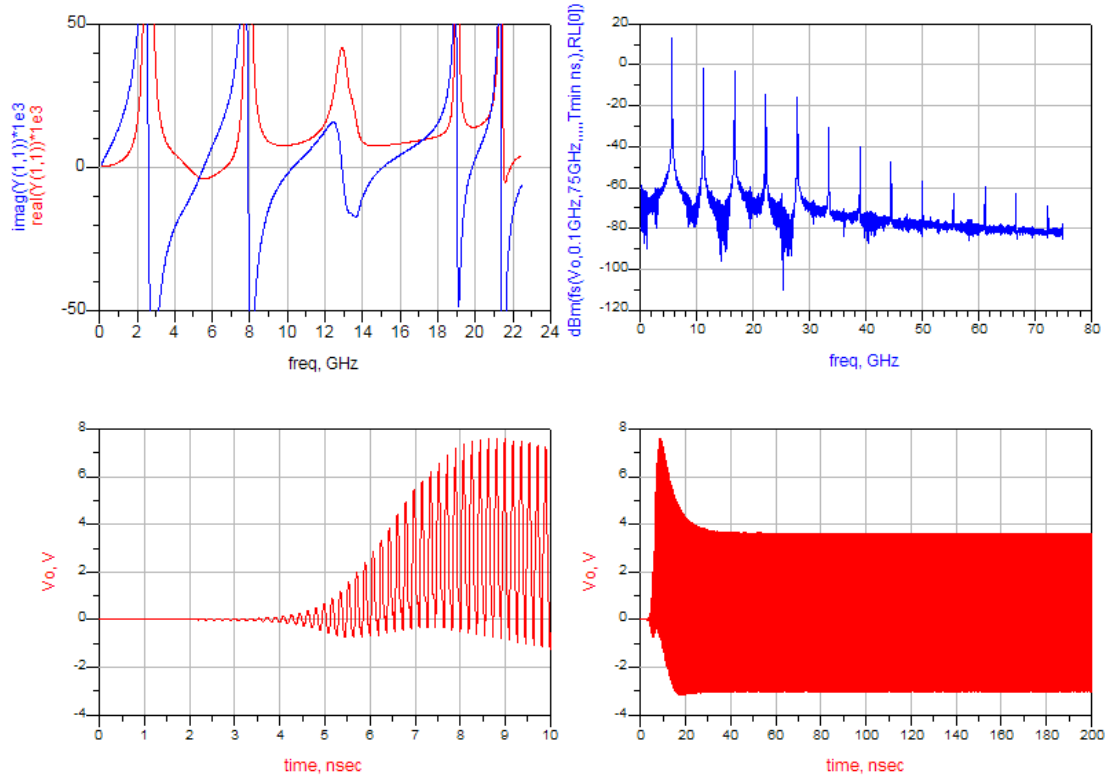

Fig.20.   Small signal admittance analysis and time domain spectrum and voltage waveforms corresponding to the structure in Fig.19
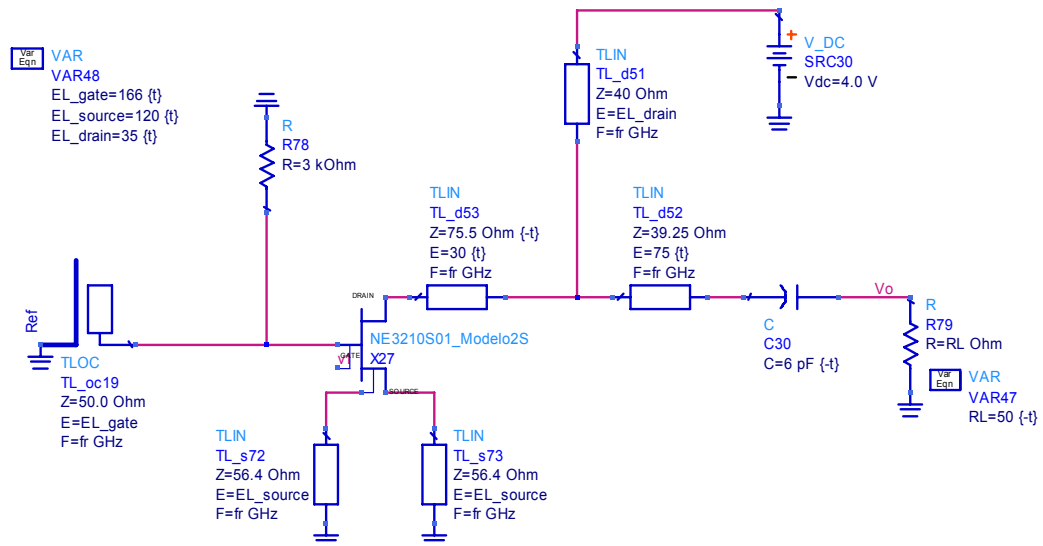

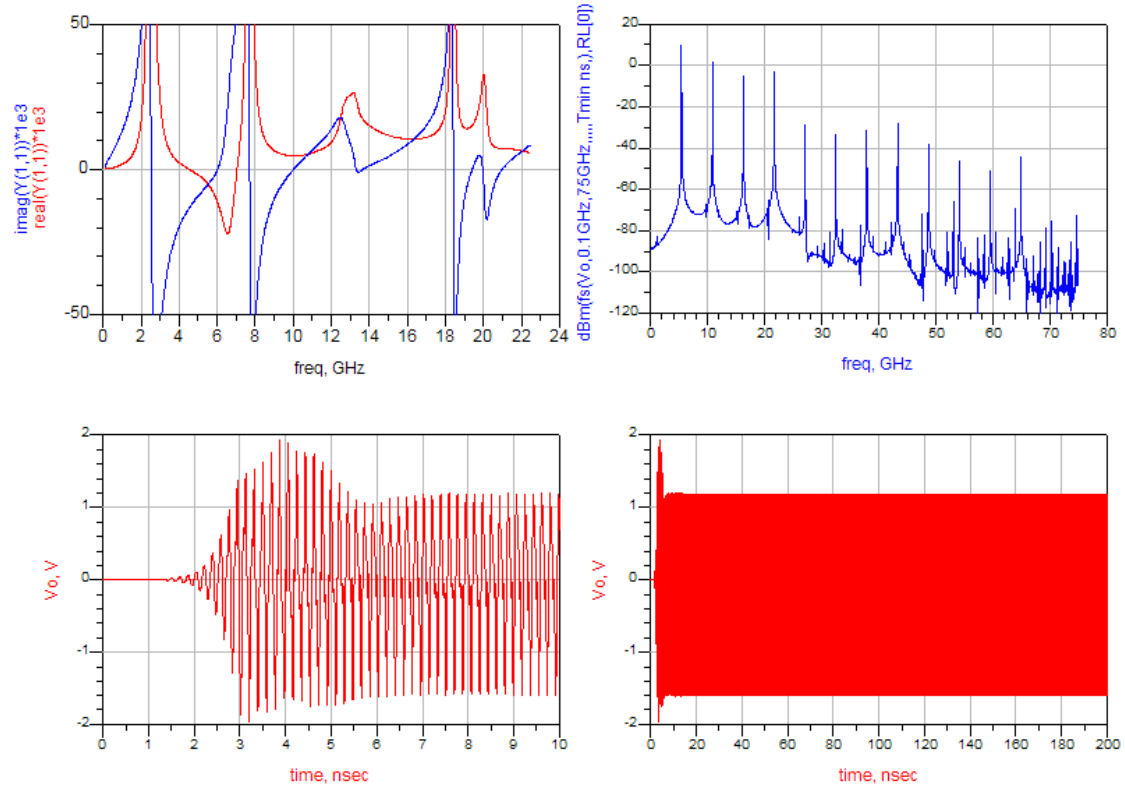Fig.21.   Basic circuit used for the Gate stub resonator oscillator.

Fig.22.　　　　Small signal admittance analysis and time domain spectrum and voltage waveforms corresponding to the structure in Fig.21
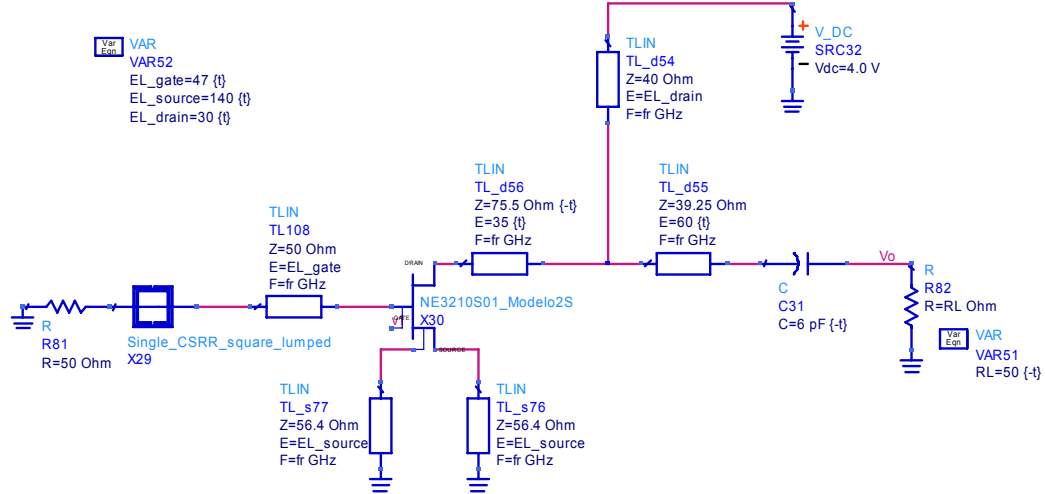
Fig.23.　　　　Basic circuit used for the CSRR resonator oscillator.

A much higher slope of 75.4 mS/GHz is observed at 5.59 GHz, compared with the 16.1 mS/GHz at 6.02 GHz form the open stub gate resonator circuit of Fig.21. The simulated output levels are +10.7 at 5.4 GHz (fo) and +4.08 at 10.8 GHz (2fo).

Both circuits in Fig.21 and Fig.23 were tuned to oscillate at 5.4 GHz. But the small signal admittance of the CSRR based structure resonates at 5.59 GHz, much closer to the nonlinear oscillation than the 6.02 GHz from the open stub gate resonator oscillator; this is a consequence of the higher Q of the CSRR based resonator. In high Q circuits

the small signal resonance is close to the actual nonlinear oscillation. Table 3 shows a comparative of the performance obtained with these two basic topologies.

Fig.24.   Small signal admittance analysis and time domain spectrum and voltage waveforms corresponding to the structure in Fig.23

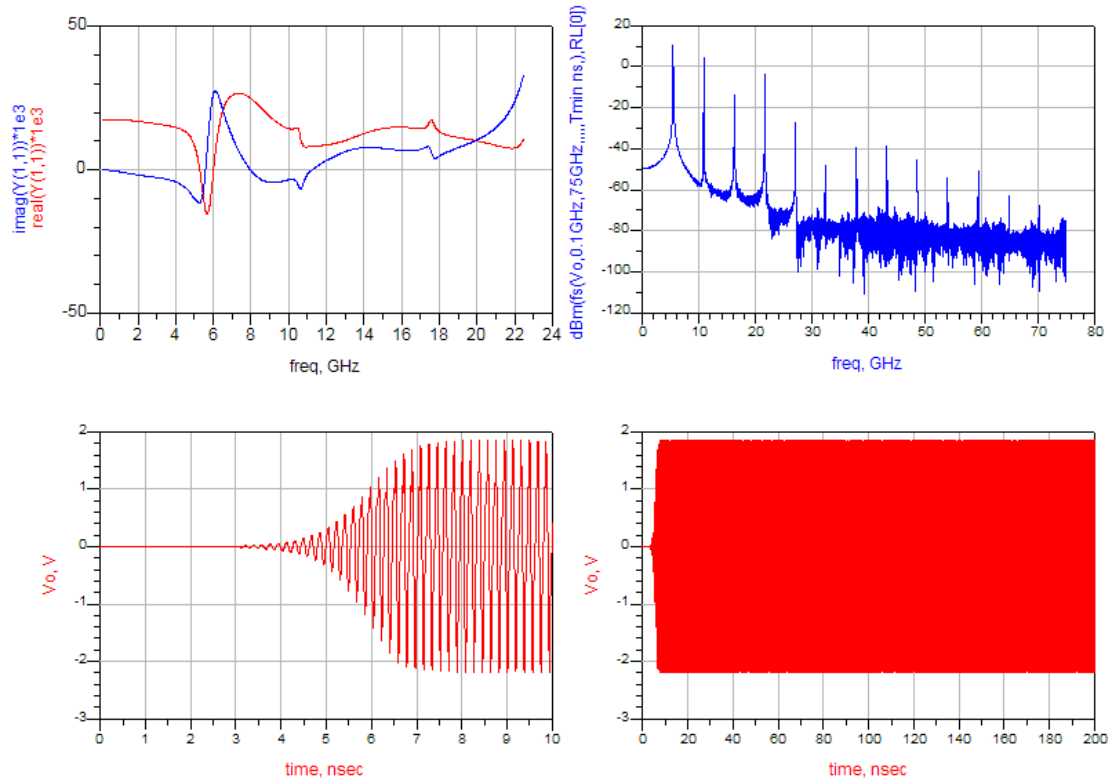|	ss resonance (GHz)	Slope (mS/GHz)	H1 (GHz)	P1 (dBm)	H2 (GHz)	P2 (dBm)
Open stub	6.02	16.1	5.4	+9.78	10.8	+1.78
CSRR	5.59	75.4	5.4	+10.7	10.8	+4.08

Table 3   Comparative results from the Open Stub and CSRR based resonator oscillators. H_n, P_n mean frequency and level of the n-th harmonic from the nonlinear simulation

4.2 Design of the 2-push (push-push) structure

Two active circuits as the one in Fig.23 have been coupled together through passive networks containing the stub or CSRR based resonators and a section of transmission line optimized to stimulate the 2-push oscillating mode in the structure. This mode could be obtained in simulation thanks to the use of ideal non dispersive line models. The schematics are shown in Fig.25 and Fig.27 with their corresponding simulation results in Fig.26 and Fig.28 respectively.

Several solutions were found for the stub coupling network in Fig.25. All have an electrical length of 180º between transistor gates, with λ/4 stubs to ground, which are also used for gate bias. The network providing for the greater second harmonic level was selected.

For the coupling network in Fig.27 four solutions were found; all of them use a λ/4 line between CSRR coupled matched stubs (ended with a 50 Ohm resistor to ground), and

the electrical length from any transistor gate to the reflection plane (the CSRR position) is a multiple of 90º. The solution offering a greater second harmonic level was selected.
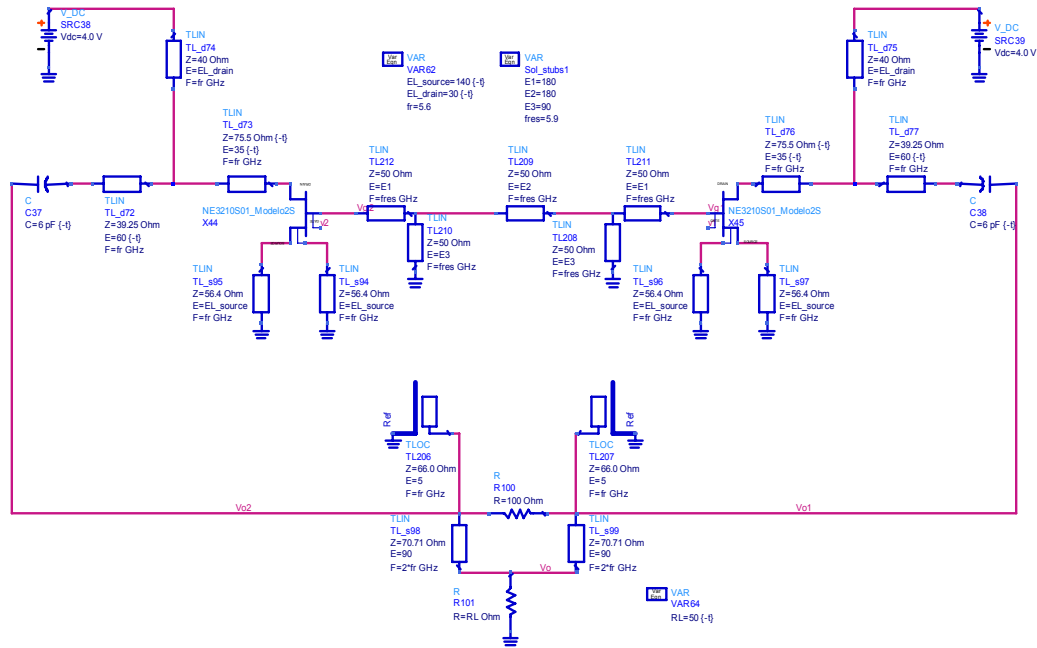

Fig.25.   Two Coupled Oscillators through a passive network containing short circuited stubs
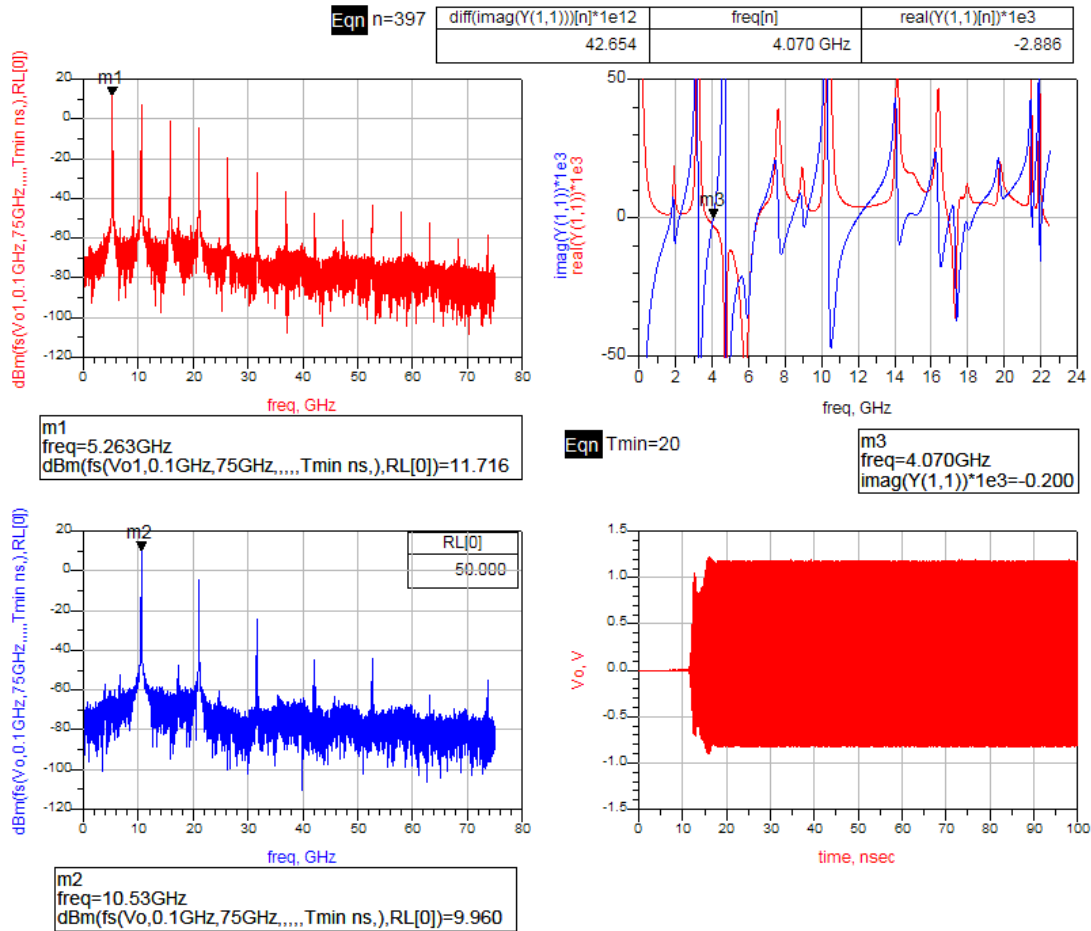

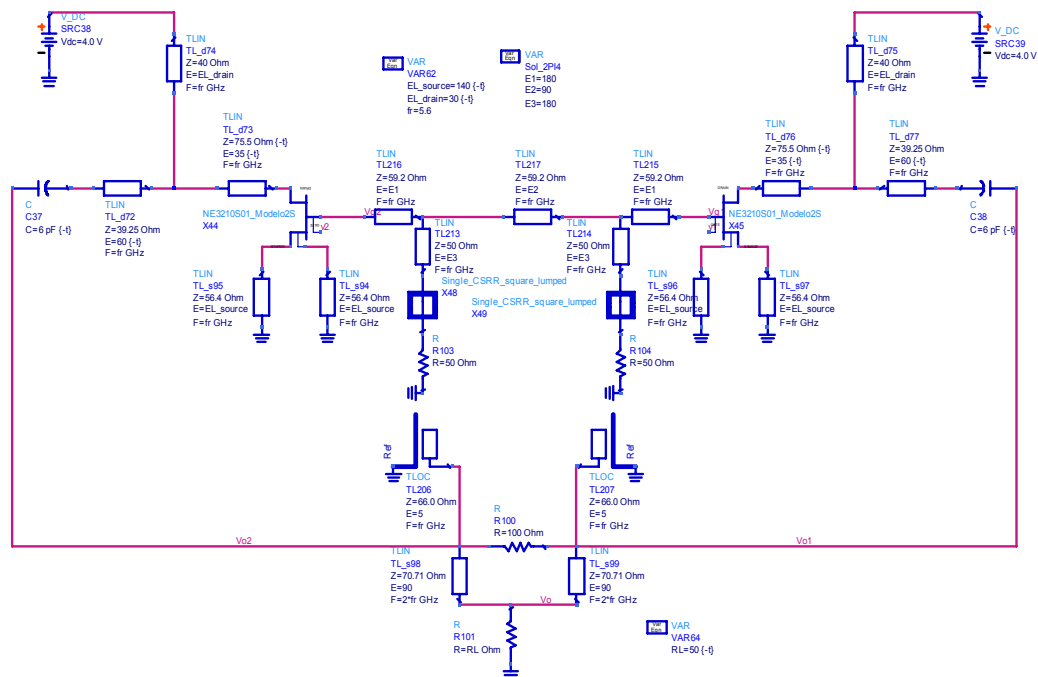Fig.26.   Simulated results from the circuit in Fig.25

Fig.27.　　　　Two Coupled Oscillators through a passive network containing CSRR based resonators
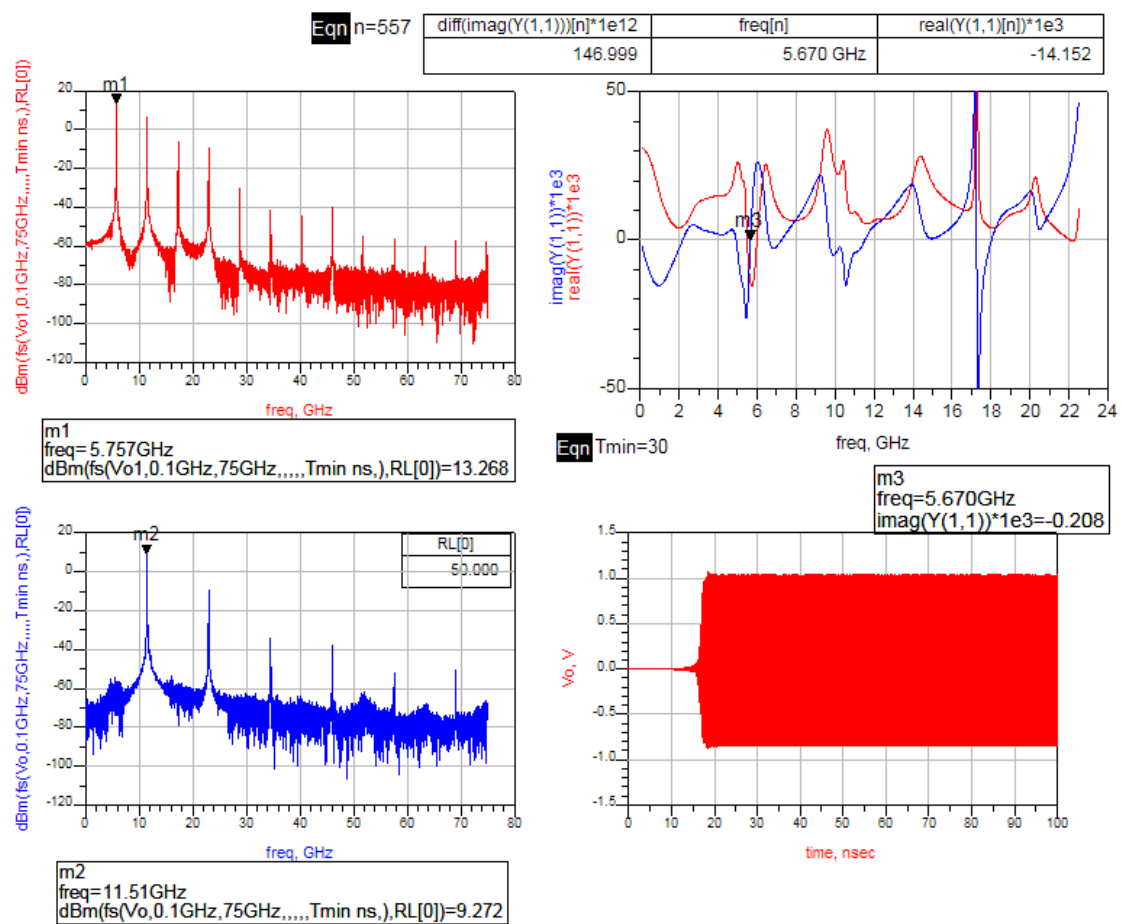

Fig.28.　　　　Simulated results from the circuit in Fig.27

With the single oscillators operating out-of-phase with respect to each other in the previous structures, it is easy to extract the 2-push mode by combining in-phase the oscillator's outputs; so that the first and odd harmonics cancel out while the second and even harmonics are added at the output of the Wilkinson power combiner. This combiner is tuned at the second harmonic frequency ($\lambda/4$ length of its branch lines). In order to avoid a potential resonance at $3f_o$ open ended stubs are placed at the combiner's input ports; the impedance presented by the combiner influences the drain load of the single oscillators, and thus their oscillation performance.

Finally both structures were reproduced using microstrip substrate line models, which are lossy and dispersive. After several optimization steps the following boards have been designed on 50mils thick RO3010 Rogers's substrate with 1oz. metallization. They can be seen in Fig.29. Their dimensions are 70 x 58 mm^2. Fig.30 shows a close-up view of the two resonator structures.

The practical realization of the basic circuits in Fig.25 and Fig.27 required the addition of new sections such as the dc decoupling networks connecting the bias to the Drain Load lines; these were carefully designed to avoid out of band resonances which might induce undesired oscillating modes. Also some capacitive-resistive coupling was added at the Source stubs in order to prevent a potentially harmful resonance in the high frequency region of the active device. Efforts have been concentrated on keeping a positive real part of the admittance out of the band of interest. The next chapter is devoted to the Frequency Domain analysis of these structures.
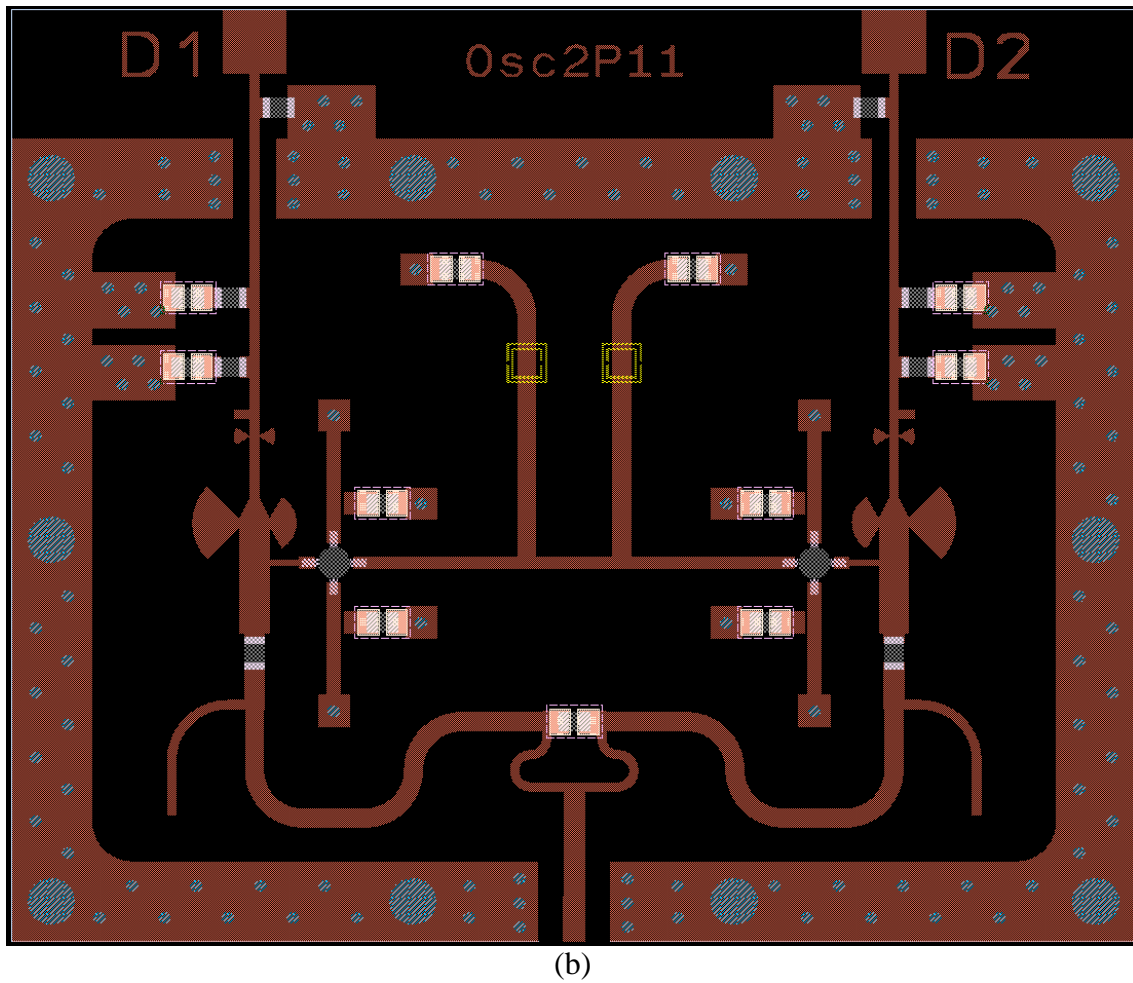

(a)

(b)
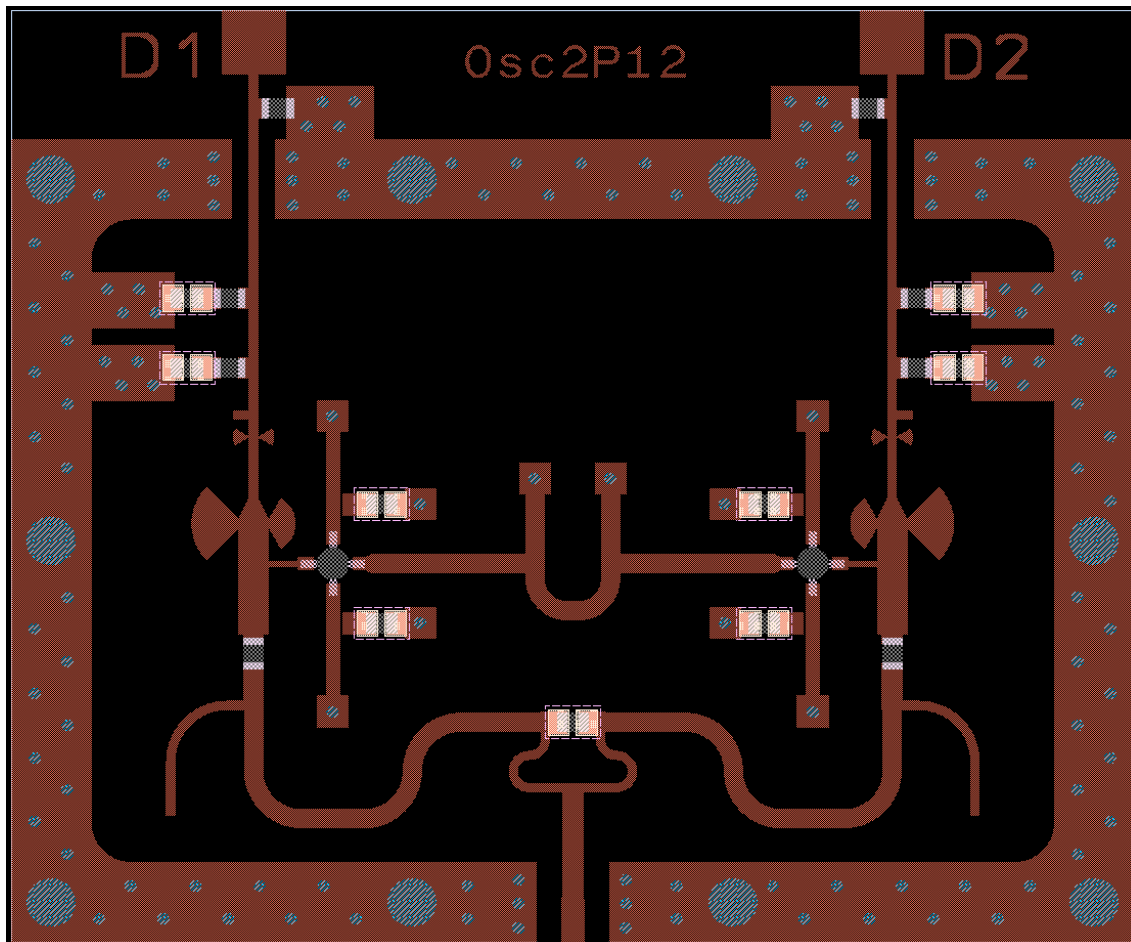
Fig.29. The 2-push test circuits implemented for evaluation of the different resonators performance. (a) Transmission Line stubs. (b) Microstrip lines coupled to CSRRs.
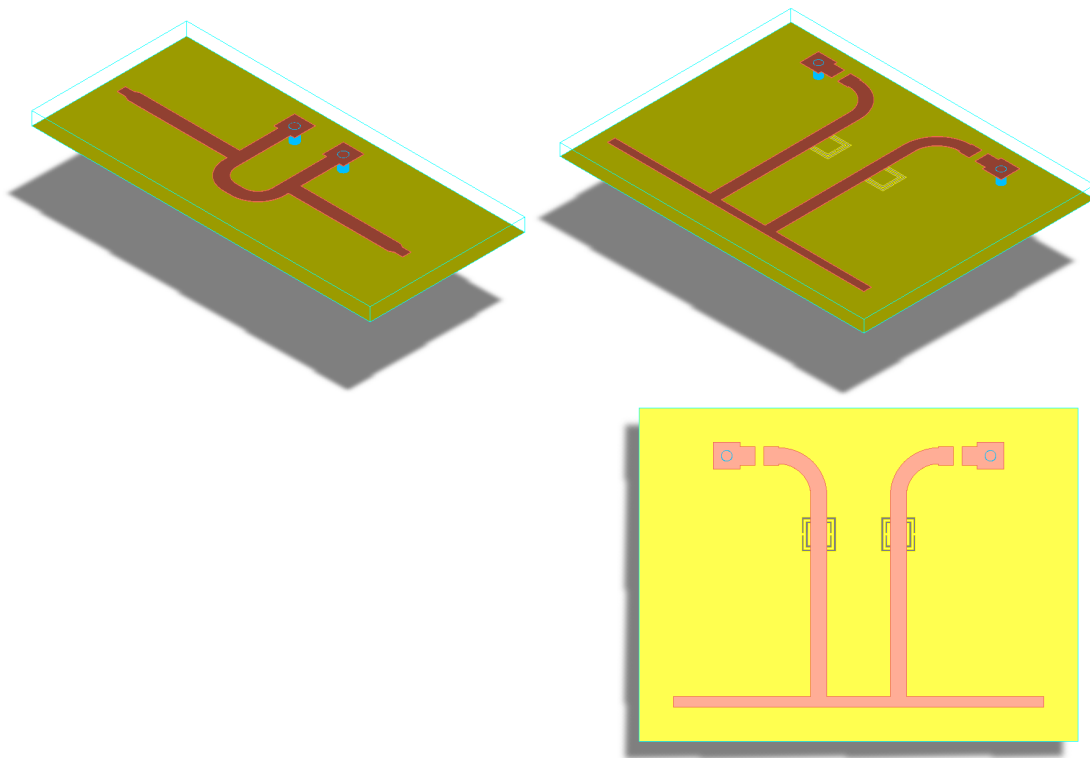

Fig.30. Close-up view of the 2-push resonators.

5 Simulation of Circuits

Undesired oscillation modes are not uncommon in coupled oscillators systems (see an example in Fig.46 of section 5.2.3.1). We have tried to dismiss their effects by approaching, as much as possible, the final designs in Fig.29 to the initial basic designs in Fig.25 and Fig.27; which showed a stable ODD mode according to the Time Domain simulations. A comparison between the real and imaginary parts of the oscillator admittance for the ideal and lossy-dispersive line model designs is presented in Fig.31; it corresponds to the CSRR resonator 2-push oscillator. A similar degree of coincidence is achieved for the stub resonator structure.

With these results it is expected that the ODD mode oscillation will also be observed from the circuits in Fig.29 which can not be efficiently and accurately simulated in Time Domain, due to the transmission line models used and the presence of discrete components defined in Frequency Domain. In fact, as the time step used in the previous results was $T_s = 0.005$ ns, the transient simulator needs to characterize the circuit elements to $F_{max} = 0.5/T_s = 100$ GHz, where frequency information for the models is not available or not accurate. Also, due to the presence of RF grounding capacitors in the bias networks, very long integration times are required to find the steady state response.
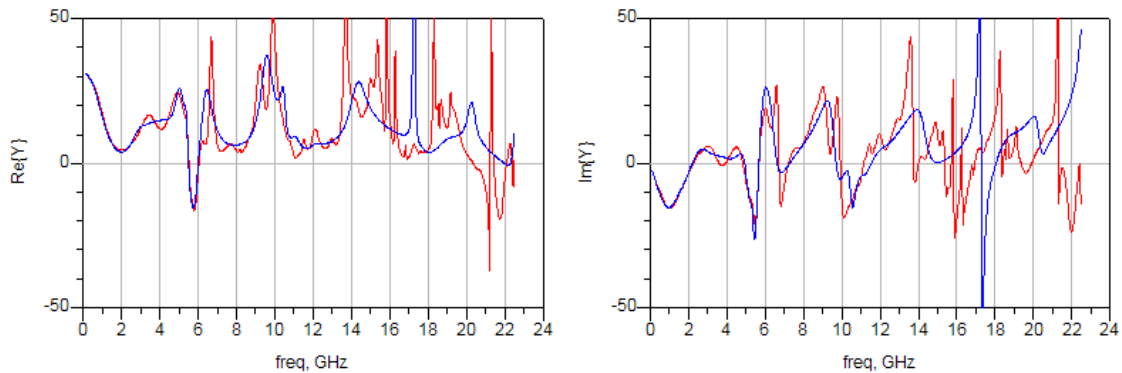
Fig.31.   Comparison between the real and imaginary parts of the CSRR resonator oscillator admittance from the ideal (blue) and lossy-dispersive (red) line model designs.

All the circuits with symmetry, such as N-push oscillators, have coexisting oscillation modes; EVEN and ODD modes are both mathematically possible, but they don't necessarily show up simultaneously in practice. A correct analysis of such circuit topologies requires the excitation of these modes, to determine parameters such as the oscillating frequency and output level. Additionally each steady-state solution must be analyzed to determine its stability under natural small signal perturbations affecting every real system. This is done through small signal perturbation and pole-zero identification techniques.

The excitation of different modes in nonlinear regime is performed by means of non perturbing large signal probes added to the circuit; this is called the Auxiliary Generator technique and it is explained in section 5.1. The stability of the different solutions is performed by a perturbation analysis of the nonlinear regimes with small signal probes and pole-zero identification of the transfer functions obtained from this analysis; it is explained in section 5.2.

5.1 Oscillator Analysis with the Auxiliary Generator Technique

In contrast to forced circuits, where the fundamental frequency ω_o of the solution is set by an external source. In autonomous circuits the solution frequency depends on the values of the circuit elements, bias sources, and other parameters. Due to this fact, the oscillation frequency is an unknown to be determined [2].

By introducing properly chosen probes into a nonlinear circuit, autonomous as well as synchronization (phase-locked) regimes can be evaluated. In [19] the synchronization phenomenon in injected oscillators and frequency dividers is analyzed in detail by means of the Auxiliary Generator (AG) technique. We have made use of this same technique to perform the nonlinear simulations of the 2-push behavior (see Fig.32). The Auxiliary Generators were first used in [20], and further improved in [19, 21, 22]. They are currently being applied to the analysis of Periodic and Quasi-Periodic stationary solutions in nonlinear microwave circuits [23].

A probe is an independent voltage[6] source added to the circuit and connected to one of its nodes, which becomes the observation port. Usually a node close to a device nonlinearity is preferred as this provides more analysis sensitivity (the transistor terminals constitute the "sources" of negative resistance), but there is no need to access the intrinsic elements in the device model; this is an advantage because the technique can also be used with "black box" transistor models.

It is a single tone source, so to prevent short circuiting higher harmonics at the node to which it is connected; an ideal filter is inserted between the voltage source and the circuit node, so that the source is disconnected from the node at every frequency, except its fundamental. This process is represented in Fig.32. If the frequency and complex voltage imposed by the Auxiliary Generator, at the connection node, are equal to the fundamental spectral line of an existing solution, no current will flow between the node and source, and this is equivalent to the source being disconnected from the circuit.
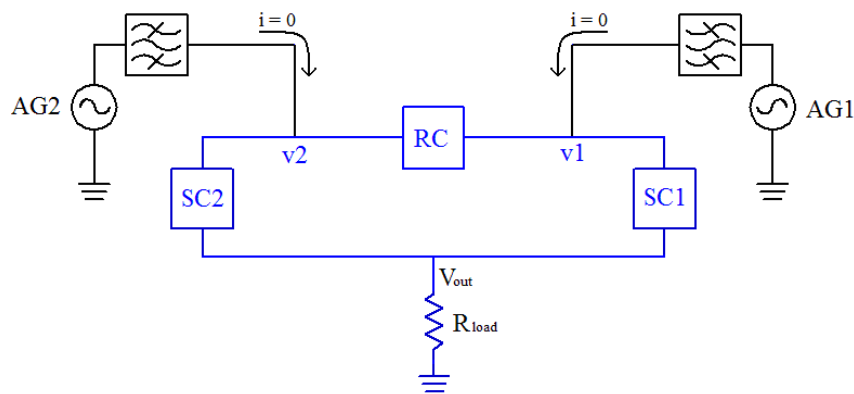

Fig.32.   Determination of the nonlinear oscillatory regime in the 2-push architectures with the Auxiliary Generator technique. (SC = sub-oscillator, RC = resonator circuit, AG = auxiliary generator). The non perturbing condition on the externally added generators (AG1, AG2) imposes *i = 0* when a solution is reached.

---

[6] It can be also a current source.

In order to perform an optimization on the frequency f_{AG} and complex voltage V_{AG} of the Auxiliary Generator, we must impose a non perturbation condition, expressed as:

$$(6) \quad Y_S = \frac{I_{AG}}{V_{AG}} = 0 + j \cdot 0$$

By means of the Auxiliary Generator, it is possible to search for nonlinear solutions at different frequencies with the aid of the Harmonic Balance algorithm, because HB by itself does not changes the frequency of a solution; it only solves for the *Kirchoff*'s laws in a circuit and optimizes the amplitude and phase of the harmonics until a solution is reached. HB always starts from an initial solution based on the signal generators (when they exist). A short note further clarifies this at the end of the section.

By adding external probes into a nonlinear autonomous circuit it is possible to perform an optimization process on variables, such as amplitude, phase, or frequency, in order to satisfy the non perturbing equation (6) and find new solutions. Including the node voltage in the denominator of (6) prevents HB from converging towards the trivial *dc* solution ($V_{AG} = 0$).

Harmonic Balance is well suited for the optimization of non linear tuned circuits, but because the type of response to which HB converges is imposed by the signal generators present in the circuit description, it will find no solution for free running oscillators other than *dc*. In order to explore other solutions, external elements must be added; some examples are the OSCAPROBE used for oscillator analysis in AWR/Microwave Office or the OscPort used in ADS. They can find oscillatory solutions in autonomous circuits, but actual simulations using these special devices are limited to only one probe/port per circuit and they are not compatible with the presence of other signal generators. Also they cannot be used to impose a particular oscillating frequency by optimizing other variables in the system [24].

The Auxiliary Generator works on a similar manner, but it allows for much greater flexibility because any one of its three parameters (Amplitude, Frequency and Phase) can be fixed while the two others are optimized, and it can be applied to autonomous as well as forced circuits.

Using Auxiliary Generators offers many advantages in nonlinear Harmonic Balance simulations:

- Having access to the three AG parameters allows for the optimization of nonlinear circuits in order to produce a particular desired solution, such as damping unwanted oscillations in amplifiers, increasing the locking bandwidth in injected oscillators, or fixing a particular frequency in a free running oscillator.

- The probe can be set to a free frequency (to search for autonomous oscillations inside the circuit) or to the same frequency as the input, or a sub-harmonic of it, in order to search for synchronous solutions.

- When performing a parametric sweep (frequency, power, control voltage, component value ...) we sometimes observe jumps in the response, no matter

how fine we set the sweep step. This is a common phenomenon associated with the existence of multi-valued sections[7] in a curve which lead to infinite slopes at some point during the sweep, and can not be solved by the Newton-Raphson convergence algorithm used by Harmonic Balance. With the aid of an Auxiliary Generator and thanks to its flexibility in using any sweep parameter, we can perform a *parameter switching* and change the sweeping parameter to avoid the infinite slope. Curve sections that are hidden by normal HB sweeps can be reproduced by this method.

According to the test bench of Fig.32, we now proceed to search for even and odd mode solutions in the circuits of Fig.29 by optimizing the parameters in the auxiliary generators, which excite the desired solutions in the two sub-oscillators.

Each auxiliary generator is a single tone voltage source characterized by three parameters; its frequency and the complex voltage (f_{AG}, V_{AG}, Φ_{AG}), so we have six unknowns. By imposing the non perturbing condition (6) at both generators, four equations are obtained, which set a zero target value on the real and imaginary parts of the complex admittances seen by each generator. Now we need two more conditions in order to have an independent set of equations.

> ➢ As the sub-oscillators are coupled together we assume that they will synchronize shortly after switch on, and so the system will freely oscillate at a unique frequency f_o, which corresponds to the fundamental or first harmonic of the output voltage. Then **$f_{AG1} = f_{AG2} = f_o$**.

> ➢ The second condition comes from the phase relationship between the voltage signals from the two sub-oscillators, $\Delta\Phi$; that we set to 0º and 180º for the even and odd oscillation modes respectively. Thus we can fix **$\Phi_{AG1} = 0^o$** and **$\Phi_{AG2} = \Delta\Phi$**, because the phase reference is undefined in autonomous circuits and thus the particular values of Φ_{AG1} and Φ_{AG2} are irrelevant; only their phase difference makes sense under synchronization operation.

We then perform a *Gradient* optimization on the three variables V_{AG1}, V_{AG2} and f_o, until a sufficiently low value of the *error function* is reached. The nonlinear simulations are performed with the Harmonic Balance algorithm.
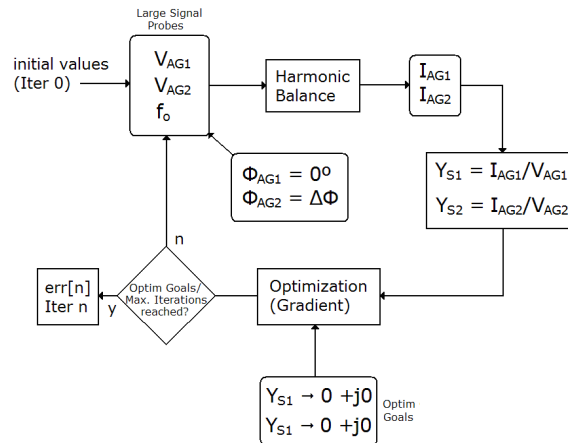

Fig.33.   Flow chart of the optimization process in the search for nonlinear solutions of the 2-push structures

---

[7] Multi-valued sections are those having more than value for the same input parameter in a curve.

Fig.33 shows a flow chart of the optimization process; the frequency f_o is optimized to find the oscillatory solution in the system that satisfies a given phase condition between sub-oscillators. Fig.34 to Fig.38 show the simulation results.
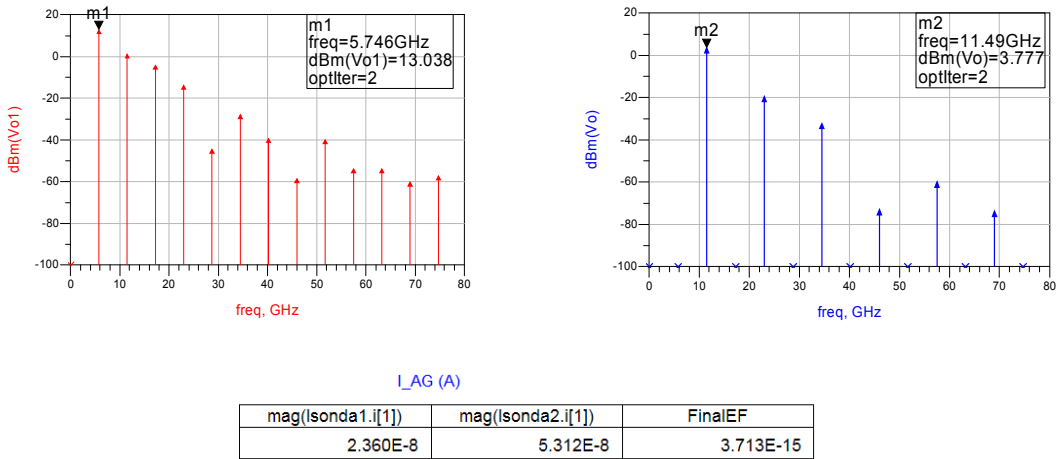
I_AG (A)

mag(Isonda1.i[1])	mag(Isonda2.i[1])	FinalEF
2.360E-8	5.312E-8	3.713E-15

Fig.34.   Odd mode solution for the 2-push structure with CSRR based resonator

I_AG (A)

mag(Isonda1.i[1])	mag(Isonda2.i[1])	FinalEF
1.256E-7	1.227E-7	3.374E-14

Fig.35.   Even mode solution for the 2-push structure with CSRR based resonator

I_AG (A)

mag(Isonda1.i[1])	mag(Isonda2.i[1])	FinalEF
4.744E-8	4.744E-8	1.568E-15

Fig.36.   Odd mode solution for the 2-push structure with short circuited stubs resonator
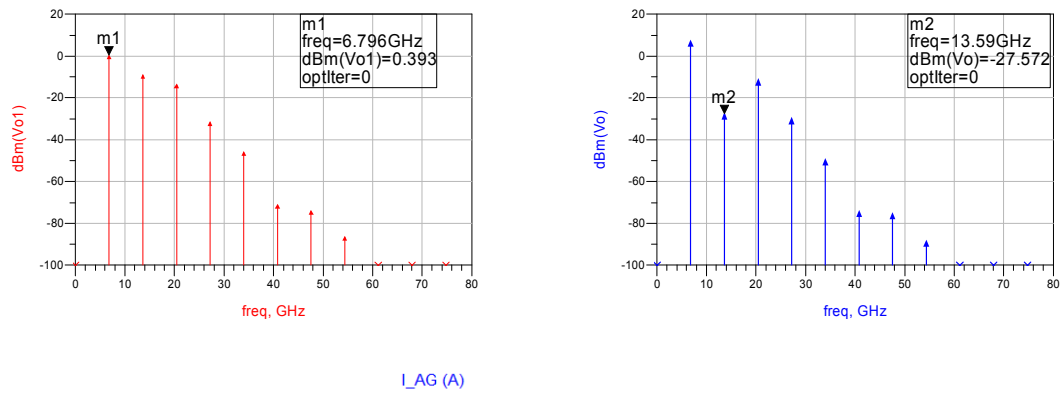
mag(Isonda1.i[1])	mag(Isonda2.i[1])	FinalEF
1.051E-4	1.051E-4	2.270E-7

Fig.37. Even mode solution for the 2-push structure with short circuited stubs resonator. Convergence error is not low enough to guarantee that this is a solution (AG currents can not be neglected)

mag(Isonda1.i[1])	mag(Isonda2.i[1])	FinalEF
1.274E-6	1.810E-6	1.362E-12

Fig.38. Another undesired even mode solution for the 2-push structure with short circuited stubs resonator
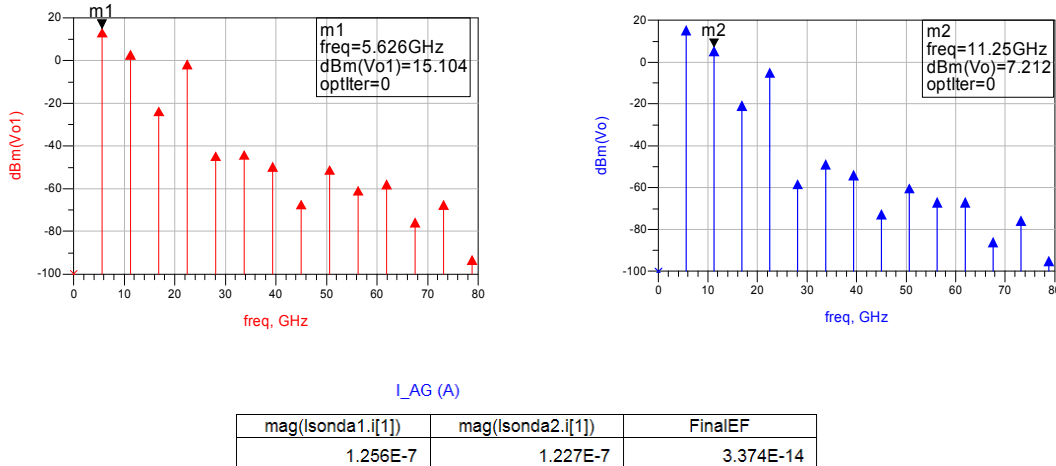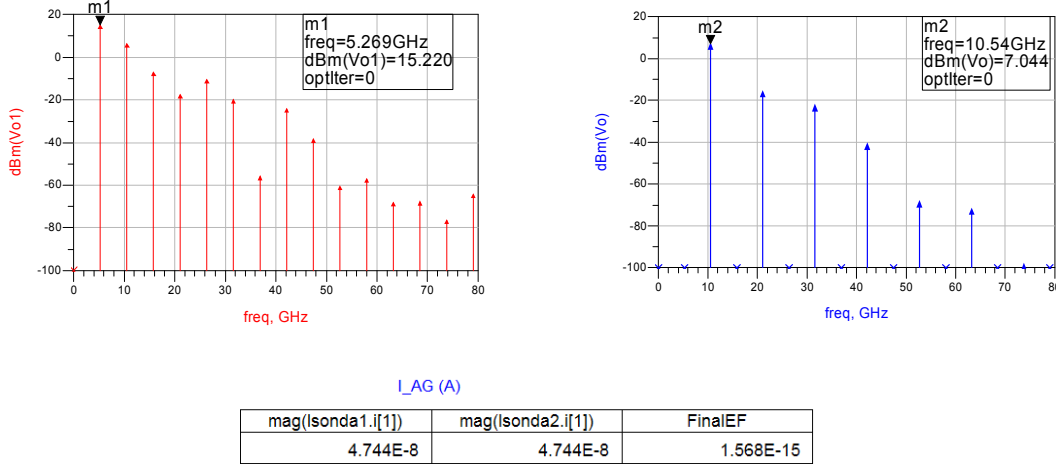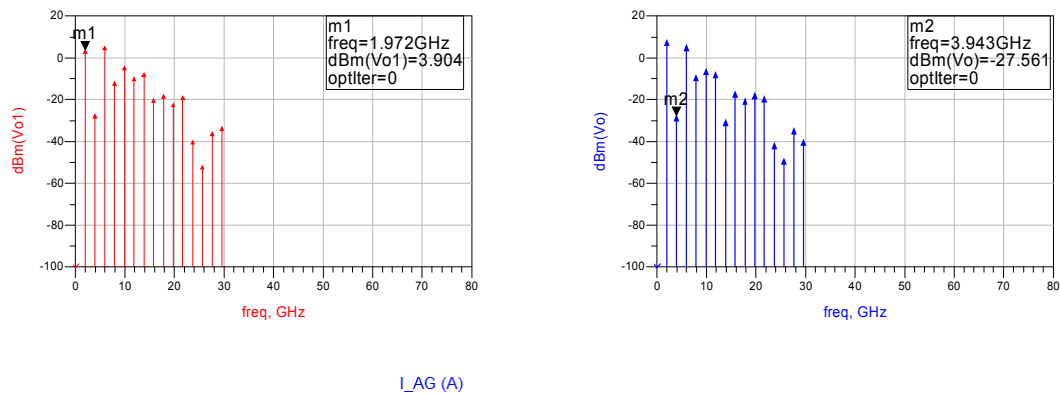
A total of five modes have been found; Two desired odd modes and three undesired even modes. No convergence was reached at other explored frequencies in odd or even phase modes.

A short note about Harmonic Balance [24]

The HB algorithm is a frequency domain method; it basically solves for the *Kirchoff*'s laws in a circuit, creating a set of nonlinear equations and imposing an initial value to the harmonics of the node voltages or branch currents based on the input or internal generators available in the circuit description. That initial value is usually not a solution to the set of equations and it results an error voltage (or current) associated to it. A *Newton-Raphson* convergence method is then applied to minimize that error vector by optimizing the amplitude and phase of the initial solution harmonics, but <u>not</u> their frequency!

Thus in no way we can reproduce an oscillation from an autonomous circuit (without input signal generators) or sub-harmonic and non-harmonically related frequencies from a forced circuit such as an injected oscillator or an amplifier. No fundamental frequency will show up from an HB analysis which is not present in the internal or external signal generators used in the non linear circuit's description unless we use external probes.

5.2 Stability Analysis

Oscillator stability can mean many different things, it can mean that the oscillator stays at one frequency without jumping to another as temperature changes (one type of perturbation), it can mean stability in the short term sense of low-phase noise, or it can mean stability in the long-term sense of minimal change in the oscillation frequency over minutes and days. In this case, we refer to the stability of an oscillator in the sense that it has a stable frequency and does not jump to another frequency if perturbed.

It is worth clarifying that we will refer to the stability of particular solutions and not of the circuits; a well designed oscillator has an unstable DC output and a stable oscillation. Unstable solutions do not withstand the natural fluctuations produced by the noise sources present in real circuits, as opposed to stable (robust) solutions which continuously recover from small signal perturbations [2].

In general, current stability analysis is characterized by linear approaches applied to linear (or linearized) systems. The simplest form of linearization calculates small-signal approximations to the nonlinear behavior about previously determined quiescent or DC operating points, which are usually assumed to remain static in nature.

Two basic and commonly used stability criterions are:

Linville or Rollett stability criteria — Scattering parameter-based approach. Determines unconditional and conditional (potentially unstable) stability for a 2-port, based on the real part of impedances presented to its input/output ports.

Kurokawa oscillation and stability criteria — Impedance-based approach. Oscillatory condition based on the presence of negative resistance (in a linearized network) that will cause oscillations to arise.

Kurokawa divides a linearized network into two sub-networks (Fig.39) at an appropriate port and establishes his oscillation condition (7):

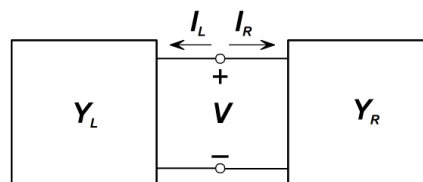$$(7) \quad Y_{tot} = Y_L + Y_R = 0$$

Fig.39.   Linearized network to determine the stability of oscillations by Kurokawa. In general L and R could be any admittance function and stand for Left/Right side. But in the Kurokawa analysis they usually refer to Linear and Resistive (non linear) admittances.

For a steady-state oscillation to be stable, the circuit must return to it exponentially under any small perturbation. In the stability analysis proposed by Kurokawa in 1969 [25] a small perturbation is applied which takes the circuit out of its steady state and a transient is generated. As a consequence of this small perturbation, small variations are assumed in the oscillation amplitude and frequency. Kurokawa makes use of impedance functions in the cited article. We reproduce here the result from an equivalent derivation by Suarez [2] based on admittance functions. The linearization of the total admittance function $Y_{tot}(V, \omega)$ about the free-running solution fulfilling $Y_{tot}(V_o, \omega_o) = 0$ leads to the criterion for a stable oscillation as:

$$(8) \quad \frac{\partial \operatorname{Re}\{Y_{tot}\}}{\partial V} \cdot \frac{\partial \operatorname{Im}\{Y_{tot}\}}{\partial \omega} - \frac{\partial \operatorname{Re}\{Y_{tot}\}}{\partial \omega} \cdot \frac{\partial \operatorname{Im}\{Y_{tot}\}}{\partial V} > 0$$

This condition was first derived by Loeb in 1953, who used equivalent linearization to extend Nyquist's linear stability method to non linear feedback systems. Initially the equation was written in terms of the linearized loop gain *GH*. A graphical representation of this criterion is due to Slater, who focused his analysis on two-terminal devices, from studies on magnetrons at Bell Labs during the 1940s, and considered the device and load as described by impedance functions *Z(A)* and *Z(ω)*, with *A* being the current amplitude [11].

Thanks to the interpretations of (8) by Loeb and Slater, several problems found in oscillators, not explained by previous simple treatments, could be understood; in particular the hysteresis in the tuning characteristic and frequency jumping. Fig.40 represents the real and imaginary parts of the active device and load lines, $\hat{Z}(A)$ and $\tilde{Z}(\omega)$, which respectively change with the current amplitude, *A* and the radian frequency, ω. The intersection points $-\hat{Z}(A) = \tilde{Z}(\omega)$ are mathematical solutions for the condition $Z_{tot} = 0$ and thus, possible points of oscillation. But only those points with intersection angles between 0° and 180° correspond to stable solutions.
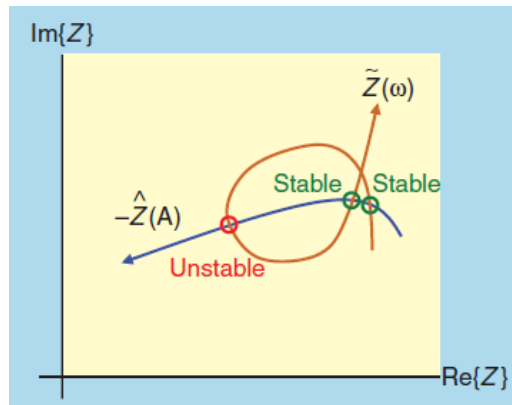

Fig.40.   Impedance plane plot of device and load lines. Stable and unstable operating points are indicated. This figure is from [11].

It is easily seen from this plot that, starting from one of the stable points as the initial solution then, in the event of an upward/downward change in one of the load

lines, $-\hat{Z}(A)$ or $\tilde{Z}(\omega)$, the intersection angles and the frequencies of the intersection would change smoothly until the oscillation became unstable and was forced to jump to another stable intersection or die out. Reversing the process from the new stable point we would have a similar behaviour but with the jump taking place at a different frequency, which explains the hysteresis phenomena. Also, in the situation where something perturbed the oscillator to the unstable intersection, the frequency would then jump to one of the stable intersections which would not necessarily be the previous one.

Kurokawa discovered that the degree of stability of an oscillator (the nearness of the intersection angle to 90º) had a direct effect on oscillator noise, in that phase noise is minimized when the intersections between the device and load lines are perpendicular. This explained the significant variations of phase noise observed within the tuning range, often experiencing a rapid increase as a frequency discontinuity point was approached.

In Kurokawa's notation the total admittance is expressed in terms of the device and load admittances, Y_R and Y_L respectively [26]. Y_R is mainly dependent on the amplitude V of the terminal voltage, because the nonlinearities responsible for the free-running oscillation are usually voltage-controlled current sources. In contrast, Y_L is a function of the radian frequency ω, so its dependence on the oscillation amplitude usually has little influence. With these assumptions the real part of the total admittance, $Re\{Y_{tot}\}$, usually has small frequency dependence because the dependence comes from the reactive elements, and the imaginary part, $Im\{Y_{tot}\}$, usually has small amplitude dependence, because it is contributed primarily by the linear elements, thus the term $\partial Re\{Y_{tot}\}/\partial\omega \cdot \partial Im\{Y_{tot}\}/\partial V$ is often small compared to the first term in (8). Also, due to the physical reduction in negative resistance with signal amplitude, the factor $\partial Re\{Y_{tot}\}/\partial V$ will generally have a positive sign, thus a positive slope on the imaginary part, $\partial Im\{Y_{tot}\}/\partial\omega > 0$, will facilitate the oscillation stability [2].

In order to guarantee the start-up of oscillations and the establishment of an oscillatory solution in the system, we have optimized the 2-push structures to follow the three Kurokawa conditions at *dc* (small signal analysis), expressed as:

$$(9) \qquad Re\{Y_{tot}\}\big|_{\omega_0} < 0$$

$$(10) \qquad Im\{Y_{tot}\}\big|_{\omega_0} = 0$$

$$(11) \qquad \frac{\partial Im\{Y_{tot}\}}{\partial\omega}\bigg|_{\omega_0} > 0$$

It contains the condition for presence of negative resistance (9) that causes oscillations to arise, due to the excess of energy, and the resonance condition at the oscillation frequency desired (10) with positive slope on the imaginary part (11), which facilitates a stable steady-state oscillation at about ω_0 according to (8).

These conditions are also associated to the instability of the *dc* solution as they help synthesize a pair of complex-conjugate poles in the right hand plane -RHP. This pair of

unstable poles shall give rise to an oscillatory transient of growing amplitude at the desired oscillation frequency ω_0.

To understand the relationship between the three Kurokawa conditions and the poles of the *dc* solution I refer to section 1.3.3 in [2], where it is shown that the phase evolution of a transfer function whose dominant contribution comes from a pair of complex-conjugate poles in RHP, has a positive slope at the resonance frequency.

When performing admittance analysis, impedance transfer functions $Z(s)$ relate the output voltage at the observation port $V(s)$, to the small-signal input current source $I_{in}(s)$ in parallel with it. These impedance functions are the inverse of the total admittance analyzed, $Z(s) = 1/Y_{tot}(s)$, and then their phase terms are related by $\tan(\varphi_Z) = -\,\mathrm{Im}\{Y_{tot}\}/\mathrm{Re}\{Y_{tot}\}$.

By assuming a small frequency variation of $\mathrm{Re}\{Y_{tot}\}$, and $\mathrm{Re}\{Y_{tot}\} < 0$; the condition $\partial\mathrm{Im}\{Y_{tot}\}/\partial\omega > 0$ will be sufficient to guarantee a positive slope of the phase associated with $Z(\omega)$, $d\varphi/d\omega > 0$, and the roots of the characteristic function of the system will be in the RHP, leading to an unstable *dc* solution. The instability of the *dc* solution guarantees that the system will not come back to this state once the transient regime caused by the perturbation has vanished.

The net negative conductance (9) will become zero as the steady state is reached because the negative conductance contributed by the active element decreases with voltage amplitude. At steady-state the oscillatory condition $Y_{tot}\,(V_o,\ \omega_{osc}) = 0$ holds, indicating zero net susceptance at resonance and zero net conductance at equilibrium between average power delivered and consumed.

For a rigorous determination of the *dc* solution poles, pole–zero identification techniques should be applied to the closed-loop transfer function $Z(\omega)$ [2].

5.2.1 Start-up conditions in N-push structures

In a typical N-push structure identical sub-oscillators are interconnected through a passive coupling network, which may also be used to combine the desired N^{th} harmonic at the output port, as is the case with the 2-push oscillators in the present study.

In general in N-push structures it is assumed that the passive coupling network presents the same load admittance at each one of its interface ports with the sub-oscillators, and that they all contribute with the same voltage amplitude, keeping a $2\pi/N$ phase shift between consecutive ports at the desired N-push oscillation mode.

The relationships between currents and voltages at the N interface ports between coupling network and sub-oscillators are determined by the vector equation

$$(12)\quad \overline{I} = [Y_L]\cdot\overline{V} = \lambda\cdot\overline{V}$$

where $\overline{I}$ and $\overline{V}$ are respectively the vectors of phasor currents and node voltages at the interface ports, $[Y_L]$ is the frequency dependent linear admittance matrix of the passive coupling network. The condition for equal load admittance at the N ports is represented by the complex scalar $\lambda = I_k / V_k$, with $k = 1..N$. From linear algebra, λ is one of the N eigenvalues of the linear admittance matrix $[Y_L]$ and $\overline{V}$ its corresponding eigenvector. Thus, the passive coupling network will present the same load admittance at its input ports when it is excited with an eigenvector of its admittance matrix [2]. Every eigenvector represents a mode of operation in the system.

We are considering linear, symmetric and passive coupling networks which in principle are reciprocal, provided they are made from isotropic materials. Reciprocity shall be considered carefully when working with split rings resonators and coupled split rings resonators, as these particles are known to have different electrical properties depending on their direction of polarization [14]. In the particular case of the planar coupling networks developed in this work, the signals propagate only in one direction through the metamaterial resonators and reciprocity can be assumed.

The vector equation (12) contains N independent conditions and N+1 unknowns (the N components of $\overline{V}$ plus λ), so it has an infinite number of solutions. By imposing the conditions for equal amplitude terms in a symmetrical and reciprocal coupling network with $2\pi/N$ phase shift between consecutive ports, we easily find (see A I) that the linear admittance matrix $[Y_L]$ for a 2-push has two eigenvalues λ_0, λ_1 corresponding to the oscillation modes 0° and 180°, which are expressed as:

$$(13) \quad \begin{aligned} \lambda_0 &= Y_{11} + Y_{12} \\ \lambda_1 &= Y_{11} - Y_{12} \end{aligned}$$

$$(14) \quad \begin{aligned} \overline{V_0} &= A_0 \cdot (1 \quad 1)^T \\ \overline{V_1} &= A_1 \cdot (1 \quad -1)^T \end{aligned}$$

Where (14) are the eigenvectors corresponding to the in-phase (n=0, even) and out-of-phase (n=1, odd) oscillation modes. The $[Y_L]$ matrix is frequency dependent and so are its eigenvalues and eigenvectors. A_n is the amplitude of the "n" oscillation mode. In general, the potential number of modes of operation is at least equal to the number of sub-circuits used in the system [2].

The possible start-up of each mode is analyzed by checking the conditions (9)-(11) with $Y_{tot} = \lambda_n + Y_D(0)$, where $Y_D(0)$ is the nonlinear admittance presented by the active sub-circuits at $A_n \approx 0$.

Both λ_n and $Y_D(A)$ are frequency dependent, so the N possible modes will have different frequencies, in general. For a given circuit, not all of the possible modes will necessarily exist. The oscillation conditions (9)-(11) may be fulfilled for none, one, or several modes at different frequencies. In fact, the objective of the small signal stability analysis is to prevent the start-up of any undesired oscillation mode from the dc regime.

In general other solutions may exist with different amplitudes at the different active blocks, even if these blocks are identical. The full system analysis requires an accurate

numerical technique such as harmonic balance with a systematic initialization method (i.e. by means of Auxiliary Generators) to obtain the various coexisting solutions, and a complementary stability analysis of each of these solutions. The additional application of pole–zero identification (or other accurate stability analysis method) is advisable [2].

5.2.2 Small Signal Admittance analysis in DC and pole-zero identification

In order to analyze the start-up conditions for each of the two possible 2-push modes considered in (13)-(14) we have implemented two different simulations of admittance in the 2-push circuits, as shown in Fig.41; small signal current sources are connected at the nodes of the resonator circuit in single, common and differential modes.

Each mode is analyzed by checking the conditions (9)-(11) with $Y_{tot} = \lambda_n + Y_D(0)$, where $Y_D(0)$ is the nonlinear admittance presented by the active sub-circuits at $A_n \approx 0$. The results of this analysis are presented in Fig.42 and Fig.43.
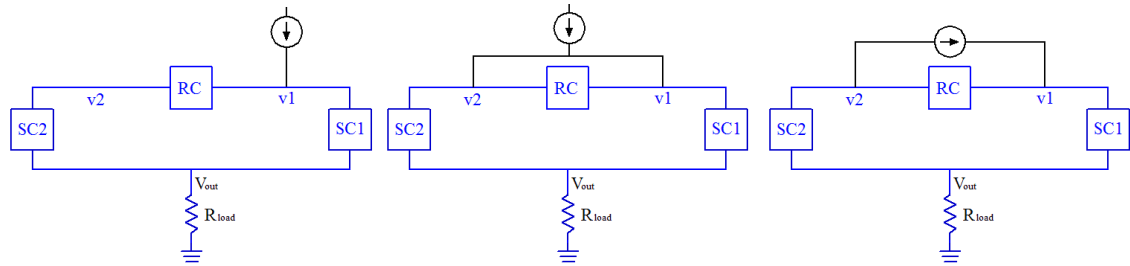

Fig.41.   Determination of the small signal admittance at a Resonator circuit node in single mode (left), common mode (center) and differential mode (right)

From a small signal analysis of the circuits in Fig.41 we have defined the common and differential mode admittances as follows:

$$(15) \quad Y_{cm} = \tfrac{1}{2}\, I_{ss}/v1 = \lambda_0 + Y_D(0)$$
$$(16) \quad Y_{dm} = 2\, I_{ss}/(v1\text{-}v2) = \lambda_1 + Y_D(0)$$

I_{ss} is the small signal current source used for the perturbation of the DC solution. This analysis can indistinctly be performed from a SPAR simulation determining $Y(1,1)$ or from an AC simulation using a linear current source.

No significant differences are observed form the CSRR based 2-push; the single, common and differential mode admittances all show a unique resonance at the frequency of oscillation of the individual oscillators (Fig.42). While in the Short Circuited Stubs structure we appreciate a much clearer resonance around 5.5 GHz in the differential mode admittance plot. As stated in the previous section, a nonlinear analysis is required to find the final oscillations modes; it was found during transient domain simulations, that an oscillation can start in common mode and become differential under large signal operation.
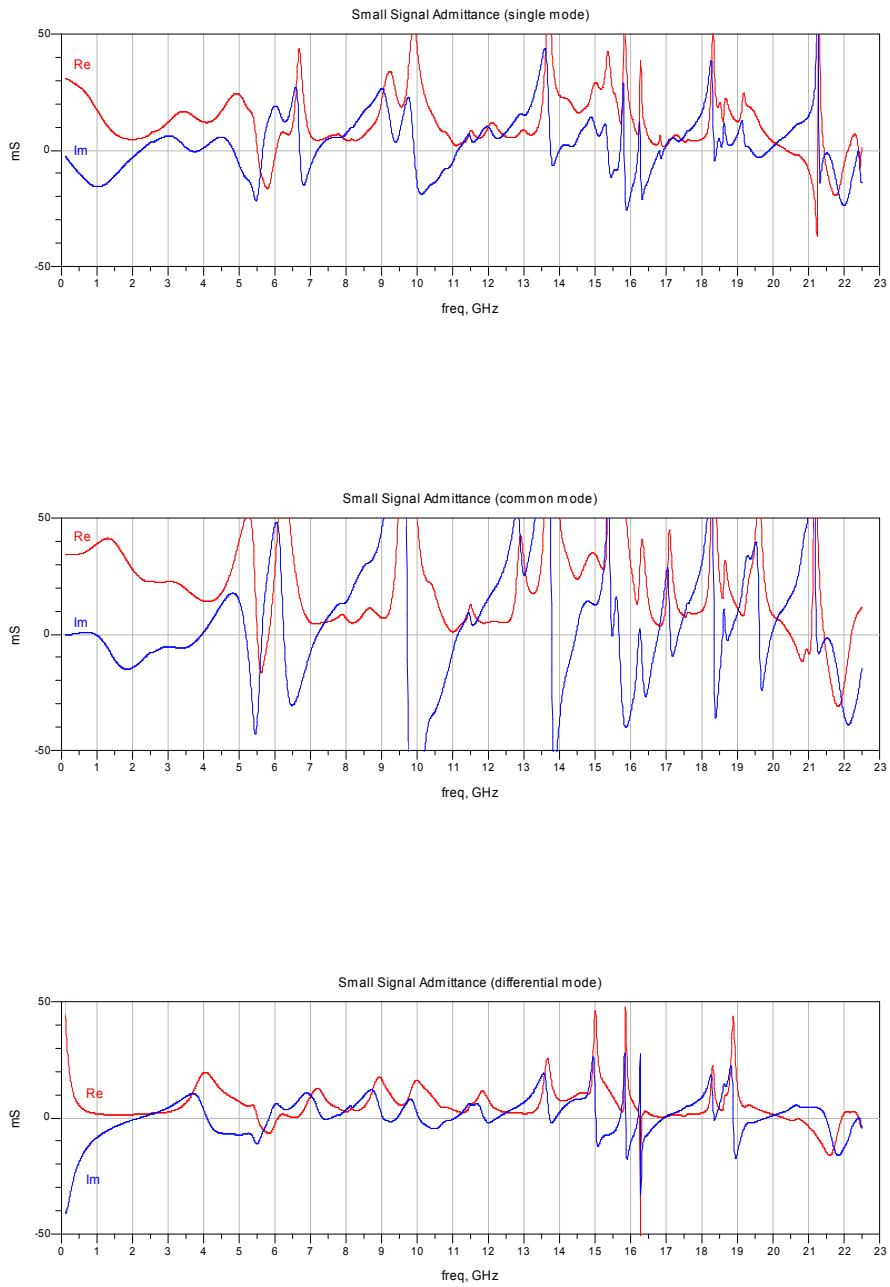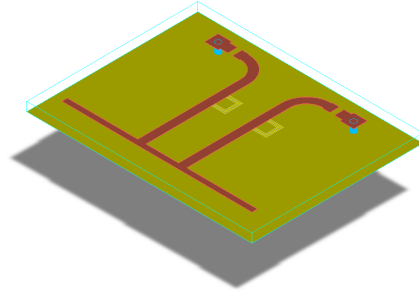
Fig.42.   Analysis of the single, common and differential mode start-up conditions for the CSRR based resonator 2-push
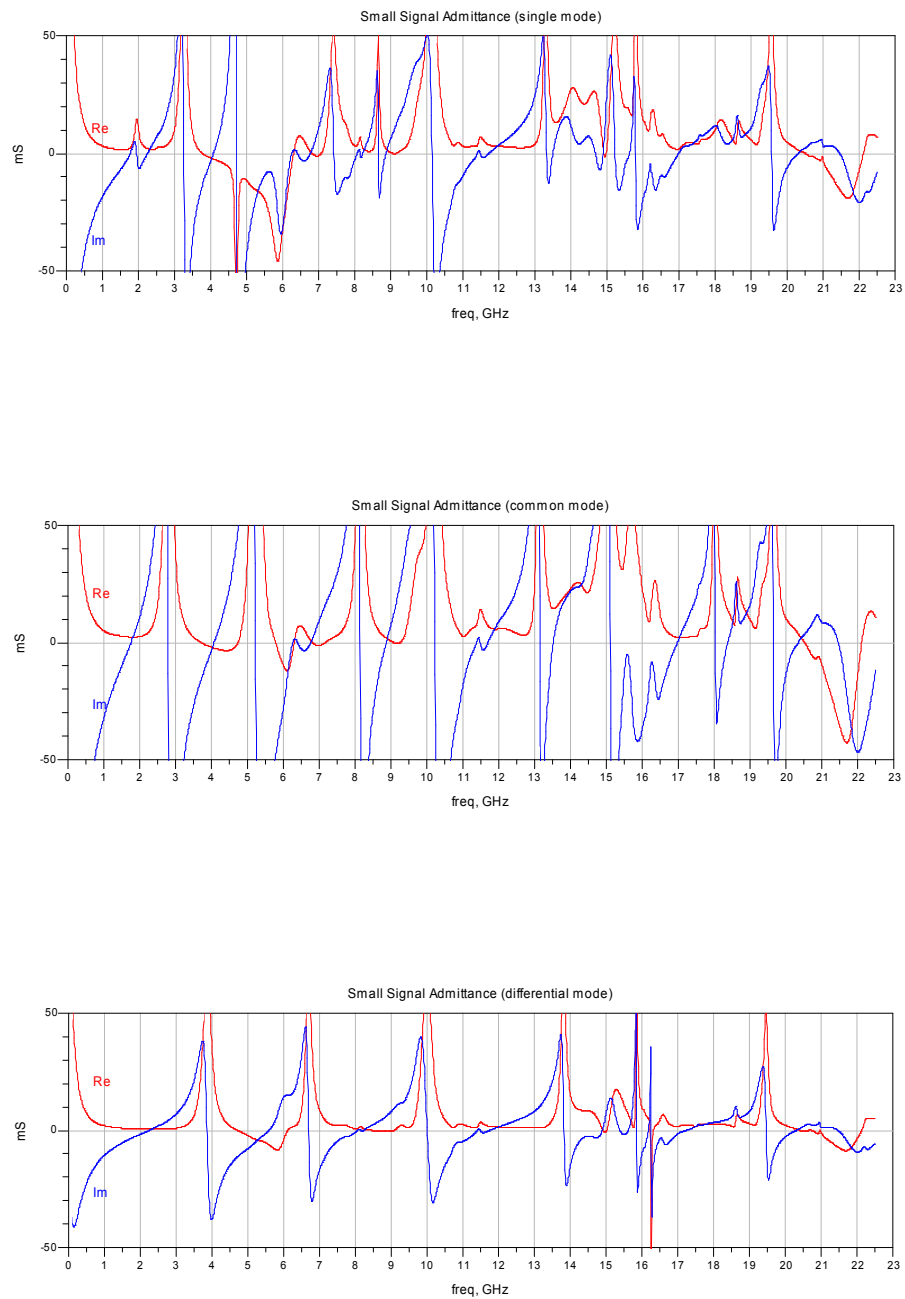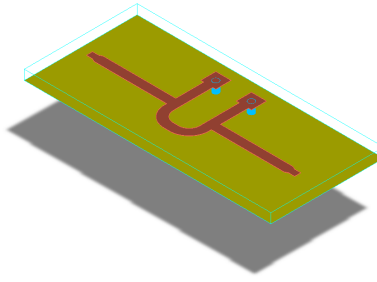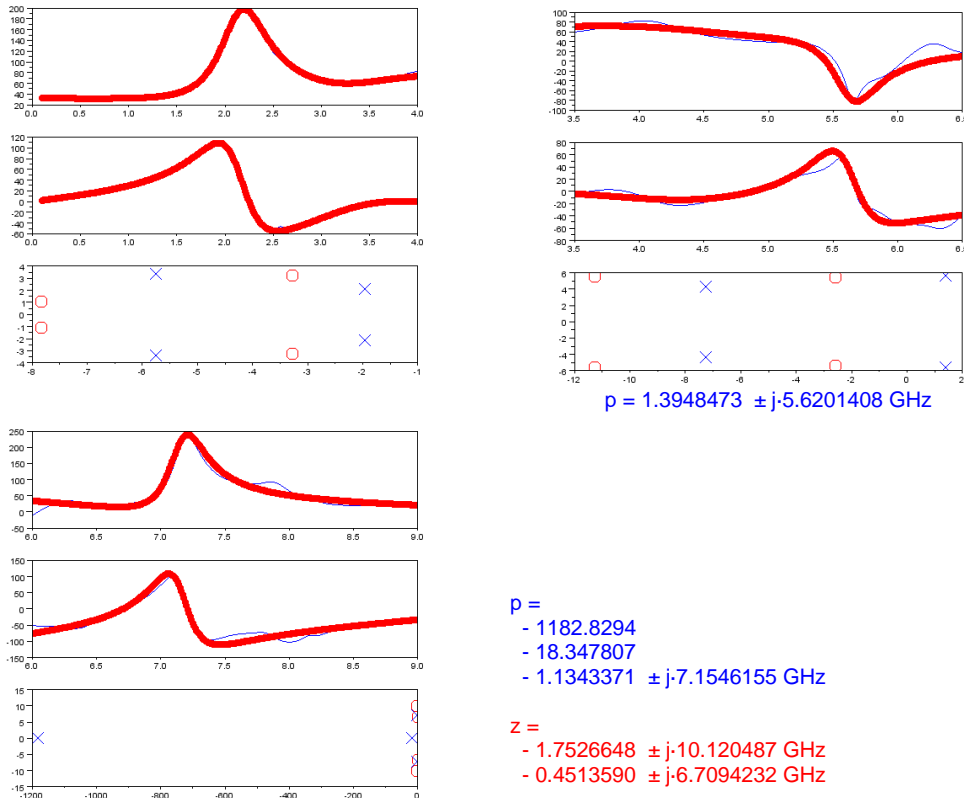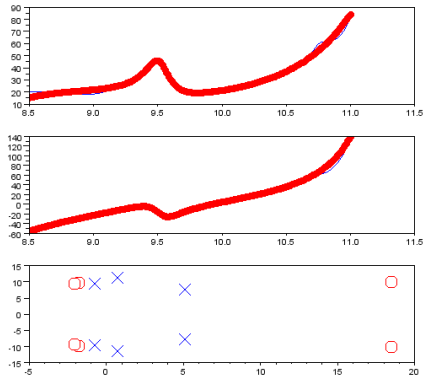
Fig.43.   Analysis of the single, common and differential mode start-up conditions for the short circuited stub resonator 2-push

Next we have performed a pole-zero identification of the transfer function H(s) = $V_n(s)/I_{ss}(s)$ resulting form the small signal perturbation of the DC solution in the CSRR based resonator 2-push (Fig.44). V_n is the voltage measured at the node where the current source I_{ss} is connected. The extraction of H(s) roots is performed at subsections of the active device's frequency band of operation. Only the roots inside the frequency band of the analysis are representative of the stability properties of the solution. An explanation of this method is given in 5.2.3.2 and the flow graph of Fig.47.

Fig.45 shows the identification of a subsection of H(s) with polynomial rational functions of order n=4 (left) and n=6 (right). The main roots are found with a 4th identification order. Higher order identifications usually led to pole-zero cancellations, which makes redundant information.

According to [2] at the initial stage of oscillation start-up the amplitude will grow according to $e^{\sigma t}$ from any small perturbation of the *dc* solution. The σ value is related linearly to Re{Y_{tot}}, in general being more positive for larger negative values of the conductance, which implies a shorter initial transient. The previous reasoning is only valid in the initial stage of the oscillation start-up, where the amplitude is small and its variation can be predicted with circuit linearization about the *dc* solution. Above a certain signal level the real part of the poles exhibits an amplitude dependence σ(V) with a decrease to the value σ = 0 at the steady state.

p = 1.3948473 ± j·5.6201408 GHz

p =
 - 1182.8294
 - 18.347807
 - 1.1343371 ± j·7.1546155 GHz

z =
 - 1.7526648 ± j·10.120487 GHz
 - 0.4513590 ± j·6.7094232 GHz

p =
- 0.7349845 ± j·9.5223329
  0.7210759 ± j·11.355853
  5.0841343 ± j·7.7012645

z =
- 2.0888394 ± j·9.3518913
- 1.7721156 ± j·9.7969146
  18.467009 ± j·9.9996872

p =
- 17.491651 ± j·19.582532
  0.1339147 ± j·21.429304

z =
- 0.1325854 ± j·21.275871
  1.8762718 ± j·21.781985

p =
- 0.0037000 ± j·22.396833
  13.148999 ± j·25.732975

z =
  0.3520361 ± j·22.436482
  1.5936372 ± j·21.963149
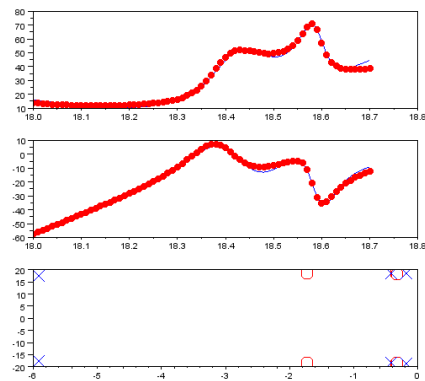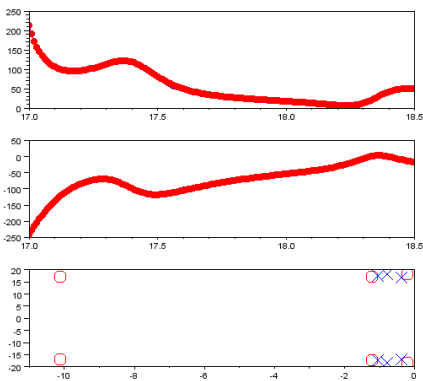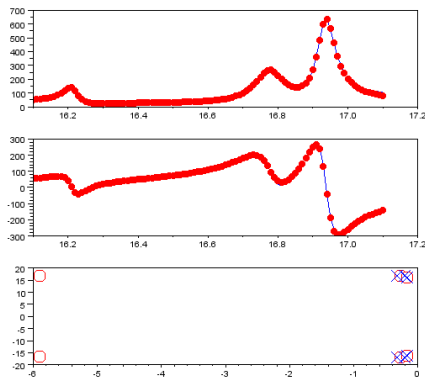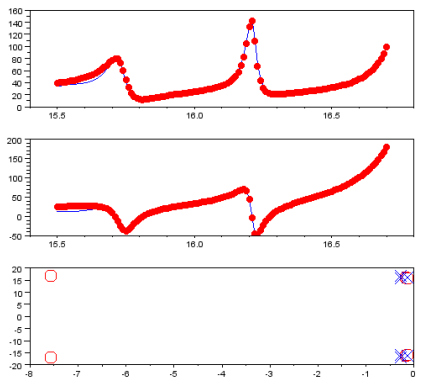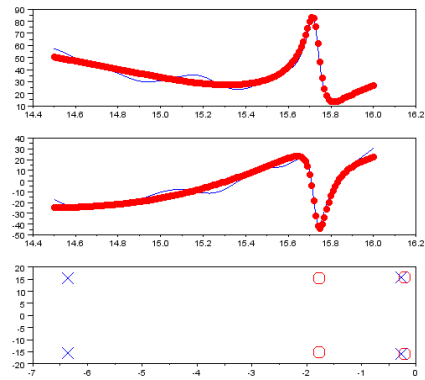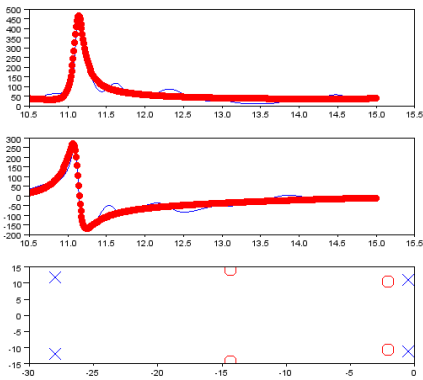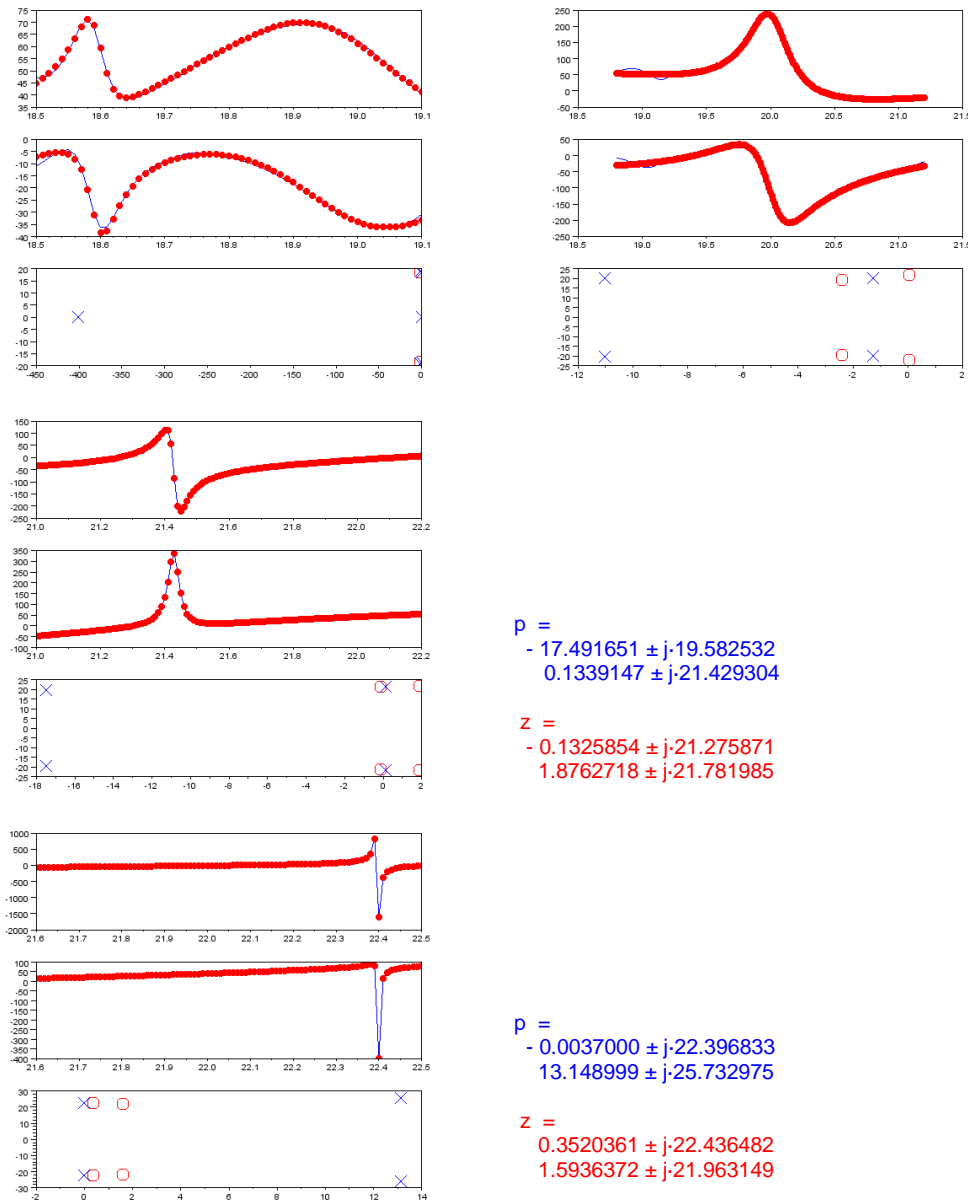
Fig.44.　　　Identification and pole-zero extraction of the transfer function H(s) = V_n(s)/I_{ss}(s) at subsections of the active device's frequency band of operation for the CSRR based resonator 2-push. V_n is the voltage measured at the node where the small signal perturbation current source I_{ss} is connected. This analysis is performed under small signal operation and implements a perturbation of the DC solution. Only roots inside the frequency band of the analysis are representative of the stability properties of the solution.
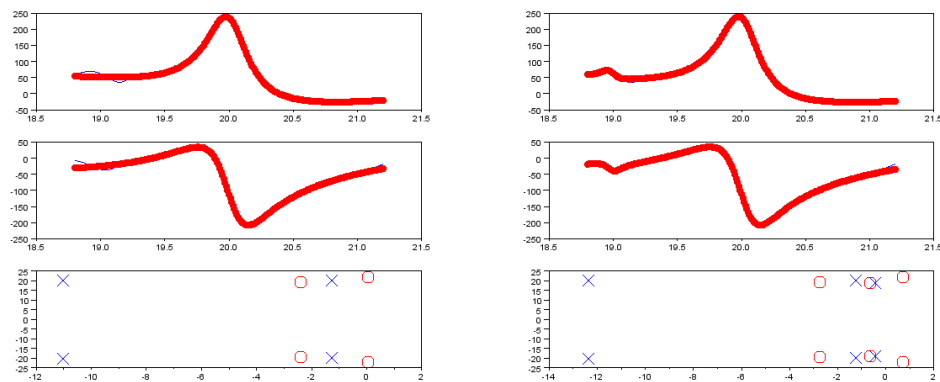
Fig.45.　　　Identification of a subsection of H(s) with polynomial rational functions of order n=4 (left) and n=6 (right). Original data is blue, model function is red. Poles and Zeros of the model function are represented respectively as crosses and circles. The main roots are found with a 4th identification order. Implementing a 6th order produces pole-zero cancellations.

5.2.3 Large Signal Stability Analysis

The small signal admittance analysis based on the Kurokawa conditions (9)-(11) is limited to a narrow band about the resonance frequency ω_0, which shall correspond to the first harmonic component of the steady-state oscillation. But a time-domain simulation would show that depending on the resonator quality factor, the final oscillation frequency ω_{osc} can differ noticeably from the resonance frequency ω_0. This discrepancy is higher for a smaller quality factor Q, due to the lower filtering of the harmonic components $n \cdot \omega_0$ with $n > 1$.

This is due to the effect that the oscillation harmonics have on the nonlinear part of Y_{tot}, which is assumed to be a real conductance in small signal (see Fig.39). The phase relationship between harmonics creates a new phase term in Y_{tot} which depends on the oscillation amplitude V, and influences the new resonance condition $\text{Im}\{Y_R (V_o, \omega_{osc})\} = 0$, at $\omega_{osc} \neq \omega_0$. Therefore, the resonance frequency ω_0 under small-signal conditions will be similar, but generally not equal, to the oscillation frequency ω_{osc}.

The presence of negative resistance can readily result in much more than simple oscillation in nonlinear systems (i.e., quasiperiodic or chaotic behavior), and the assumption of a small frequency variation in (8) is a *quasistatic* approximation that limits the validity of this condition. In practice, the small signal perturbation on a steady state oscillation can have any frequency; for instance, a common instability phenomenon is the onset of a sub-harmonic component at $\omega_o/2$, generated from a low-amplitude perturbation that clearly does not fulfil the *quasistatic* assumption. Despite of this limitation, the stability condition (8) is extremely helpful during the oscillator design stage and provides criteria for *likely* stable behavior from admittance functions accessible to the designer [2].

However, the design procedure should be complemented by a rigorous verification of oscillator stability without limiting assumptions on the frequency shift and taking into account the actual multidimensional nature of the circuit equations [2]. Unstable resonances may be hidden when inspecting the total impedance or admittance from a single observation port, and instabilities may originate when a circuit operates in its non-linear regime, being non detectable with small signal analysis techniques; for instance, a diode or transistor may present negative resistance at a particular signal level.

The approach to stability inspection implemented in this work includes conversion matrix analysis, in which quiescent points are replaced with large-signal time-varying periodic states to which a small signal perturbation is added. By frequency sweeping the perturbing signal (usually a current or voltage source) and simulating its effect on a circuit variable (branch current or node voltage), a transfer function can be obtained which is subject to pole-zero identification to determine the stability properties of the steady-state solution.

5.2.3.1 Nonlinear Dynamic Systems and Simulation Tools

In order to better understand the simulations that we have performed in this work and their results, it is worth reviewing some basic aspects from the nonlinear dynamic

theory of systems that I compiled in [24] and are partly based on notes from the course *Non linear and phase noise analysis in RF & microwave circuit*s in this master, which is given by the Microwave Engineering & Radiocommunications Systems Group, led by Prof. Almudena Suarez at the Univ. of Cantabria.

There are four basic types of stationary solution from a nonlinear system: Continuous (DC), Periodic (fundamental + harmonics), Quasi-Periodic (two or more independent frequencies plus their harmonics and mixing products), and Chaotic (continuous wideband spectrum, non periodic). All of them and even their combinations can appear in the response of a nonlinear system, depending on its parameter settings. Fig.46 shows a sequence with a full set of different responses appearing during the synchronization process of two initially uncoupled oscillators in a same board. This sequence was obtained from a test board designed at an initial phase in this Master.

Due to the manufacturing dispersions single oscillators were not identical and did not oscillate at the same frequency. By adjusting their respective gate bias a sequence of different responses was obtained until synchronization was finally achieved. During this process, the initial Quasi Periodic response gets Chaotic, then Quasi Periodic again and it finally reaches a Periodic synchronous regime.
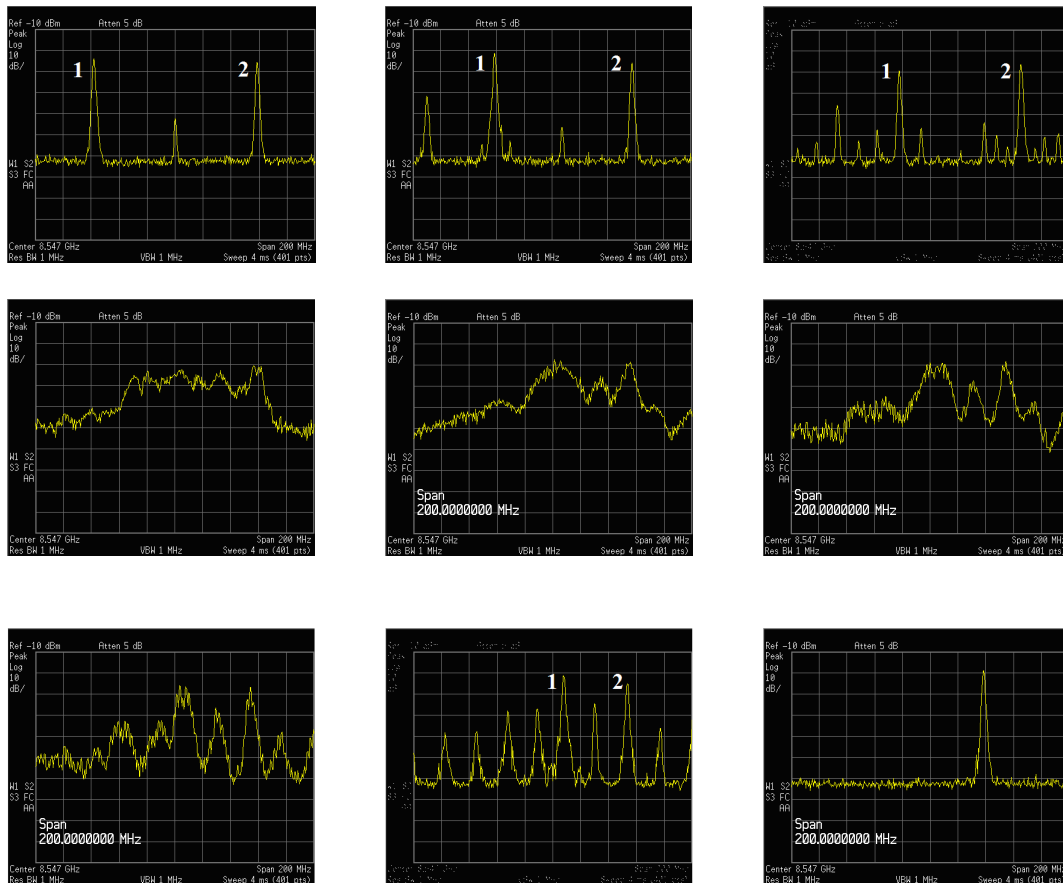
Fig.46.   Evolution of the response from a system of two initially uncoupled oscillators (Osc1 and Osc2) when the Osc1 gate bias is adjusted until both synchronize; Periodic, Quasi-periodic and Chaotic type spectrums are produced. Initially Vgs1 = Vgs2 = -0.8V at "switch ON". It was found that by increasing Vgs1 with respect to Vgs2 frequencies approached each other. Synchronization was achieved at f_o = 8.58 GHz with Vgs1 = -0.51V and Vgs2 = -0.78V.

Every circuit containing inductors, capacitors or transmission line elements is described by ordinary differential equations -ODEs. When non linear elements are also present, the resulting differential equations are non linear.

It is natural and not strange, for a nonlinear circuit to have more than one stationary solution corresponding to the same set of input parameters. Some of these solutions have no physical existence and will not be observable in practice; they are just mathematical solutions to the set of Non Linear Ordinary Differential Equations describing the circuit function. But some other solutions can be physically observable and coexist; showing up one or the other depending on the previous value of the circuit's state variables, such as node voltages and branch currents; they show up with hysteresis.

Non linear differential equations do not have explicit solutions and must be solved through numerical integration methods in time domain. Numerical integration always converges to a unique solution for a given initial condition, provided there are not integration errors caused by a poor time resolution, or bandwidth limited device models. But long transients need usually be simulated before reaching the stationary regime.

Frequency domain methods, such as Harmonic Balance -HB, avoid lengthy transients and converge directly to stationary solutions; but they could be unstable or not be unique, as these methods require for a particular type of solution to be set in advance. When properly used, Harmonic Balance can converge to stationary solutions of the DC, Periodic or Quasi-Periodic type, but can not predict stationary Chaos or give any assurance about the stability (physical existence) of the converged solutions. For these reasons large signal stability analysis techniques need to be used to explore the stability of the solutions obtained with HB simulations.

Time domain integration methods do not possess the previous limitations and more robustly converge to physically observable solutions, including cases with stationary chaos, as no particular type of solution is presumed.

Transient analysis can be effectively used to simulate ultra broadband high speed digital circuits, in which the shape of the 2-state output signal is optimized by means of eye-diagrams as the switching transients are shorter or of the same order as the minimum signal period (highest frequency).

But time domain integration is not always practical for tuned circuits because transients can be very long, particularly in high-Q circuits. Also the amount of time samples required can be very high when low and high frequency signals coexist in the simulation, as we need to integrate over a sufficient time to observe the stationary regime of the lowest frequencies, which leads to very long and complex simulations. Additionally convergence problems may arise in the integration method associated to the distributed elements models. Finally, time integration is not well suited for the study of common phenomena observed in non linear circuits, such as hysteresis or memory effects in their response (oscillations that may show up or not for a same value of the VCO control voltage, depending on its sweep direction). This is because time integration always start at $t=0$ and keeps no memory from the previous state, unless the designer imposes different initial conditions.

Harmonic Balance is best suited for the optimization of non linear tuned circuits, but a time domain integration simulator (transient), when applicable, can be very useful to extract information about the stability of the wanted solution. Both simulation techniques are complementary in non linear microwave circuit design.

Mixed time–frequency methods are intended to solutions with multiple harmonic terms, and allow the analysis of microwave circuits containing modulations, (which would require a short integration step during a long simulation interval in standard time-domain integration). They also enable efficient determination of the envelope of the oscillation startup transient and the analysis of steady-state solutions with complex dynamics [2].

With the help of Auxiliary Generators (non-perturbing current/voltage probes) we can induce different solutions in non-linear systems, and study their stability through pole-zero identification, which provides local stability results based on large-signal/small-signal (conversion matrix) analysis with Harmonic Balance.

5.2.3.2 Stability Analysis of the Steady State Solutions

In this sub-section we perform a stability analysis of the steady-state solutions found previously (Fig.34-Fig.38 in section 5.1). Through a conversion matrix analysis, small signal perturbations of different large signal responses are studied. This large-signal/small-signal method is used when some signal sources have much smaller amplitude than others, and are assumed not to exercise circuit nonlinearities; thus faster simulations are achieved.

The analysis procedure is similar to the perturbation of the DC solution performed in 5.2.2, but now the quiescent points are replaced with large-signal time-varying periodic states induced with the aid of non-perturbing Auxiliary Generator probes, whose parameters were previously found through an optimization with Harmonic Balance to fulfil the non perturbation condition (6). By frequency sweeping the perturbing signal (usually a current or voltage source) and simulating its effect on a circuit variable (branch current or node voltage), a transfer function can be obtained which is subject to pole-zero identification in order to determine the stability properties of the corresponding steady-state solution.

We are using a small signal perturbing current source, connected in single mode as in Fig.41. The resulting "v1" node voltage contains 3xN+2 harmonics; being N the max order of the Harmonic Balance simulation. Those harmonics correspond to dc, f_{ss}, F_n and $F_n \pm f_{ss}$, where F_n is the n-th harmonic, n = 1...N, from the large signal steady state solution, and f_{ss} is the small signal tone frequency mixing with it. The frequency of this small signal tone is swept over the band where the active devices can oscillate. The $H(j\omega)$ transfer function is obtained by relating the f_{ss} component of the nonlinear "v1" node voltage to the small signal current amplitude of the perturbing probe –which is a single tone of frequency f_{ss}.

Using frequency dependent real and imaginary data from $H(j\omega)$ an identification with a polynomial rational function H(s) is performed. A SciLab (v5.3.3) script has been used for this purpose; it is based on the function *frep2tf* -frequency response to transfer

function, which transforms frequency dependent complex data into a rational transfer function of the form H(s) = Num(s)/Den(s) using n-th order polynomials where 'n' is an input parameter setting the degree of the linear system.

The order 'n' of H(s) is set to minimize the fitting error with the available data, which is usually treated in sub-bands of frequency in order not to excessively increase the polynomials order. The function *repfreq* is used to extract the frequency response of H(s), which can then be plotted against the real and imaginary parts of H(jω) in order to see how close H(s) is modelling the system. Fig.47 shows a flow graph of this process.
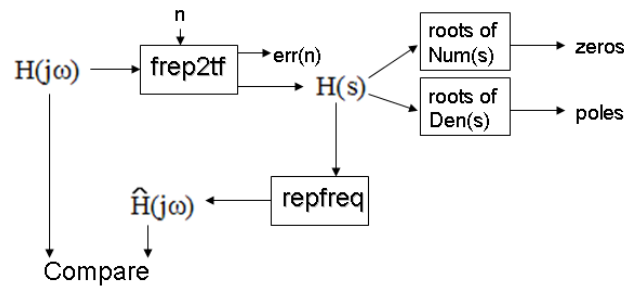

Fig.47.   Extracting poles and zeros from a transfer function. H(jω) complex frequency dependent data is processed by a SciLab (v5.3.3) script

The roots of H(s) are then extracted and plotted in the complex plane. If the poles lie on the LHP the small signal perturbation is not taking the system out of its current steady state solution, which is said to be in a stable *basin of attraction*. On the contrary, if there are system poles in RHP the solution will not stand any noisy perturbation at the poles frequency, being an unstable solution and thus non observable in practice.

Usually an excessive value of the real part of a pole (negative or positive) may indicate that it is not a root of the system, which is only approximated by the rational function H(s). Additionally, the poles appearing at frequencies outside a sub-band of H(jω) data must be later confirmed or discarded by an analysis at another sub-band including that frequency.

As an example Fig.48 shows the perturbation analysis and pole-zero identification for the odd mode solution in the circuit of Fig.27. We know already from the time domain simulation results in Fig.28 that the odd mode is a stable solution in this circuit, and the results from this analysis are in agreement with it as the system poles are in LHP.
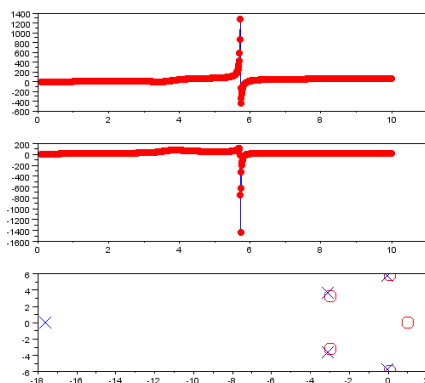
p =
   - 17.636387
   - 3.1003507 ± j·3.6642053 GHz
   - 0.0498598 ± j·5.7251665 GHz

z =
   - 2.9816007 ± j·3.2191838 GHz
     0.0836729 ± j·5.9233817 GHz
     1.0070854

p =
 - 1.2397719 ± j·18.032261 GHz
 - 0.0028768 ± j·11.451394 GHz

z =
 - 3.1198501 ± j·17.555254 GHz
   1.8885048 ± j·11.661486 GHz

p =
 - 6.3219705 ± j·21.215009 GHz
 - 1.2522136 ± j·18.05203   GHz

z =
 - 5.3655041 ± j·22.181563 GHz
 - 3.2535185 ± j·17.441912 GHz

Fig.48.   Perturbation analysis and pole-zero identification for the ODD mode solution in the CSRR based resonator 2-push structure of Fig.27.

The same analysis performed on the even mode solution shows poles in RHP (Fig.49), indicating that this solution is unstable.
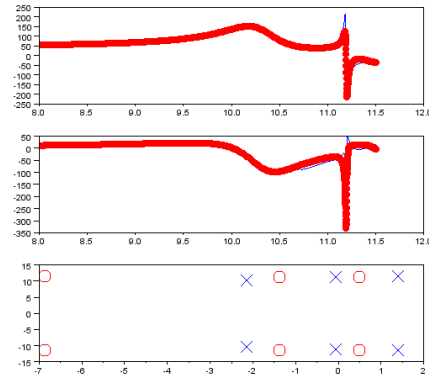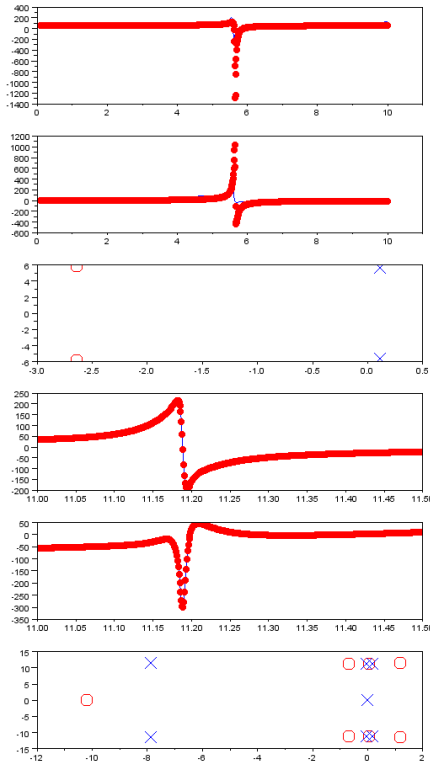
p =
 - 7.8701445 ± j·11.463947 GHz
 - 0.0342478 ± j·11.189032 GHz
 - 0.0000329
   0.1863567 ± j·11.189659 GHz

z =
 - 10.216012
   1.1793857 ± j·11.513899 GHz
 - 0.6977238 ± j·11.174430 GHz
   0.0611078 ± j·11.191355 GHz

p =
 - 14.382187
 - 10.573827 ± j·18.587583 GHz
 - 1.6885046 ± j·18.138688 GHz
 - 0.0000122
   0.1544750 ± j·16.784887 GHz

z =
 - 59.999822
 - 12.617056 ± j·16.966378 GHz
 - 4.6029255 ± j·18.068914 GHz
 - 0.0000555
   0.2329288 ± j·16.789119 GHz
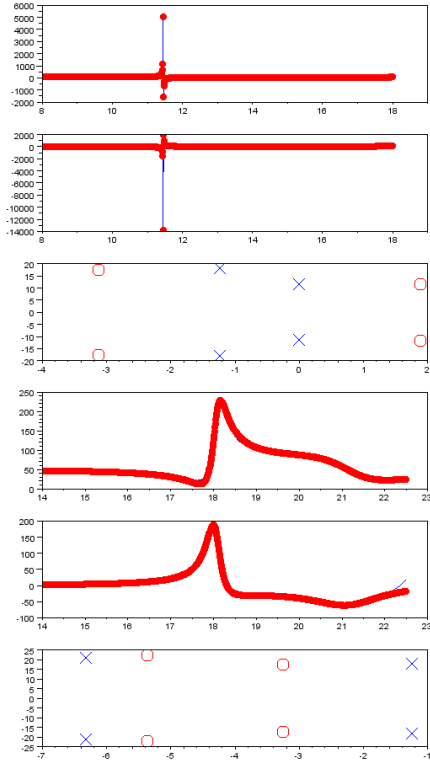
Fig.49.   Perturbation analysis and pole-zero identification for the EVEN mode solution in the CSRR based resonator 2-push structure of Fig.27.

The two analyses performed in Fig.48 and Fig.49 have benefitted form the previous knowledge of the stability of the solutions under study, thanks to the time domain simulations that could easily be performed on the circuit in Fig.27. This allow us to corroborate the stability of the odd mode solution and the instability of the even mode solution with the aid of pole-zero identification of the system's response to a small signal perturbation.

Now we will determine the stability of the different solutions found with Harmonic Balance using the Auxiliary Generator technique on the two circuits in Fig.29, which are modelled using microstrip lines and other planar elements defined in frequency domain.

5.2.3.3 Mode Stabilization Resistor

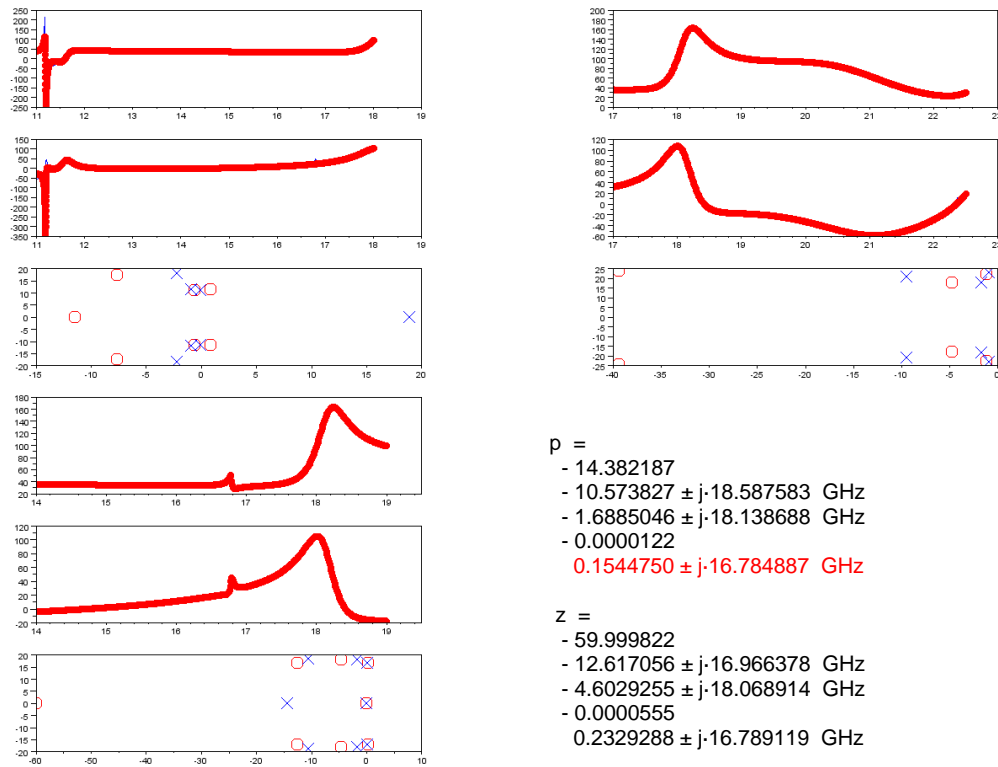Based on the small signal analysis of 5.2.2, a resistor was initially coupled to each transistor source stub in order to avoid a resonance at the high frequency portion of the active device band; which was showing a potential risk for the start of undesired oscillations. The coupling of low/medium value resistors annihilates that resonance.

As expected, the HB analysis with AG converged to the odd and even modes at the desired frequency, and no other spurious frequencies were found during this analysis – which was nevertheless limited to even/odd operation modes of the structure. But when the large signal stability analysis was performed, RHP poles were found in the two cases. It was assumed that the system would not have a synchronized solution and that it might have instead a Quasi-Periodic or a Chaotic type response; QP responses have not been explored, and Chaotic responses can not be reproduced with the AG technique. In

fact, as our desired response is Periodic, we analyzed the resulting RHP poles for the wanted odd mode solution with different values of the source coupled resistor; they are plotted in Fig.50.
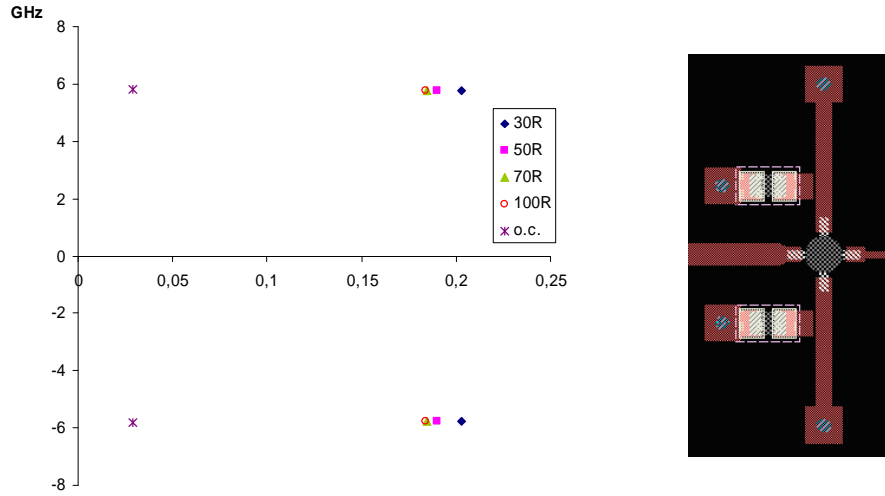
Fig.50.   Resulting RHP poles from the odd mode stability analysis of the 2-push oscillator in Fig.29 (b) for different values of the source coupled resistor. The lowest real part is obtained with no resistor (open circuit)

We found that none of the resistor values led to a stable solution, having a pair of complex conjugate dominant poles in RHP, which approached the imaginary axis as the resistor value increased. In the limit, with no resistor connected (open circuit) the resulting poles were still in RHP. This resistor was obviously not contributing to stabilize the wanted solution, even though it guaranteed that the small signal condition for the start of oscillations was accomplished at the desired frequency only. We then placed the resistors in series with the source stubs, and studied their effect on the dominant pole locations, which now appeared in LHP. The results are in Fig.51.
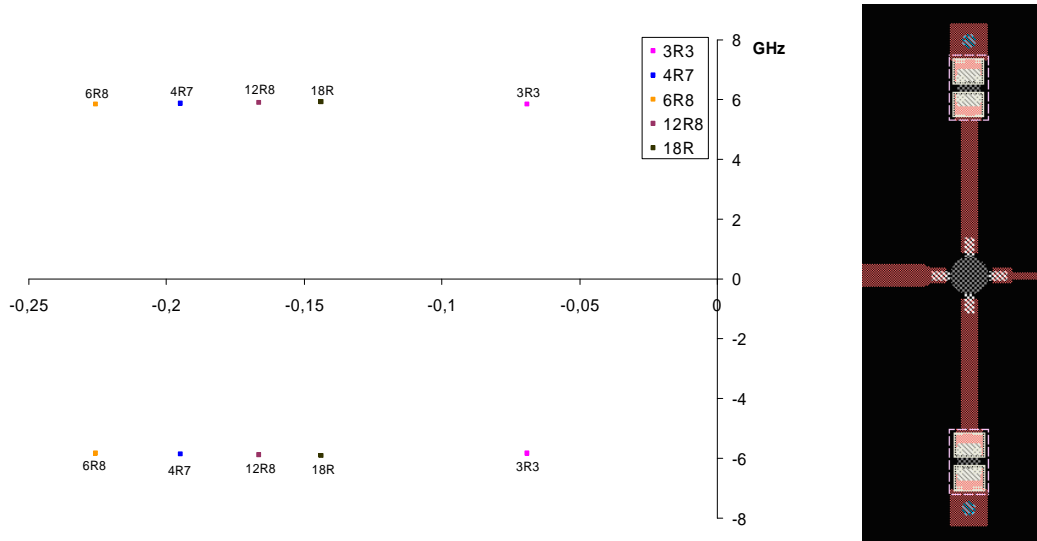
Fig.51.   Representation of the pair of dominant poles from the oscillator structure in Fig.29 (b) for different values of the series source resistor. The dominant poles are those which are the closest to the imaginary axis. A resistor value around 7Ω keeps the dominant pair at a maximum distance from the RHP.

We set a design criteria here; in that the small signal analysis can not guarantee a desired operation mode in a coupled structure. It is then required to perform a stability

analysis on every mode for which we have had convergence with HB using the AG technique. By relating the perturbing small signal current at frequency f_{ss} to the corresponding spectral component of the nonlinear node voltage at which the current probe was added, we determine the admittance function Y_{bif} which, in our analysis, happens to be the inverse of $H(j\omega)$; in general $H(j\omega)$ can be any function relating a perturbing parameter to the corresponding effect observed on any circuit variable. Three admittance functions are represented in Fig.52, corresponding to different stabilization mode solutions.
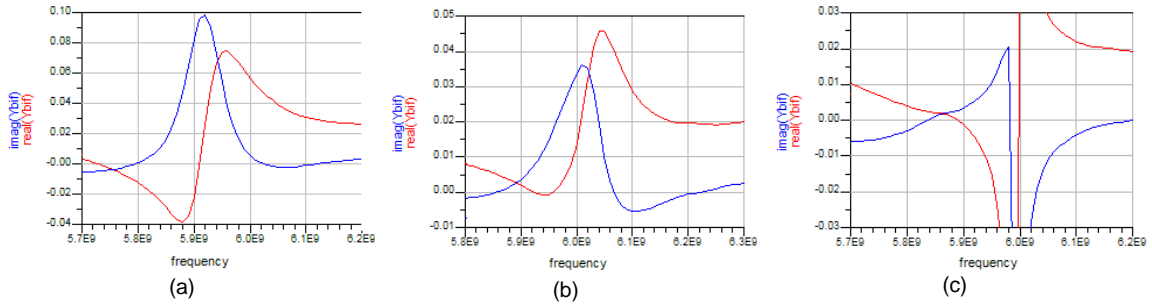
Fig.52.   Real and imaginary parts of the admittance function relating the small signal perturbing current to its effect on the nonlinear voltage at the connecting node. Three mode stabilization solutions are represented, corresponding to the implementations of Fig.50 and Fig.51. The value of the Y_{bif} conductance at the zero crossing with positive slope of its susceptance is shown. (a) Capacitive coupled 10 ohm resistor, -11.3 mS. (b) Series 12R8 resistor, +4.9 mS. (c) Series 6R8 resistor, +2.3 mS.

If we apply the Kurokawa conditions (9),(10),(11) to Y_{bif} we deduce that the capacitive coupled resistor produces an unstable solution while the series resistive resistors give the desired stability. In this case the highest positive real conductance is obtained with a 12.8 ohm resistor, which does not seem to corroborate the results of the pole-zero analysis in Fig.51, where the maximum distance of the dominant poles from the RHP was obtained for a 6.8 ohm resistor. The pole-zero analysis for these three cases is shown in Fig.53.

| - 1.4470278 ± j·5.3166552 GHz | - 0.7299106 ± j·6.2154920 GHz | - 0.2813959 ± j·5.8969783 GHz |
| +0.2284567 ± j·5.7437651 GHz | - 0.1664395 ± j·5.8935032 GHz | - 0.2257006 ± j·5.8390801 GHz |
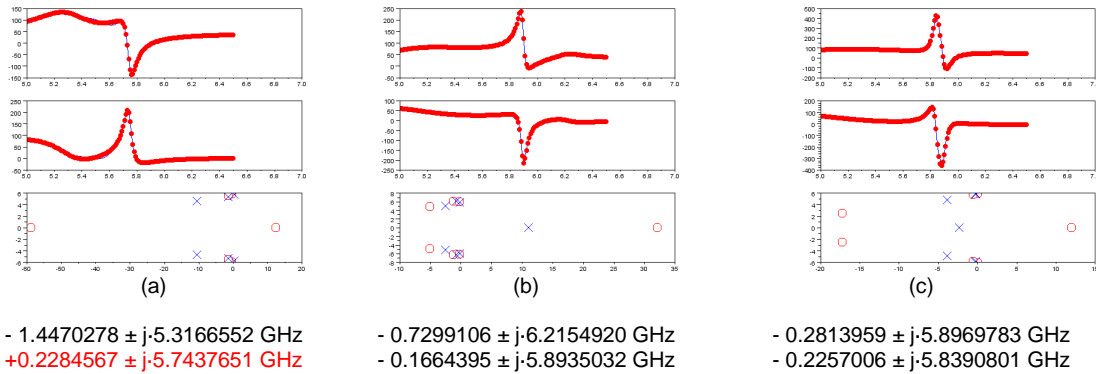
Fig.53.   Results of the pole-zero identification of the system with the three stabilization approaches of Fig.52.

Even though the small signal admittance can give some clues on the stability properties of a solution, it is the pole-zero identification of the transfer function which shows a clearer picture on the location of the dominant system poles, and their evolution with the variation of a circuit parameter. The sensitivity of the solution stability to that parameter will provide a means for stability control. In our design a resistor in series with the source stub proved to be more efficient than the coupled resistor. An this

efficiency for stability control could only be evaluated through a nonlinear stability analysis.

5.2.3.4 Stability Analysis of the Final Oscillator

In this subsection we proceed to analyze the stability properties of the odd and even mode solutions found for the circuit in Fig.29 (b) with 12.8 ohm series resistors connected to the source stubs. Fig.54 shows the plots of the admittances extracted during the stability analysis of the DC (small signal) and Oscillatory (large signal) solutions in both odd and even modes.
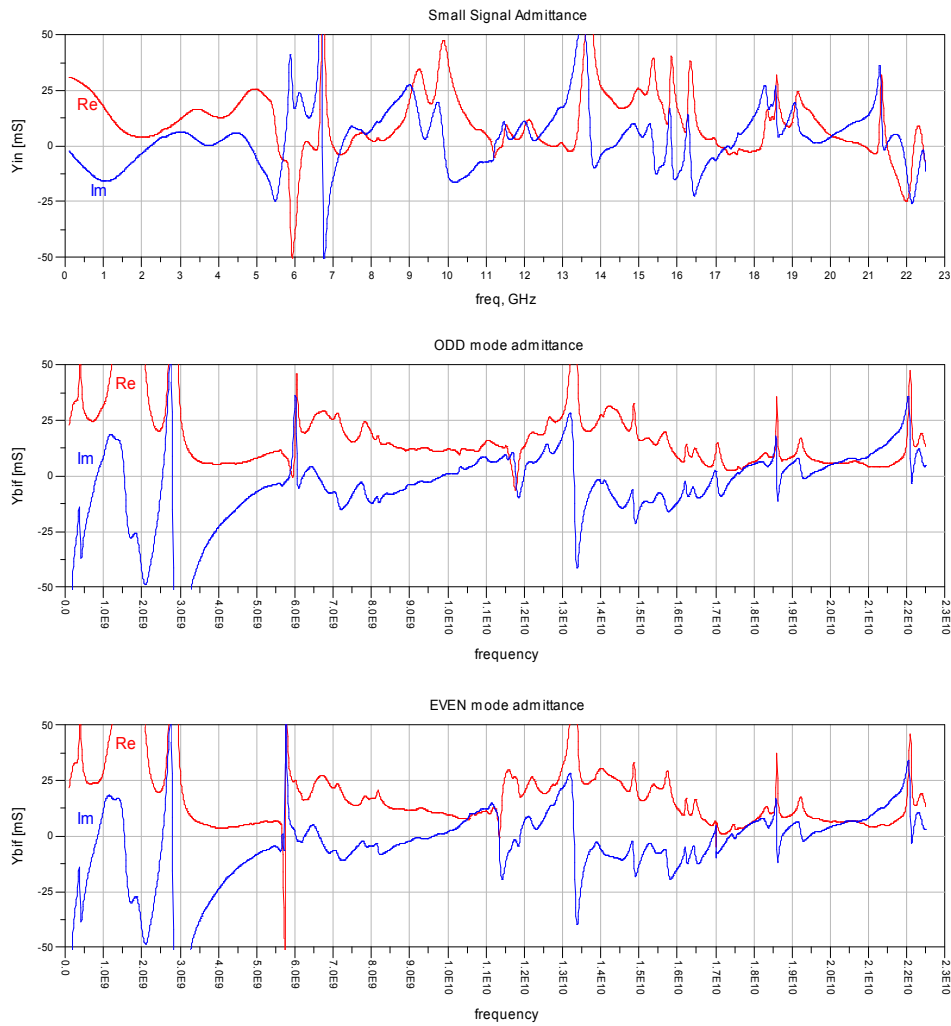
Fig.54.　　Admittance functions extracted during the stability analysis of the DC and Oscillatory solutions (odd and even modes). The Kurokawa condition is satisfied at DC (top), meaning that this solution is unstable. The odd mode oscillatory solution (middle) does not verify that condition, while the even mode (bottom) does; this may indicate that the odd mode is stable (observable) and the even mode is unstable (non observable). A pole-zero analysis is required to corroborate this assumption.

The DC solution satisfies the Kurokawa conditions (9),(10),(11), indicating that it is unstable, so the system will start an oscillation; there are two possible oscillating modes in a 2-push structure: odd and even –provided there are no implementation errors or important differences in the active device's performance due to statistical variations or

malfunction. The odd mode oscillatory solution does not verify (9)-(11) , while the even mode does; this may indicate that the odd mode is stable (observable) and the even mode is unstable (non observable). It is nevertheless recommended to perform a pole-zero analysis to corroborate this assumption.

The pole zero identification of the perturbation transfer function, H(jω), for both mode solutions in the CSRR based resonator 2-push structure are plotted in Fig.55 and Fig.56. In order to determine that the odd mode solution is stable we have performed the identification in overlapping sub-bands covering the full frequency range of active device operation (Fig.55). For the even mode we just identified the dominant poles in the RHP, which proves the instability of this solution (Fig.56). The same analysis is performed on the stub resonator circuit of Fig.29(a) obtaining similar results.

p =
 - 5.2633210 ± j·4.9452051 GHz
 - 1.4453663 ± j·0.7812292 GHz
 - 0.5672262 ± j·2.5349748 GHz
 - 0.4577610

z =
 - 17.386774
 - 5.0700533
 - 4.5086350 ± j·1.6398549 GHz
 - 0.7601279 ± j·2.8041918 GHz
   0.3071199

p =
 - 24.298208 ± j·0.4727394 GHz
 - 0.1622062 ± j·5.8955808 GHz

z =
   20.807116 ± j·7.0880647 GHz
 - 0.2974560 ± j·5.9899992 GHz
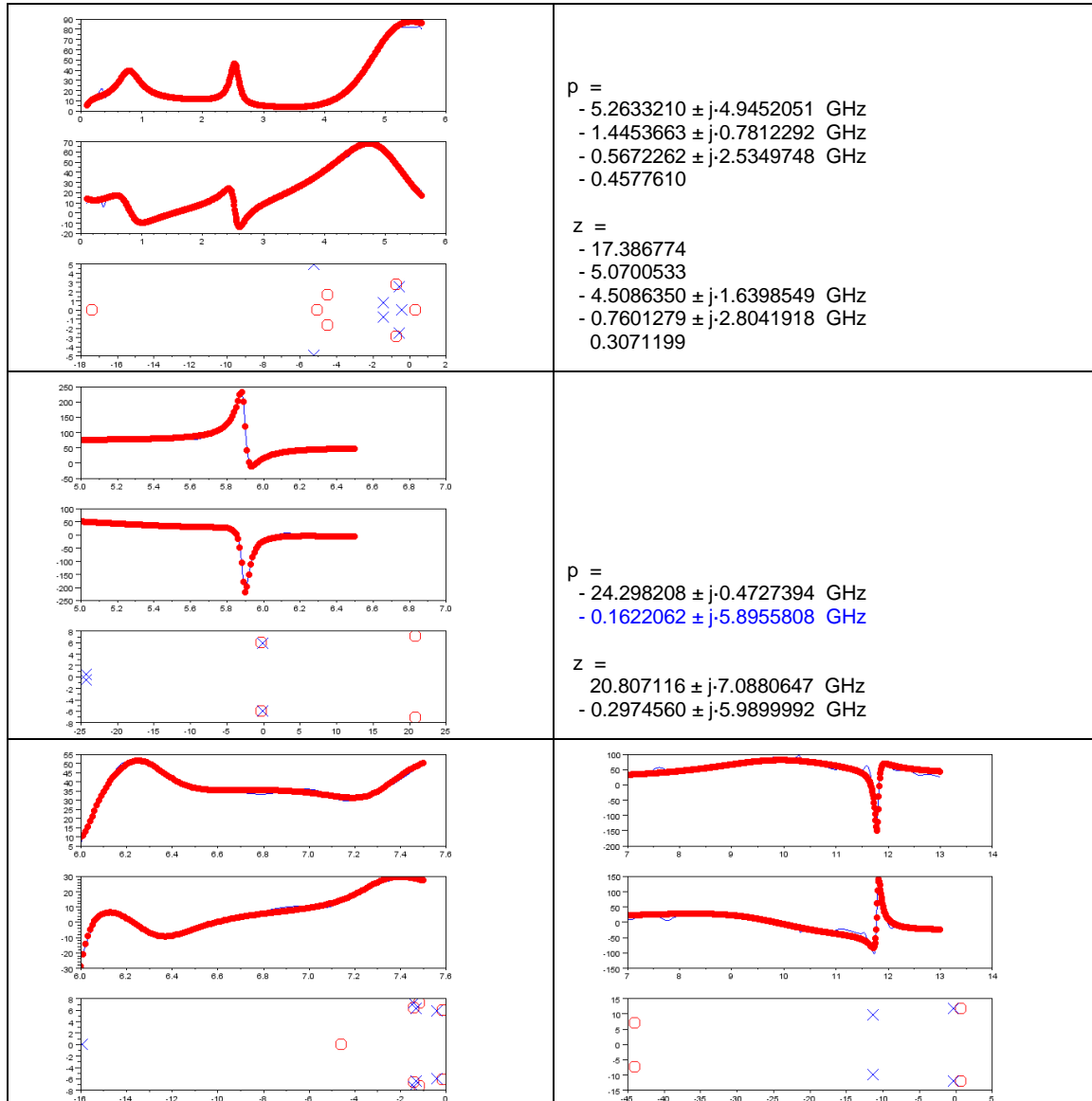
Fig.55.   Pole-zero identification of the perturbation transfer function for the ODD mode solution in the CSRR based resonator 2-push structure of Fig.29 (b)

p =
 - 0.8317366 ± j·17.462109 GHz
 - 0.4584267 ± j·16.916221 GHz
 - 0.3360714 ± j·16.168231 GHz
 - 0.0000021
   2326.4896

z =
 - 7.7705514 ± j·16.749084 GHz
 - 0.7016143 ± j·16.193545 GHz
 - 0.4409595 ± j·17.048318 GHz
   0.0000054
   598.79428

p = 0.0009869 ± j·5.6679696 GHz

p = - 0.0027367 ± j·5.6691037 GHz
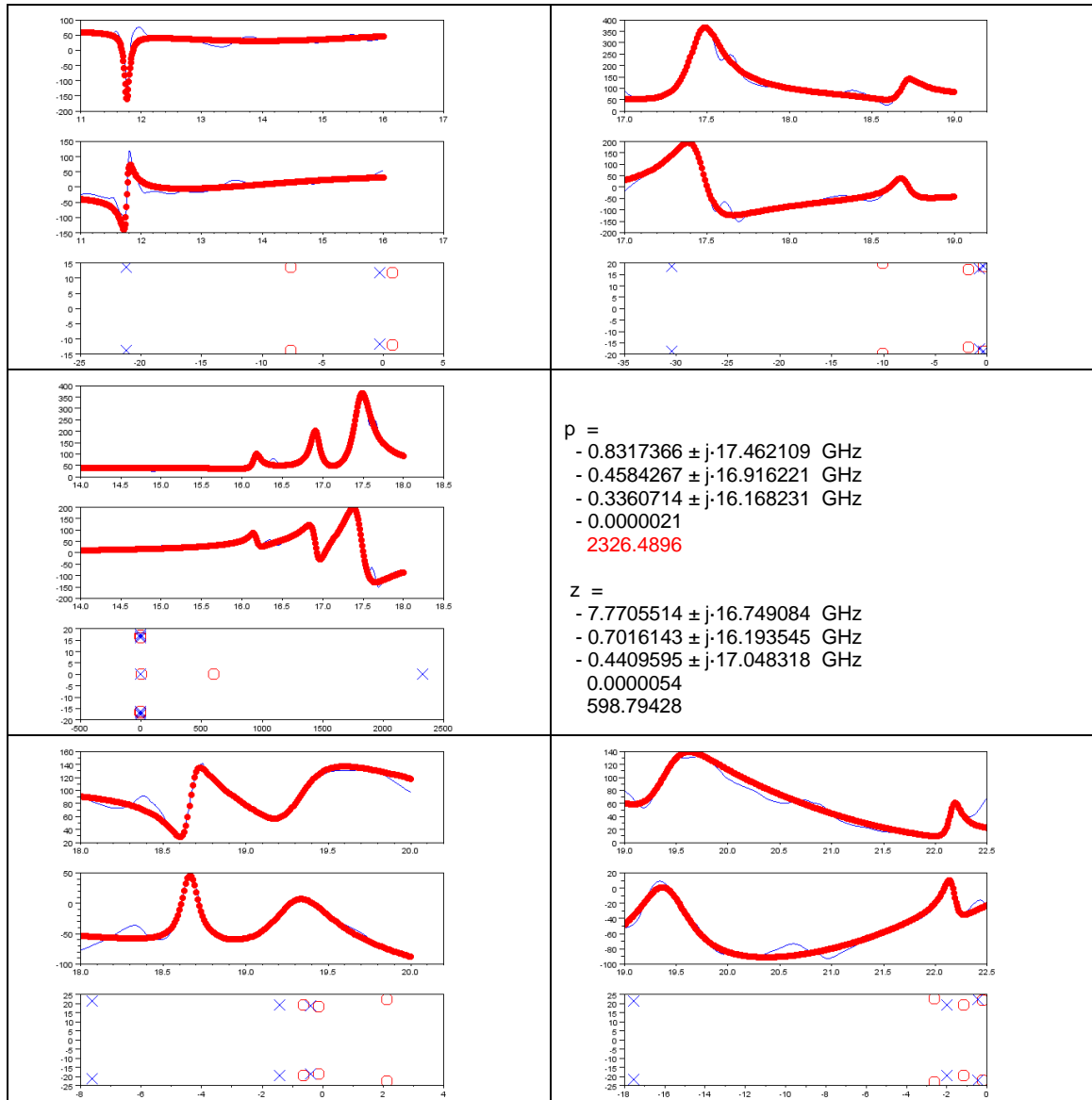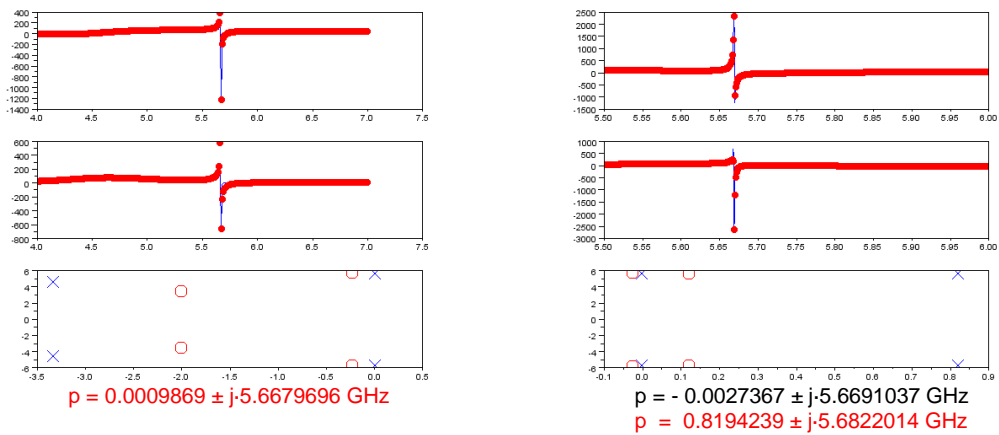p = 0.8194239 ± j·5.6822014 GHz

Fig.56.   Pole-zero identification of the perturbation transfer function for the EVEN mode solution in the CSRR based resonator 2-push structure of Fig.29 (b)

5.3 Output Impedance

Determining the output impedance of an oscillator from a small signal analysis has no sense, unless we can assume that the output port has enough isolation from the active device's operation. As the 2-push oscillator operates in large signal on a highly nonlinear region of the active devices, it is not possible to simulate its output match by applying linear techniques such as S-parameter or AC analysis, which perform a linearization of the circuit elements about the DC operating point. A correct evaluation of the output match must be performed under large signal operation, and once again the Auxiliary Generator is of great help to this end.

The current-to-voltage ratio is simulated at the load node with the help of a small signal current generator whose frequency is swept in a band around the second harmonic of the large signal oscillatory solution; this determines the total admittance seen at the output port. By subtracting the load admittance (1/50 Ω^{-1}) we obtain the part corresponding to the oscillator circuit alone, whose reflection coefficient is plotted in Fig.57.
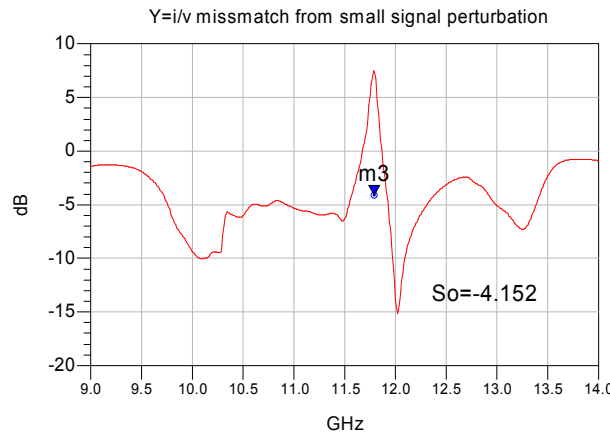
Fig.57.   Output match simulated with a perturbation analysis measuring the small signal voltage to current variations on the load node

This method requires that the small and large signals be incommensurate, so the admittance result at the second harmonic frequency is no taken into account. Instead we determine the internal circuit impedance at this frequency by a direct method; the output port matching can be evaluated by considering the circuit as a signal source and applying the voltage divider formula (17) to determine its generator impedance.

$$(17) \quad V_{out} = \frac{R_{load}}{R_{load} + Z_{generator}} \cdot V_{generator}$$

$V_{generator}$ is the voltage simulated at the unloaded output node (in open circuit or with a very high R_{load}) with the circuit operating under the oscillatory solution imposed by two Auxiliary Generators, whose parameters have been previously optimized to induce the normal operating mode (loaded). V_{out} is the voltage simulated under normal load condition. The impedance is calculated as:

$$(18) \quad Z_{generator} = R_{load} \cdot \left(\frac{V_{generator}}{V_{out}} - 1 \right)$$

It is not possible to establish a linear relationship between $V_{generator}$ and V_{out}; in fact (18) is a nonlinear expression where $Z_{generator}$ is a complex vector on the harmonics of V_{out}. The output match marked as "*m3*" in Fig.57 is calculated as $S_o = 20 \cdot \log_{10}(\Gamma^{H2})$, with Γ^{H2} = $(Z_{generator} - R_{load})/(Z_{generator} + R_{load})$ evaluated at the second harmonic frequency; it represents a first order approximation to the generator impedance.

5.4 Phase Noise

We have already studied the oscillator stability in terms of the robustness of the 2-push system to stay at one frequency and phase mode without jumping to another state under the effect of small signal perturbations. In this section we will approach the oscillator stability in the short term sense of phase noise. There is another concept of stability in the long-term sense referring to the changes in the oscillation frequency over minutes and days, which is of relevance in reference oscillator performance for accurate frequency synthesis, but it is not addressed in this work.

Oscillator noise forms sidebands around the carrier power spectrum. The spectral density of its phase component has a f^{-2} evolution near the carrier, when the noise is dominated by white noise. But when $1/f$ or *Flicker* noise influences the noise sidebands, they take on an f^{-3} characteristic.

Several regions can be identified on a phase noise spectral density function: a flat region at large offset frequencies where the oscillator amplifies the broadband noise floor, an f^{-2} region within the oscillator loop bandwidth where the oscillator loop gain magnifies the phase noise, and an f^{-3} region where the low-frequency $1/f$ noise from the device modulates the signal's phase to create an even more rapidly increasing noise. [11] suggests that the resonator might also possibly contribute to $1/f$ noise. Fig.58 shows these regions.
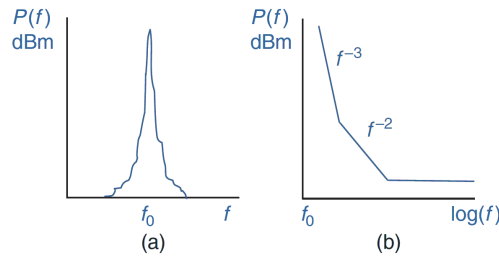
Fig.58.   Oscillator spectrum as seen on a spectrum analyzer and (b) as seen if referenced to the center frequency, averaged, and plotted on a logarithmic frequency scale [11].

In Leeson's model for phase noise the spectrum increases as f^{-2} when Δf is less than $f_0/2Q$ and as f^{-3} when Δf is also less than a value "f_k", which is almost always less than the measured device $1/f$ corner frequency because the modulation conversion does not raise the noise above the thermal floor [11].

5.4.1 Noise modeling and simulation

All passive lossy elements in a circuit are noisy and can generate an available noise power equal to K·T·B, where K is the Boltzmann constant, T is the element temperature in Kelvin and B the integration bandwidth (in Hz) where the effect of noise is accounted for. The term K·T is the white noise spectral power density which, at an ambient temperature of 25ºC, has the value -174 dBm/Hz. As the available power from a resistor R in terms of its effective voltage or current noise is $|v_n|^2/4R$ or $R·|i_n|^2$, it follows that the spectral noise densities associated to $|v_n|^2$ and $|i_n|^2$ are:

$$\frac{<v_{th}^2>}{\Delta f} = 4KTR \qquad V^2/Hz \qquad\qquad \frac{<i_{th}^2>}{\Delta f} = \frac{4KT}{R} \quad A^2/Hz$$

When dealing with random processes we do not consider the time or frequency domain waveforms of the currents or voltages because their functional form is not known, instead we only care about their power, and this requires the mean-square values of the magnitudes.

Each resistive noisy element in a network can be modeled as a noiseless resistor having a series voltage noise source or a shunt current noise source. The combined effect of all noise sources in multiport networks is expressed by a *noise-correlation matrix*, which in the case of currents is obtained from the admittance matrix **Y** of the component as:

$$C_i = 4KT·\text{Re}\{Y\}$$

The current correlation matrix **C$_i$** contains the mean-square values of the noise current sources and their crossed correlations and it is used to determine the contributed noise power at a particular device port.

Other sources of noise in electrical circuits arise from the physical processes in semiconductor devices and are bias dependant. The most common are:

o   Flicker noise, also known as *1/f*. Due to imperfections on the semiconductor crystals (surface and volume phenomena, temperature fluctuations...). It is the dominant contributor to low frequency noise and is modeled as a current source with Power Spectral Density (PSD)

$$\frac{<i_{fl}^2>}{\Delta f} = \frac{K_f·I^{Af}}{f^{Ffe}}$$

K_f is a constant, $A_f \approx 2$, $F_{fe} \approx 1$

o   Shot noise. Caused by the granular nature of electricity: Every current **I** can be considered as a succession of independent current impulses. The associated PSD is of the form

$$\frac{<i_{sh}^2>}{\Delta f} = 2·q_e·I$$

o Generation-recombination (GR) noise. Due to fluctuations in the number N of free carriers caused by recombination and trapping processes. The associated PSD is constant up to the cutoff frequency $F_c = 1/(2\pi\tau)$, where τ is the carrier lifetime. F_c is of the order of 1.5 KHz. Above that frequency the PSD decreases as $1/f^2$.

$$\frac{<i_{gr}^2>}{\Delta f} = \frac{4 \cdot I^2 \cdot \overline{\Delta N}}{N^2} \cdot \frac{\tau}{1+(\omega\tau)^2}$$

HEMT device models usually consider the thermal noise associated to the contact resistors of gate, source and drain. Shot noise from the gate current and Flicker noise form the drain and gate currents. Shot noise from the drain current is neglected with respect to the thermal noise in the channel. Also $1/f^2$ GR noise is neglected with respect to the $1/f$ Flicker noise.

Thermal noise in the channel is dependent on the equivalent noise channel resistance, $R_{id}(V_{gs}, V_{ds})$, which is a function of the bias. This drain current fluctuation gives raise to variations in the depletion region under the gate, creating an input thermal noise which is strongly correlated to the thermal channel noise. The correlation between these two noise sources takes place through the C_{gs} capacitance and so the correlation coefficient is essentially imaginary.

Appendix A III shows a comparative table between the noise models from the very complete Chalmer's Angelov and the Agilent's EEHEMT1 available to this project – used for our nonlinear analysis. Flicker noise sources are not included in the ADS2009 version of the EEHEMT1 model, which suggests the use of bias-dependent noise sources connected external to the nonlinear device.

After connecting three nonlinear noise current sources external to the EEHEMT1 model, in order to take into account the flicker noise associated to the nonlinearities C_{GS}, C_{GD} and I_{DS}, unsatisfactory results were obtained. In the simulated phase noise spectral density from such device the f^{-3} region is not observed or it is very narrow; instead, the phase noise grows as $1/f$ in the close to carrier region, which does not fit the expected behaviour of real transistors[11].

In order to investigate the possible causes of these results, a very simple oscillator was designed with the only noisy elements being the transistor and the resistive part of the resonator. Also an Angelov model was fitted to reproduce the same nonlinear performance of the NE3210S01 device, based on its available EEHEMT1 model and datasheet information (see Appendix A II). The test circuit and transistor model are shown in Fig.59. A comparison of the I_g, I_d from this new fitted Angelov model and the original EEHEMT1 is presented in Fig.60.
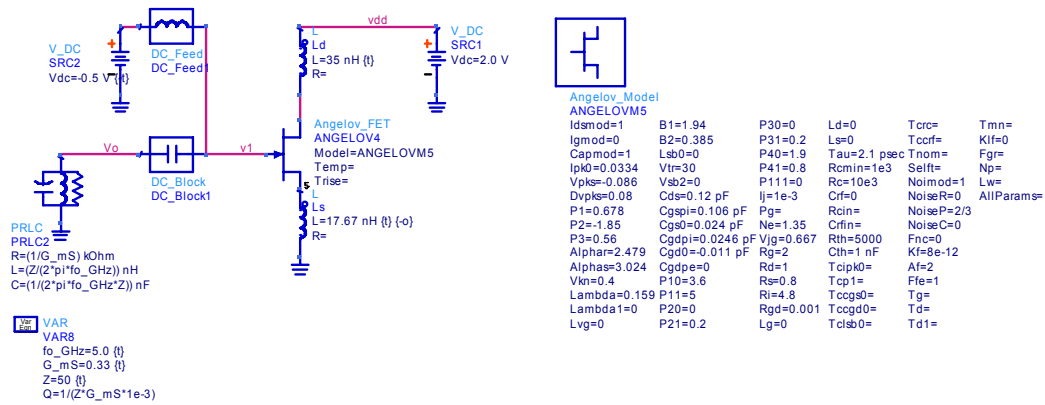
Fig.59.   Basic oscillator circuit used to compare the noise performance of different transistor models and configurations for the NE3210S01 device

The noise spectral density simulated from this oscillator, using two different noise models, is shown in Fig.61. From this result I conclude that the addition of external noise sources is not an efficient method for simulating HEMT phase noise in ADS2009.
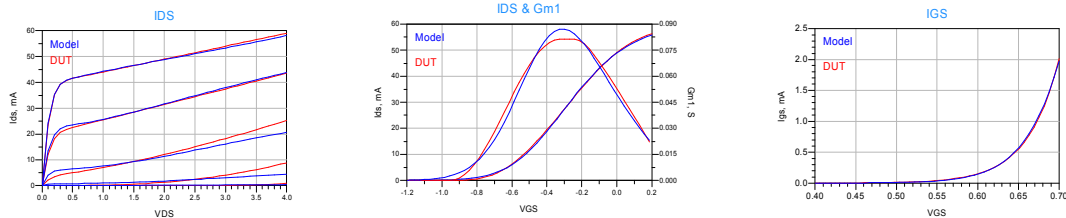
Fig.60.   Fitting of the I_d and I_g Angelov equations with respect to the available NEC 3210S01 EEHEMT1 model (DUT)
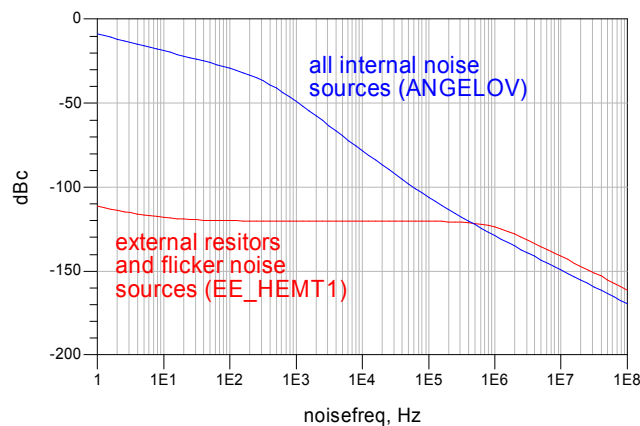
Fig.61.   Noise spectral density simulated from a basic test oscillator circuit using with two models of a same transistor

A probable explanation to this result could be that the noise contributions of the internal noise sources in a model are being computed analytically, by using an equation, instead of performing a nonlinear harmonic balance simulation. This could explain the differences observed in the simulated phase noise at the gate port using two configurations of the same transistor model (Fig.62); one with the parasitic resistors R_G, R_D, R_S embedded in the model and the other with external resistors.

Fig.62. Noise spectral density simulated from a basic test oscillator circuit using two configurations of a same transistor model: with all internal noise sources (original, blue) and some external noise sources (modified, red)

Using the Angelov HEMT model with all internal noise sources, a simulation of phase noise has been performed on the two circuits of Fig.29, corresponding to the odd mode of oscillation, the results are in Fig.63.
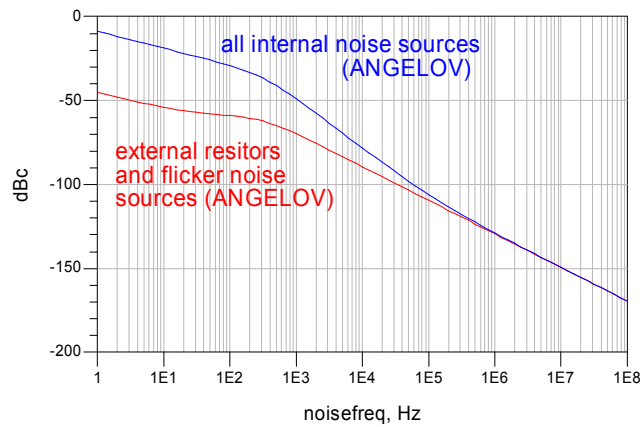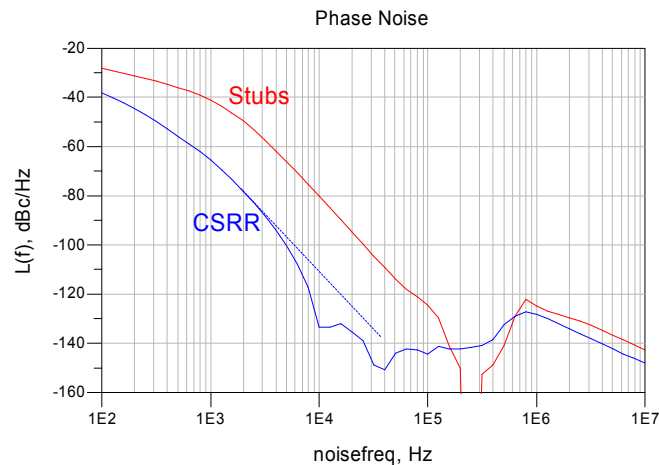

Fig.63. Phase noise simulation results from the CSRR and Stub based resonator 2-push structures in Fig.29, corresponding to the odd oscillation mode. The higher quality factor of the CSRR based resonator results in a much lower phase noise contribution. The dashed line is an estimation of a more likely phase noise level.

The most important aspect to stress out from those results is the much lower phase noise contribution from the CSRR based resonator 2-push with respect to its classic microstrip stub counterpart; this is due to the higher quality factor from the CSRR coupled lines. But we remain nevertheless a bit skeptic about the wonderful low phase noise obtained at 10 KHz offset from the carrier in the CSRR case. We can not exclude the possibility of a simulation error –as it happens with the stub curve at around 2e5 Hz, and believe that the most likely values for the phase noise would be along the dashed line. This result requires a deeper study in order to understand the causes for some points not being properly calculated, and also a comparison with measured boards.

6 Literature Surveys

An extensive literature survey has been carried out during the realization of this master. It was required in order to understand the role of the coupling and power combining networks used to implement oscillators working on the N-push principle. It was also required in order to verify that no other works have been published to date –and to our knowledge- using CSRR based resonators in the coupling networks of 2-push oscillators. We believe that it is worth including this work in the present document.

The referenced articles are summarized and commented, giving their relevant conclusions. Understanding and summarizing the results has not been an easy task, as most of the articles are from Research Groups in Asian Universities, and the language used seems to have been translated by automatic tools. I think they present very interesting ideas; but an interpretation of the texts has been necessary, which was only possible after an in-depth reading to fully understand the work done. I hope that the following summaries will be useful to future continuations of this work.

The first section "*Resonator Combiner Networks in N-Push Oscillators*" presents four articles which implement different structures to perform the resonator + coupling + power combining functions in N-push structures. None of them makes use of CSRRs.

The second section "*Ring Resonator based Negative Resistance Oscillators*" presents five articles which implement oscillators using different resonators; some of them are based on CSRR or their dual counterpart, the SRR. But they are for the most part single oscillator structures. Only one mentions the design of a 2-push VCO; but the paper only concentrates on the design of the resonator using multiple concentric SRR's and makes no mention to the active part of the circuit.

6.1 Resonator Combiner Networks in N-Push Oscillators

The reference works found on this topic are all from Prof. Masayoshi Aikawa and Dr. Takayuki Tanaka, from Saga University in Japan. They are listed below.

A Low Phase Noise Ku-Band Push-Push Oscillator Using Slot Ring Resonator	2004	Hai Xiao; Tanaka, T.; Aikawa, M.
A Wideband Push-Push VCO Using a Phase Shifter in the Common Feedback Loop	2007	Tsutsumi,M.; Tanaka, T.; Aikawa, M.
V-band 8th Harmonic Push-Push Oscillator Using Microstrip Ring Resonator	2009	Kawasaki,K.; Tanaka, T.; Aikawa, M.
An Octa-Push Oscillator at V-Band	2010	Kawasaki,K.; Tanaka, T.; Aikawa, M.

I proceed to comment and summarize the conclusions from these four articles.

6.1.1 A Low Phase Noise Ku-Band Push-Push Oscillator Using Slot Ring Resonator

Ku-band push-push oscillator using a common one-wavelength slot ring resonator loosely coupled to the active sub-circuits in order to achieve low phase noise performance at the desired second harmonic of 16 GHz. In order to prevent resonance instability caused by the loose coupling, a method of stabilizing the fundamental resonance mode is proposed, thus making the active sub-circuits oscillate in accurate and stable out of phase mode at the fundamental frequency f_o.

Open circuited stubs at the access ports play the double role of coupling the sub-circuits to the slot ring resonator and power combining (see Fig.64). This simplifies the circuit structure by eliminating additional power combiner circuits required in conventional push-push oscillators such as a Wilkinson.

The output is obtained from a microstrip line coupled to the slot ring resonator on its symmetry plane, where the fundamental and odd harmonic signals are cancelled out.
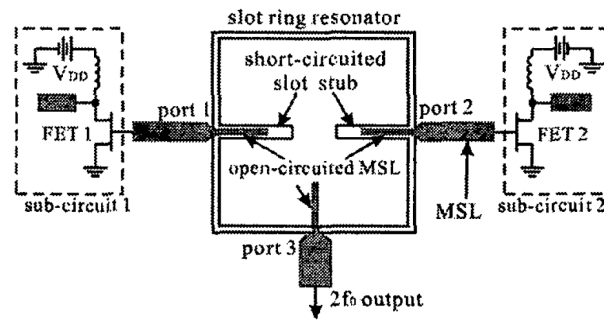
Fig.64.   Circuit configuration of push-push oscillator using slot ring resonator [27].

Coupling between the microstrip access lines and the slot ring resonator is controlled by the value of the open-circuited microstrip stubs impedance $Z_{open} = -jZ_0 \cdot \cot(\beta\ell)$. Then by adjusting the length and width of open-circuited stubs, the coupling with the active sub-circuits can be optimized, together with the transmission characteristic for proper push-push operation.

Stabilization of the fundamental resonance mode is done by means of two short-circuited slot stubs in series with the input ports; they make the resonance current zero and thus the resonance voltage is maximum and out of phase for the fundamental resonance frequency f_o.

Active sub-circuits are designed as one-port negative resistance oscillators at the fundamental frequency of 8 *GHz*. They are HEMT based (Fujitu's FHX35LG) and biased in nonlinear range at 4 V_{drain} / 0 V_{gate}, to generate high power at the desired second harmonic frequency.

Measured output power at 16.0 GHz ($2f_o$) is +10 dBm, with a phase noise of -103.8 dBc/Hz at 100 KHz and -121.3 dBc/Hz at 1 MHz offset frequencies. Suppressions of

the undesired fundamental and 3rd, 4th harmonics at the output port are -37.5 dBc, -40.0 dBc and -42.2 dBc respectively.

In order to confirm the resonance stabilizing effect of the short-circuited slot stub, the same circuit without the stubs is fabricated and measured. As a result, the suppression for the f_o signal degrades to slightly -10 dBc (27.5 dB worse)

6.1.2 A Wideband Push-Push VCO Using a Phase Shifter in the Common Feedback Loop

A push-push VCO with electrically tunable positive feedback loops is proposed.

For wideband VCOs, feedback oscillators are more suitable than the negative resistance type because the electrical length of feedback loops can be changed easily while the negative resistance oscillators need tunable negative resistance circuits and a common resonator whose resonant frequency should be variable, making the tunable frequency ranges comparatively narrow.
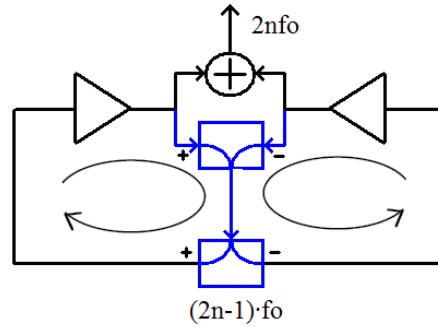
Fig.65.   Working principle of the feedback push-push oscillator based on microstrip-slotline transitions, showing how the slotline (blue) is part of both; the output combiner and the positive feedback loops (resonator). Drawing made by J.L. Flores.
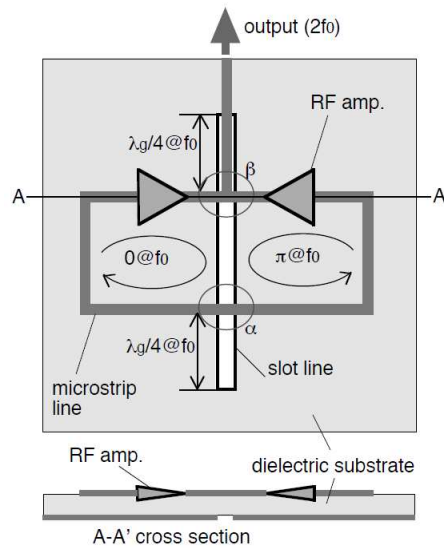
Fig.66.   Basic schematic of the feedback push-push oscillator [28]

The working principle and schematic of a basic feedback push-push oscillator are presented in Fig.65 and Fig.66 respectively. This structure exploits the phase shifting

principle of the microstrip-to-slotline transitions (see Fig.67), which provide a 180° phase reversal quite independent from the frequency, and make a high bandwidth phase shifter [29].

Fig.67.   Working principlie of the 180° reciprocal phase shifters based on microstrip-slotline transitions [29]

The direction of the electrical field in the slotline is switched $\pm \pi/2$ with respect to the direction of the electrical field in the microstrip, and the sign depends on which side in the slotline both electrical fields are coupled.

The key to understand the operation of the structure in Fig.66 is in the common slotline and the microstrip-to-slotline transitions. The electrical length of the feedback loops i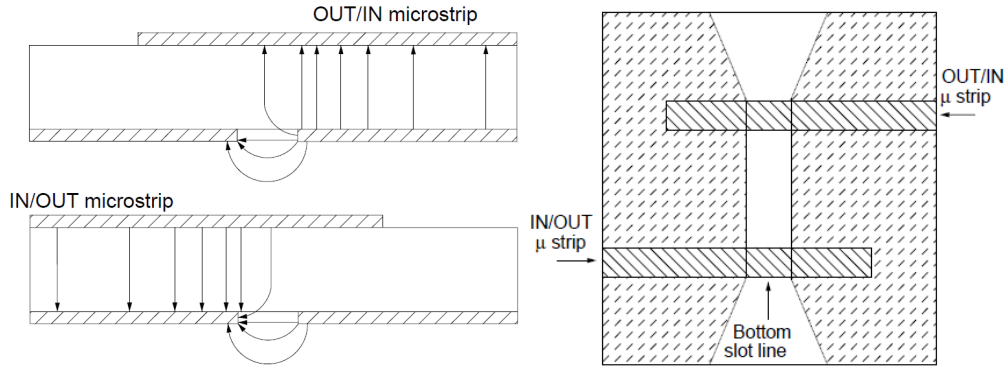s designed to be $2n\pi$ (n integer) at the fundamental frequency f_0, which determines the oscillating frequency. The slot line is a common part of the positive feedback loops, so by changing its electrical length both loops can be simultaneously tuned.

The 2-push operation mode is guaranteed by the phase changes that take place in the microstrip-slotline transitions. The strip-slot T-junction (β) combines out-of-phase the output signals from the two amplifiers and feeds them back to the slot-strip T-junction (α) where they are split out-of-phase, so there is no net phase change in the loops. But the input signals to the amplifiers are in opposition.

Now, an interesting phenomenon takes place in the combiner network. Due to the nonlinear function of the amplifiers, their fundamentals and odd harmonics appear out of phase at the symmetry plane of the structure (where the output signals are combined) and the even harmonics appear in-phase. At this point the in-phase signals add constructively at the output microstrip line, while the out-of-phase signals add constructively at the slotline, and so only the even harmonics are transmitted to the output port, while the fundamental (and odd harmonics) are fed-back through the slotline.

The authors claim that a high suppression of undesired odd harmonics is achieved and thus a high frequency signal of good quality can be generated with this structure.

The VCO achieves frequency tuning by means of a varactor phase shifter placed in the common slot line, which changes the electrical length of the feedback loops. This provides for a 11.6 % (1.85 GHz) tuning range in Ku-band (15.21 - 17.06 GHz) with

phase noise around -77 dBc/Hz and -100 dBc/Hz at 100 kHz and 1 MHz respectively, over the band.

6.1.3 V-band 8th Harmonic Push-Push Oscillator Using Microstrip Ring Resonator

In an "N-push oscillator" the order of the output harmonic is the same as the number of active sub-circuits. Here, the authors demonstrate an 8th harmonic push-push oscillator, using only two active sub-circuits (hence the name push-push) and they implement a new type of resonator combiner that resonates at the fundamental f_o but adds in-phase the 8th harmonic only.

To achieve an eighth harmonic oscillator utilizing the push–push resonant mode, two identical sub-circuits are connected to a one-wavelength (λ_g) microstrip ring resonator at opposite points, having a 180º phase difference at the fundamental frequency f_o. This is similar to what would be done in a classical push-push structure, but instead of just combining the signals at the ring's symmetry plane, which would enhance all even harmonics (see Fig.69, top), the output circuit in the inside area of the resonator is connected at eight ring points spaced $\lambda_g/8$. This effectively combines in-phase the resonant 8th harmonics (see Fig.69, bottom).
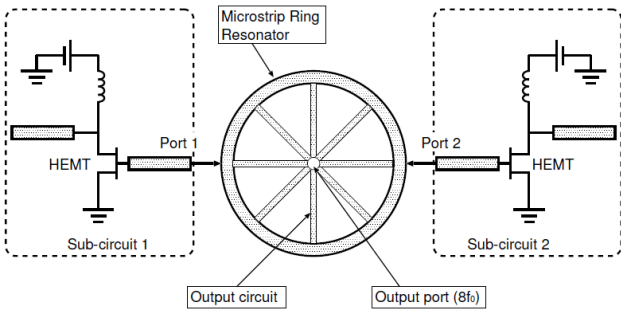
Fig.68.   Circuit configuration of the 8th harmonic push-push oscillator [30]

This way the 8th harmonic is obtained at the output port, while the other undesired even harmonics are combined out of phase and cancel out.

Output harmonic	Circuit Structure	Technical feature
$2f_0$		Basic Push-Push modes
$8f_0$		Harmonic resonant modes

Fig.69.   Operation principles of the basic and harmonic resonant push-push oscillators [30]

The active HEMT based sub-circuits (Fujitsu's FHX35LG), are designed to show the negative resistance at the gate ports at the fundamental oscillating frequency f_o. Microstrip open stub are connected to the drain ports of the HEMTs to provide negative resistance at the gate.

The operating bias voltage is +3.9 V / 0 V (max. drain voltage is +4.0 V). The resonant frequency of the ring resonator is f_o = 6.4 GHz, and the 8th harmonic is at $8 \cdot f_o$. = 51 GHz.

A MIC technology is adopted on a teflon glass fiber substrate.

Measured output level is -12.33 dBm at 51 GHz, but the power of the undesired 2nd harmonic is -12 dBm. This poor suppression is attributed to the unbalance of the sub-circuits and the resonant mode.

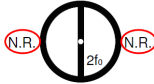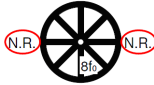Measured phase noise is -93 dBc/Hz at 1 MHz and -69 dBc/Hz at 100 kHz. As the loss in the connector used in the oscillator is about -6 dB at the output frequency, the practical output power can be estimated to be about -6 dBm.

Authors claim the this new oscillator is a very promising method to generate millimeter and sub-millimeter signals, and suggest that the balance shall be improved by adopting a multi active sub-circuit (i.e., using 4 or 8 sub-circuits) on MMIC technology. In my opinion this would turn the circuit into a classical topology like the 8-push or an 8th harmonic 4-push, at best, but it would no longer demonstrate an 8th harmonic push-push oscillator, which was the main contribution of that work.

6.1.4 An Octa-Push (8-push) Oscillator at V-Band

In this paper, the authors propose what they call the *simplified structure harmonic oscillator* (SSHO), where a common resonator is also part of the power combiner. No additional in-phase power-combiners (usually necessary in conventional push–push oscillators) are required.

The SSHO has several technical advantages. First, this concept enables high-order harmonic generation with high efficiency. Second, it is suitable to generate with multi-semiconductor devices.

The resonator plays a main role by working with the output circuit to extract the desired harmonic signal.

The eight sub-circuits operate at the resonant frequency of a one-wavelength ring resonator. At the output circuit, the in-phase power combining enhances the desired eighth harmonics and the fundamental and other undesired harmonics are suppressed.

The sub-circuits and microstrip ring resonator are designed at the fundamental frequency in C-band, while the eighth harmonic output signal is experimentally confirmed in V-band.

The sub-circuits are designed to show negative resistance at the gate port at the fundamental frequency f_o.

Active device, HEMTs (Fujitsu's FHX35LG). The operating bias voltage is +3.9 V / 0 V, Id = 350 mA. Max. drain voltage is +4.0 V

A microstrip open stub is connected to the drain to provide the N.R. (negative resistance) at the gate. Another microstrip open stub is connected to the source for intentional distortion of the fundamental frequency signal (to enhance harmonics). Finally a chip coupling capacitor is mounted at the coupling point of the S.C. (sub-circuits) and the resonator

In order to stabilize the resonance mode at the eighth harmonic frequency, an octagon-shaped resonator is adopted to form a discontinuity boundary condition at the fourth and the eighth harmonic frequencies. The circle-shaped ring resonator resulted in unsatisfactory performance mainly due to the instability of the eighth harmonic resonant modes.

Gap capacitors of about 0.02 pF are formed at the coupling points between the output circuit and the resonator (s = 0.1 mm, w = 0.5 mm). In the previous work the output circuit was directly connected to the resonator and the phase noise performance was not so good due to the tight coupling.

The discontinuous layout of the octagon resonator and the gap capacitor are very important points in design used to obtain the eighth harmonic signal steadily, while improving the low noise performances.

The characteristic impedance of the microstrip line of the ring resonator is 116 Ω.

	$8f_o$ (GHz)	P_{out} (dBm) (*)	PN (dBc/Hz)	PN (dBc/Hz)
8th 2-push	51	-12.33	-69 @ 100 KHz	-93 @ 1 MHz
8-push	51.8	-10.17	-78.8 @ 100 KHz	-99.8 @ 1 MHz

(*) Subminiature A (SMA) connector (Gigalane, PSFS00) has 6 dB I.L. at 50 GHz. Not accounted for in the results

Suppression of the undesired signals is mostly good: from -15.33 dBc (at $4f_o$) to -45.00 dBc (at $7f_o$).

Relatively better characteristics of the output power, phase noise and suppression of undesired harmonics are obtained when compared with the previous 8th Harmonic Push-Push Oscillator. The output power is 1.6 times better and the phase noise is also much better. However, the power efficiency is worse because eight HEMTs are used instead of two.

In both designs the output power is more than -15 dBm with the drain bias voltage varied from 3.0 V to 3.9 V. But the variation rate of output frequency is about 0.35 % (from 50.96 GHz to 51.14 GHz) in the 8th push-push, and 0.77% (from 51.84 to 52.24 GHz in the 8-push.

The frequency sensitivity to Vd is also higher in the 8-push, probably due to the higher number of HEMT devices [J.L. Flores].

Table IV in [13] shows the comparison with other oscillators. The authors comparatively achieve good phase noise and output power in V-band in spite of using a commercially available X-band device and a simple structure.

6.2 Ring Resonator based Negative Resistance Oscillators

The next four articles cover the design of single negative resistance oscillators using different types of resonators based on SRR and CSRR particles. The number five in the list is about a 2-push VCO and it is the closest work to our subject found to date. But it concentrates only on the design of the resonators, which are made from multiple concentric SRRs.

The five works are listed below:

A Dual-band Oscillator with Reconfigurable Cavity-Backed Complementary Split-Ring Resonator	2012	Yuandan Dong, Tatsuo Itoh
A Low Phase-Noise Microwave Oscillator Using a Substrate Integrated Waveguide Resonator based on Complementary Split Ring Resonator	2011	Woo-Young Park, Sungjoon Lim
Design of Low Phase Noise VCO using Microstrip Complimentary Split Ring Resonator	2009	Duwon Jung, Chulhun Seo, Seungki Ko
High Quality Factor mm-Wave Coplanar Strip Resonator Based on Split Ring Resonators	2011	Ali K. Horestani, Zahra Shaterian, Said Al-Sarawi, Derek Abbott
Low Phase Noise Push-Push VCO using Microstrip Square Open Loop Multiple Split Ring Resonator and Rat Race Coupler	2010	Jaewon Choi, Chulhun Seo

I proceed to comment and summarize the conclusions from these articles.

6.2.1 A Dual-band Oscillator with Reconfigurable Cavity-Backed Complementary Split-Ring Resonator

In [31] a reconfigurable resonator is implemented by loading a SIW (substrate integrated waveguide) cavity with a CSRR resonator which can be configured by means of a PIN diode switch across the inside ring slot. This is used to control the resonance frequency.

The dual resonance frequency of the SIW-CSRR is achieved by selecting either the single/double-ring CSRR resonator configuration by means of a PIN diode switch.

In the reflective cavity resonator the vias form a closed cavity structure. Access line is CPW. SIW structures exhibit low-loss, high-quality (Q) factor, good power handling capability, and easy integration with other planar circuits. Nevertheless, they are still voluminous, especially at low frequencies.

Complementary split-ring resonators (CSRRs) are metamaterial resonators that exhibit negative permittivity and can be applied to miniaturized and high-Q microwave devices [14].

SIW cavity loaded with a CSRR resonator is able to generate lower frequency resonances compared with the dominant waveguide mode resulting in size reduction. Thus, miniaturization is obtained by loading this metamaterial resonator. The experimental results indicate that high-Q and low phase noise are achieved.
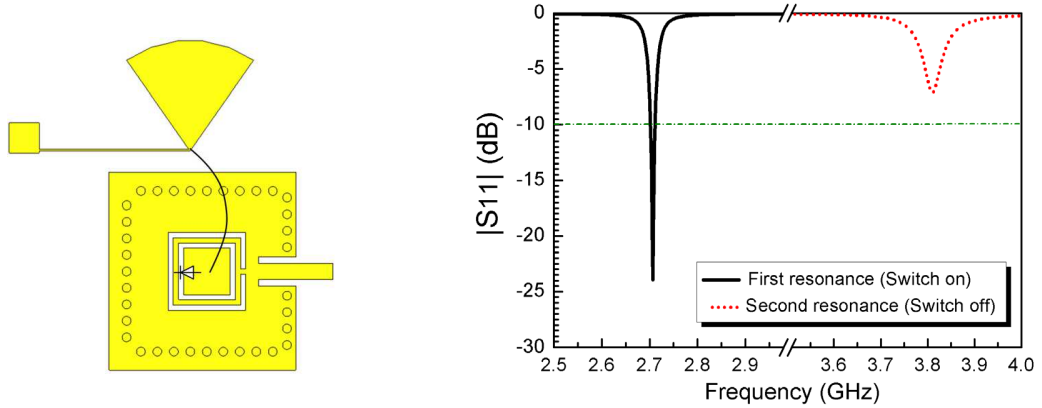

Fig.70.   Reconfigurable SIW-CSRR resonator and reflection coefficient (simulated) [31]

This resonator is used to implement a C-band low phase noise dual-band reflective oscillator. When the PIN diode is ON, the CSRR becomes a double-ring resonator and the resonance frequency of the SIW-CSRR resonator drops down to 2.71 GHz from the 3.82 GHz obtained with a single-ring CSRR when the diode is OFF. The figure of merit (FOM) is calculated as

$$FOM = -L(\Delta f) + 20\log\left(f_0 \middle/ \Delta f\right) - 10\log(P)$$

where L is the phase noise at the offset Δf, f_0 is the oscillation frequency and P(mW) is the DC power consumption of the VCO.

[Coment by JL Flores]

It should be pointed out that these two resonance frequencies can be easily adjusted by changing the split length, as well as the length and width of the two ring slots of the CSRR. Rings separation affects the equivalent capacitance of the SRR.

The outside microstrip line length does not affect the resonance frequency, but can change the phase of the reflected wave, which is an important parameter for oscillator design. This length is adjusted for establishing the required negative conductance and meeting the oscillation conditions at the two resonance frequencies.

6.2.2 A Low Phase-Noise Microwave Oscillator Using a Substrate Integrated Waveguide Resonator based on Complementary Split Ring Resonator

Here is an interesting article [32], very useful to complement 6.2.1 with notions about SIW and discussions on Q factor, phase noise and CSRR miniaturization [JL Flores]

For reducing phase-noise, it is important to increase resonator's loaded-Q factor $Q_L = Q_u / (1 + \beta_c)$ as Leeson's model denotes, where Q_L, Q_u, and β_c are the loaded Q-factor, unloaded Q-factor, and coupling coefficient to resonator, respectively.

Waveguide-like structures called a substrate integrated waveguide (SIW) have been synthesized in a planar form by using metallic via arrays in a printed circuit board (PCB) or low temperature co-fired ceramic (LTCC). Such SIW structures largely preserve the advantages of conventional rectangular waveguides, such as low loss, high-Q factor, and high power capacity, etc.

Split-ring resonators (SRRs) and complementary split-ring resonators (CSRRs) are sub-wavelength particles showing a strong self-resonant behavior with high-Q factor in nature, and many researchers have used these benefits of the CSRR in the SIW cavity resonator design

The SIW/CSRR cavity resonator consists of two metalized via arrays in a substrate to form the electric side-walls in a dielectrically filled rectangular waveguide. The propagation mode of the SIW is very similar to the TE_{10} mode of a rectangular waveguide. Thus, the resonant frequency of SIW cavity is determined by L and W like a rectangular waveguide cavity resonator. Spaces between vias and via diameter are determined in order to optimize return loss and insertion loss. Consequently, the structure has almost no leakage along the guide at the operating frequency. They use a via hole diameter of 0.8 mm, and via spacing of 1.5 mm.

Width and length of the stepped access lines to the resonator determine the phase response and a coupling level to the cavity. Access line and CSRR are designed to maximize the unloaded Q factor of the cavity, which follows the equation

$$(1) \quad 1/Q_u = 1/Q_c + 1/Q_d + 1/Q_{leak}$$

where Q_c, Q_d, and Q_{leak} are the Q factors of the conductor, dielectric, and leakage losses, respectively.

Access line is made of 65 Ω and 95 Ω microstrip sections with lengths adjusted to satisfy the oscillation conditions at the gate side

From Eq. (1), the measured unloaded Q factor of SIW-CSRR cavity is calculated to be 1960, while without the CSRR it was only 350. The resonance occurs at 9.3 GHz

The CSRR not only increases coupling level between the microstrip and cavity, but also increases the Q factor of the SIW-CSRR resonator, which is employed to implement a low phase-noise oscillator.

6.2.3 Design of Low Phase Noise VCO using microstrip CSRR

In [33] the phase noise of a VCO using a microstrip CSRR is reduced by 19 dB compared with that of the conventional VCO using a microstrip line resonator in the tuning range 5.7-5.8 GHz

The phase noise of VCO depends on the Q factor of the resonator. But the resonator using a microstrip line has the limitation for reducing the phase noise because of the low Q factor.
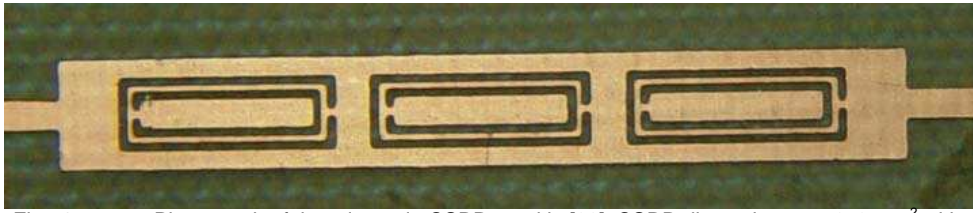

Fig.71. Photograph of the microstrip CSRR used in [33]. CSRR dimensions are 6x2 mm^2 with 1 mm separation. It presents a sharp notch of -57.67 dB at 5.75 GHz (measured).

An array of CSRRs etched on the center line of a microstrip (see Fig.71). A deep rejection band is obtained around the resonant frequency of the CSRRs (5.75 GHz) with sharp cutoff in stopband. As shown by experimental results, a rejection notch of -57.67 dB is measured at the resonance frequency.

The microstrip CSRRs have more high rejection property and high-Q compared to conventional microstrip line resonators. Lower phase noise than the conventional VCO have been obtained by this structure.

6.2.4 High Q Factor mm-Wave Coplanar Strip Resonator Based on Split Ring Resonators

This paper [34] demonstrates the design of high quality factor coplanar strip (CPS) resonator using SRRs in a 90 nm CMOS process, which is applicable in a 60 GHz oscillator.

The main drawback of CMOS technology in the mm-wave regime is the fact that due to low resistivity of the silicon substrate, passive components suffer from substrate conductive loss, and as a result design of high Q factor passive components in this technology is a challenge.

For a conventional $\lambda/4$ short ended TL, resonance occurs at a frequency where Γ_{in} phase is 0º and Γ_{in} phase changes linearly with frequency. A resonator's Q is determined by the rate of deviation of $\Gamma_{in}(f)$ from $\Gamma_{in}(f_r)$.

To modify TL frequency response, split ring resonators aligned with the slot of a Coplanar Strips CPS line and placed in lower metal layers are able to inhibit wave propagation in a narrow frequency range below or above the resonance frequency .

Since the resonator's Q is directly proportional to the deviation rate of Γ_{in}, the quality factor issue in TL resonators in CMOS technology can be addressed by using SRRs to increase the deviation rate around the resonance frequency and consequently increasing the quality factor.

The proposed structure is composed of a short ended conventional CPS designed to operate as a balanced quarter wavelength resonator at 60 GHz, and SRRs symmetrically laid out below the slot between the CPS strips to obtain high inductive coupling at resonance and improve the resonator's quality factor.

In order to achieve a high-Q SRR based CPS resonator, the introduced SRRs were tuned to resonate at 65 GHz. The rejection band caused by SRRs leads to increased phase and amplitude deviation rate of the Γ_{in} at frequencies above the resonance frequency.

From a normalized input impedance plot, the SRR loaded CPS resonator shows a narrower −3 dB bandwidth compared to the conventional resonators, which implies a higher quality factor. A Q = 17.7 is obtained at 60 GHz, which is a 52% greater than the 11.6 value from the conventional CPS resonator. The input impedance of the CPS-SRR is also 2 dB higher at resonance which would result in lower loss and thus lower power consumption in oscillators.

6.2.5 Low Phase Noise Push-Push VCO using Microstrip Square Open Loop Multiple Split Ring Resonator and Rat Race Coupler

The use of multiple concentric rings is studied in [8].

The phase noise of VCO in the $1/f^3$ region depends on the value of the Q factor of the resonator. A larger coupling coefficient of the resonator improves the quality factor value. A basic idea to increase the coupling coefficient of the resonator is to use multiple concentric SRRs with increased distributed capacitance.

A square-shaped multiple SRR consists of N concentric split rings. As N increases a progressive increase of the distributed inter-ring capacitances and reduction of the ring's inductance takes place. But above a certain value of N, as the rings become progressively smaller, the increasing rate of the total distributed capacitance and the decreasing rate of the total inductance are less significant. The resonant frequency of a multiple SRR can be reduced appreciably up to five rings. The introduction of further rings may be used for fine tuning.
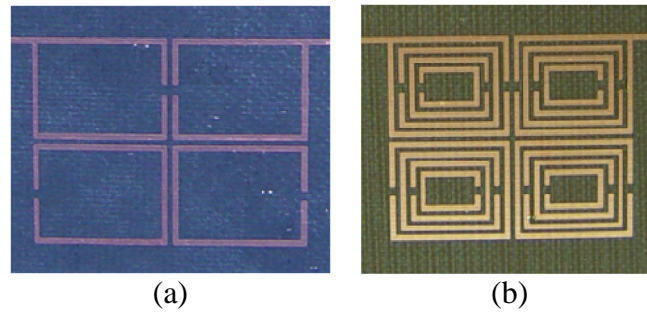
Fig.72. The microstrip square open loop resonator (a) and Microstrip square open loop multiple SRR (b) compared in [8]. Measured respective rejections are - 38.8 dB and -86.3 dB at 2.9 GHz, showing the higher rejection and steeper skirt performance of (b).

Square-shaped multiple SRRs exhibit larger coupling coefficient and higher frequency selectivity than conventional SRR, and have already been used (magnetically coupled to a microstrip) to fabricate efficient stop-band structures. They are a potential candidate for the design of low phase noise VCO due to their improved quality factor Q.

The Q factor can be improved by increasing the mutual capacitance and inductance of the rings, which is accomplished through a decrease of the inter-rings separation and the separation between multiple-SRR structures. The high electric and magnetic couplings obtained with this structure translate to high rejection stop bands. (Electric coupling between concentric rings, magnetic coupling between different multiple-SRRs and with the microstrip).

[Comment from JL Flores]

A weak point in this paper is that the authors claim to have implemented a 2-push VCO but make no mention to its design, and in particular to the stabilization of the odd oscillation mode (out-of-phase sub-oscillators), which has been one of the difficult aspects found in my study. The authors just say "*The correct phase difference between the sub-VCOs is enforced by a properly designed microstrip line*"

Conclusions

The Complementary Split Ring Resonators or CSRR are sub-wavelength particles which offer a good potential for reducing phase noise in oscillators thanks to their small dimensions and higher Q factor as compared to classical approaches to planar resonator design by means of stubs ended in short or open circuit.

A good fitting of both the amplitude and phase of the 2 port parameters is essential to use the lumped element CSRR models in the design of resonator coupling networks for 2-push oscillators, where the achievement of the out-of-phase or odd oscillating mode is critical to obtain the performance benefits of these structures.

The only means of extracting information about the oscillating mode, frequency and level from a 2-push is by performing a nonlinear simulation. The time domain integration is the most straightforward approach to this end, as it converges to the stable solutions which are observed in practice –provided the circuit models are adequate and operate under their validity range. But this method is not practical when the schematic contains high frequency tuned resonant structures and bias decoupling circuitry with low frequency filtering components; the time integration required to reach the stationary regime is very long, and the integration step must be small to accommodate the high frequency solution. An additional limitation comes from the use of distributed element models in the schematic, which slows down the simulation because every component needs to be characterized in the frequency band set by the time step. As an example, the simulation of a 2-push in 0-100 ns with a time integration of 0.01 ns required the characterization of the distributed elements up to 100 GHz and lasted 5140.36 seconds (1 hour and 25 min.!)

The characterization of components up to such high frequency is limited by the validity of their models. And we must assume that the simulation reached the stationary regime within the first 100ns. Of course we can simulate longer times at the cost of extra computing time. Optimizing a design under such limited analysis capability is not practical, so we used Harmonic Balance, which is a frequency domain technique, to solve the previous problems as it reaches the steady-state regime directly. But Harmonic Balance alone can only explore a limited number of solutions and it may give unrealistic results (non observable or unstable solutions) as well.

To help HB explore and converge to a broader set of solutions we have used the technique known as Auxiliary Generator. With it we have been able to induce desired and non desired oscillation modes in the 2-push structures and HB has converged at many of them. Unfortunately there is no means of distinguishing the observable (stable) solutions from the unstable ones, unless we apply a nonlinear stability analysis on them. The stability analysis implemented in this project is based on the small signal perturbation of an oscillatory solution and the extraction of a cause-effect transfer function H(s) whose poles are identified to determine whether they are in LHP (stable solution) or in RHP (unstable). The frequency response H(jω) is obtained from the linearization of the system about the steady state regime imposed by the large signal oscillation. Then pole-zero identification is performed by modelling H(s) as a quotient of polynomials to fit the frequency response H(jω).

More simple to say than to apply; the pole-zero identification requires splitting $H(j\omega)$ in sub-bands of frequency to reduce the order of the $H(s)$ polynomials. Sub-bands must overlap with each other and a separate identification is performed on each one. The rational function $H(s)$ is optimized to fit the frequency response $H(j\omega)$ in a sub-band of frequency, but as $H(s)$ is defined in the whole complex plane, it always gives extrapolated information. It then may happen that poles in RHP are found at frequencies outside the input data during the identification at a particular sub-band. In that case the suspicious poles must be looked at in detail by analyzing another sub-band containing their frequency; this must be done before extracting any conclusion relevant to the stability of the oscillatory solution.

We exclude form the analysis those poles appearing at frequencies above the f_t of the active devices, and also the poles with a very high real part, as they are not dominant and have a negligible effect on the system's response.

The stability analysis must be performed on every solution found in the system. If a solution is found with no poles in RHP it may be the one that we will observe in practice. But we must discard other possible solutions. The AG analysis is valid for Periodic and Quasi Periodic solutions, but it can not find Chaotic type responses, which may exist in a nonlinear system. It is important to induce as many oscillatory solutions as we suspect that the system can have; this is done by setting different parameter values in the Auxiliary Generators. For instance in a 2-push oscillator we may expect solutions with the two sub-oscillators in-phase or out-of-phase, but both can not happen at the same time (for a given configuration of the circuit), so one of them will be unstable. If both are unstable, then the system has a different solution which may be quasi periodic or chaotic. We were not interested in those solutions, so we have only analyzed the stability of the even and odd modes and have modified the circuit in order to stabilize the odd mode, which is the wanted solution in a 2-push. We found that the insertion of a small value resistor in series with the Source stub in the transistors offered a means to stabilize the odd mode solution. The system dominant poles were plotted for different resistor values and it was found that a value around 7-8 ohm produced the lowest negative real part on the system's dominant poles.

The 2-push using a CSRR based resonator coupling network achieves a stable odd mode with a second harmonic output ($2f_o$) of +3.7 dBm at 11.5 GHz ($f_o = 5.75$ GHz).

The 2-push using a resonator coupling network made of microstrip stubs achieves a stable odd mode with a second harmonic output ($2f_o$) of +7.0 dBm at 10.54 GHz ($f_o = 5.27$ GHz).

There is a double explanation for the frequency difference between both oscillators. First, the stub resonator was tuned at a lower frequency to avoid harmonic resonances (at $2f_o$, $3f_o$...) which appeared at the small signal DC analysis and were difficult to eliminate. We initially paid a big effort to assure that the oscillations would start at the wanted frequency only, because we had trouble with undesired oscillation modes in previous designs during their characterization in the Lab. Secondly, the higher quality factor Q of the CSRR resonators has the effect that the large signal oscillation is close to the small signal resonance where the start up condition is achieved. This is directly related to the slope of the small signal admittance's imaginary part at its zero crossing, which takes place at the resonances.

The CSRR based 2-push resonates at 5.67 GHz with a slope of +147 mS/GHz, and its large signal oscillation has the fundamental frequency f_o = 5.75 GHz.

The microstrip stubs 2-push resonates at 4.07 GHz with a slope of +42.6 mS/GHz, and its large signal oscillation has the fundamental frequency f_o = 5.27 GHz.

The small signal analysis is the easiest tool to use when designing circuits, even oscillators, as it allows for a rapid optimization of the circuit elements to verify the start up condition at the desired frequency. But spending too much time on this is not very efficient because in the end the solution is a large signal oscillation. As soon as a small signal oscillation starts growing in a circuit, changes are produced in the impedance of its nonlinear elements (capacitors, current sources...); the resonances move and some disappear. From the experience gained during this project I believe that rather than fighting to eliminate undesired small signal resonances, it is more appropriate to perform a nonlinear analysis with the frequency of the Auxiliary Generators set close to the suspicious frequencies, and if convergence is achieved then performing a stability analysis of the solution. It is always preferable not to have undesired resonances, but in some cases it may be very difficult, even impossible, to get rid of all of them. And after the nonlinear analysis we may find that those resonances did not produce a steady oscillation. There must be a trade between the small and large signal analysis until the desired performance is achieved.

High slope values on the imaginary part of the small signal admittance at the resonances are also related with low frequency sensitivity to noise fluctuations, and thus a reduced phase noise. In order to simulate the phase noise spectrum of the oscillatory solutions we needed to add bias dependent noise sources to the transistor model; they are responsible for the Shot and Flicker noise affecting close to carrier phase noise. But the noise simulations performed with this extended model did not produce credible results; close to carrier phase noise was not being correctly accounted for. By fitting an Angelov model –which includes bias dependent noise sources, we discovered that the simulated phase noise spectrum showed differences depending on whether the internal noise sources were used or replaced by external sources with identical parameter settings. We conclude that the phase noise contribution from the bias dependent elements is probably computed by equations in the simulator used (ADS2009) and it is not the result of a nonlinear analysis converging to a solution. This is a hypothesis only but the results are conclusive.

From the phase noise spectrum computed using the Angelov transistor model, we have obtained a much lower phase noise in the CSRR based 2-push of about -110 dBc/Hz at 10 kHz offset from the carrier, compared to -80 dBc/Hz at 10 kHz obtained with the stub based resonator 2-push.

These results confirm that the high Q factor of the CSRR based resonator (verified by measurement) contributes to a reduced phase noise in the 2-push oscillator.

References

[1] U. L. Rohde, A. K. Poddar and G. Böck, Eds., *The Design of Modern Microwave Oscillators for Wireless Applications.* John Wiley & Sons, Inc., 2005.

[2] A. Suárez, *Analysis and Design of Autonomous Microwave Circuits.* Piscataway, NJ: IEEE Press, 2009.

[3] U. L. Rohde and A. K. Poddar, "Configurable adaptive ultra low noise wideband VCOs," in *Ultra-Wideband, 2005. ICU 2005. 2005 IEEE International Conference on,* 2005, pp. 6 pp.

[4] Jonghoon Choi and A. Mortazawi, "Design of push-push and triple-push oscillators for reducing 1/f noise upconversion," *Microwave Theory and Techniques, IEEE Transactions on,* vol. 53, pp. 3407-3414, 2005.

[5] U. L. Rohde, A. K. Poddar, J. Schoepf, R. Rebel and P. Patel, "Low noise low cost ultra wideband N-push VCO," in *Microwave Symposium Digest, 2005 IEEE MTT-S International,* 2005, pp. 4 pp.

[6] U. L. Rohde and A. K. Poddar, "Ultrawideband (UWB) RF signal source," in *Wireless Communication Systems, 2005. 2nd International Symposium on,* 2005, pp. 255-258.

[7] U. L. Rohde and A. K. Poddar, "Technological scaling and impact on UWB configurable RF signal source," in *Sarnoff Symposium, 2006 IEEE,* 2006, pp. 1-4.

[8] Jaewon Choi and Chulhun Seo, "Low phase noise push-push VCO using microstrip square open loop multiple split ring resonator and rat race coupler," in *Microwave Conference Proceedings (APMC), 2010 Asia-Pacific,* 2010, pp. 394-397.

[9] A. Hajimiri and T. H. Lee, "A general theory of phase noise in electrical oscillators," *Solid-State Circuits, IEEE Journal of,* vol. 33, pp. 179-194, 1998.

[10] A. Hajimiri and T. H. Lee, "Corrections to "A General Theory of Phase Noise in Electrical Oscillators"," *Solid-State Circuits, IEEE Journal of,* vol. 33, pp. 928-928, 1998.

[11] A. Riddle, "A Long, Winding Road," *Microwave Magazine, IEEE,* vol. 11, pp. 70-81, 2010.

[12] J. E. Post Jr., I. R. Linscott and M. H. Oslick, "Waveform symmetry properties and phase noise in oscillators," *Electronics Letters,* vol. 34, pp. 1547-1548, 1998.

[13] K. Kawasaki, T. Tanaka and M. Aikawa, "An Octa-Push Oscillator at V-Band," *Microwave Theory and Techniques, IEEE Transactions on,* vol. 58, pp. 1696-1702, 2010.

[14] J. D. Baena, J. Bonache, F. Martin, R. M. Sillero, F. Falcone, T. Lopetegi, M. A. G. Laso, J. Garcia-Garcia, I. Gil, M. F. Portillo and M. Sorolla, "Equivalent-circuit models for split-ring resonators and complementary split-ring resonators coupled to planar transmission lines," *Microwave Theory and Techniques, IEEE Transactions on,* vol. 53, pp. 1451-1461, 2005.

[15] I. Gil, J. Bonache, J. Garcia-Garcia and F. Martin, "Tunable metamaterial transmission lines based on varactor-loaded split-ring resonators," *Microwave Theory and Techniques, IEEE Transactions on,* vol. 54, pp. 2665-2674, 2006.

[16] J. B. Pendry, "Negative refraction," *Contemporary Physics,* vol. 45, pp. 191-202, 2004.

[17] M. C. K. Wiltshire, "Bending Light the Wrong Way," *Science,* vol. 292, pp. 60-61, 6 April, 2001.

[18] I. Gil, J. Bonache, M. Gil, J. Garcia-Garcia, F. Martin and R. Marques, "Modelling complementary-split-rings-resonator (CSRR) left-handed lines with inter-resonator's coupling," in *Electrotechnical Conference, 2006. MELECON 2006. IEEE Mediterranean,* 2006, pp. 225-228.

[19] A. Suarez, J. Morales and R. Quere, "Synchronization analysis of autonomous microwave circuits using new global-stability analysis tools," *Microwave Theory and Techniques, IEEE Transactions on,* vol. 46, pp. 494-504, 1998.

[20] A. Suarez, R. Quere, M. Camiade and E. Ngoya, "Large signal design of broadband monolithic microwave frequency dividers," in *Microwave Symposium Digest, 1992., IEEE MTT-S International,* 1992, pp. 1595-1598 vol.3.

[21] R. Quere, E. Ngoya, M. Camiade, A. Suarez, M. Hessane and J. Obregon, "Large signal design of broadband monolithic microwave frequency dividers and phase-locked oscillators," *Microwave Theory and Techniques, IEEE Transactions on,* vol. 41, pp. 1928-1938, 1993.

[22] A. Suarez and R. Melville. Simulation-assisted design and analysis of varactor-based frequency multipliers and dividers. *Microwave Theory and Techniques, IEEE Transactions on 54(3),* pp. 1166-1179. 2006.

[23] A. Suarez, E. Fernandez, F. Ramirez and S. Sancho, "Stability and Bifurcation Analysis of Self-Oscillating Quasi-Periodic Regimes," *Microwave Theory and Techniques, IEEE Transactions on,* vol. 60, pp. 528-541, 2012.

[24] J. L. Flores and A. Suárez. On the use of the auxiliary generator technique to improve nonlinear microwave circuit analysis and design. Presented at ARMMS RF & Microwave Society Conference. 2013, . DOI: http://www.armms.org/conferences/.

[25] K. Kurokawa, "Some basic characteristics of broadband negative resistance oscillator circuits," *The Bell System Technical Journal,* pp. 1937-1955, July-August, 1969.

[26] K. Kurokawa, J. P. Beccone and N. D. Kenyon, "Broadband negative resistance oscillator circuits," in *Microwave Symposium, 1969 G-MTT International,* 1969, pp. 281-284.

[27] Hai Xiao, T. Tanaka and M. Aikawa, "A low phase noise ku band push-push oscillator using slot ring resonator," in *Microwave Symposium Digest, 2004 IEEE MTT-S International,* 2004, pp. 1333-1336 Vol.3.

[28] T. Tanaka, M. Tsutsumi and M. Aikawa, "A wideband push-push VCO jusing a phase shifter in the common feedback loop," in *Microwave Conference, 2007. European,* 2007, pp. 747-750.

[29] F. DiPaolo, Ed., *Networks and Devices using Planar Transmission Lines.* CRC Press LLC, 2000.

[30] K. Kawasaki, T. Tanaka and M. Aikawa, "V-band 8th harmonic push-push oscillator using microstrip ring resonator," in *Microwave Symposium Digest, 2009. MTT '09. IEEE MTT-S International,* 2009, pp. 697-700.

[31] Y. Dong and T. Itoh, "A dual-band oscillator with reconfigurable cavity-backed complementary split-ring resonator," in *Microwave Symposium Digest (MTT), 2012 IEEE MTT-S International,* 2012, pp. 1-3.

[32] Woo-Young Park and Sungjoon Lim, "A low phase-noise microwave oscillator using a substrate integrated waveguide resonator based on complementary split ring resonator," in *Microwave Conference Proceedings (APMC), 2011 Asia-Pacific,* 2011, pp. 371-374.

[33] Duwon Jung, Chulhun Seo and Seungki Ko, "Design of low phase noise VCO using microstrip complimentary split ring resonator," in *Microwave Conference, 2009. APMC 2009. Asia Pacific,* 2009, pp. 1707-1710.

[34] A. K. Horestani, Z. Shaterian, S. Al-Sarawi and D. Abbott, "High quality factor mm-wave coplanar strip resonator based on split ring resonators," in *Infrared, Millimeter and Terahertz Waves (IRMMW-THz), 2011 36th International Conference on,* 2011, pp. 1-2.

A I. Determination of the eigenvectors and eigenvalues for the 2-push coupling network

Writing relationship between currents and voltages in a linear two port represented by its admittance matrix parameters, and imposing the condition $[Y_L] \cdot \overline{V} = \lambda \cdot \overline{V}$ in order to find the eigenvalues and eigenvectors of $[Y_L]$ we obtain

$$Y_{11}V_1 + Y_{12}V_2 = \lambda V_1$$
$$Y_{21}V_1 + Y_{22}V_2 = \lambda V_2$$

which is equivalent to

$$(Y_{11} - \lambda) \cdot V_1 + Y_{12}V_2 = 0$$
$$Y_{21}V_1 + (Y_{22} - \lambda) \cdot V_2 = 0$$

any linear combination of the above equations leads to the expression

$$(Y_{11} - \lambda) \cdot V_1 + Y_{12}V_2 + \alpha \cdot Y_{21}V_1 + \alpha \cdot (Y_{22} - \lambda) \cdot V_2 = 0$$

with α being any complex value. A general condition relating the two components of $\overline{V}$ is

$$\frac{V_2}{V_1} = -\frac{Y_{11} + \alpha \cdot Y_{21} - \lambda}{\alpha \cdot Y_{22} + Y_{12} - \alpha \cdot \lambda}$$

if we impose the equal amplitude condition $|V_2/V_1| = 1$ the former expression becomes

$$-\frac{Y_{11} + \alpha \cdot Y_{21} - \lambda}{\alpha \cdot Y_{22} + Y_{12} - \alpha \cdot \lambda} = e^{j\theta} \qquad ; \theta \in [0, 2\pi]$$

Thus the eigenvectors of equal amplitude terms have the form $\overline{V}_\theta = A_\theta \cdot \begin{pmatrix} 1 & e^{j\theta} \end{pmatrix}^T$, with A_θ being the voltage amplitude of the "θ" oscillation mode, and the corresponding eigenvalues verify

$$\lambda_\theta = \frac{Y_{11} + \alpha e^{j\theta} Y_{22} + \alpha Y_{21} + e^{j\theta} Y_{12}}{1 + \alpha e^{j\theta}}$$

In case of a symmetrical ($Y_{11} = Y_{22}$) and reciprocal ($Y_{21} = Y_{12}$) coupling network the former expression simplifies to

$$\lambda_\theta = Y_{11} + \frac{\alpha + e^{j\theta}}{1 + \alpha e^{j\theta}} \cdot Y_{12}$$

The modes with a $2\pi/N$ phase shift between adjacent nodes have, for the N=2 case, θ values of 0 and π, whose corresponding eigenvalues are ($\theta = n\pi$, $n = 0, 1$)
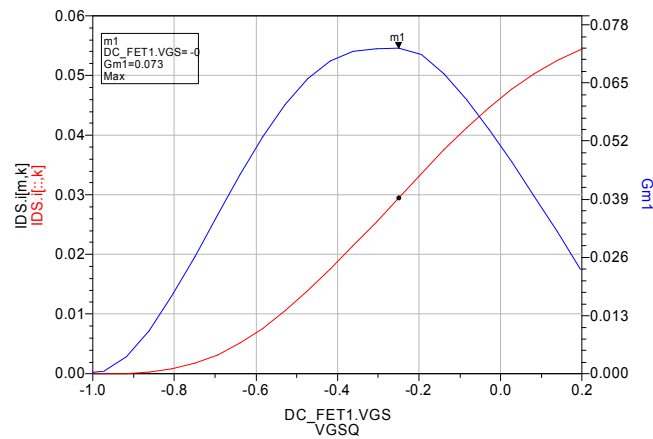
$$\lambda_0 = Y_{11} + Y_{12}$$
$$\lambda_1 = Y_{11} - Y_{12}$$

A II. Selection of the transistor model

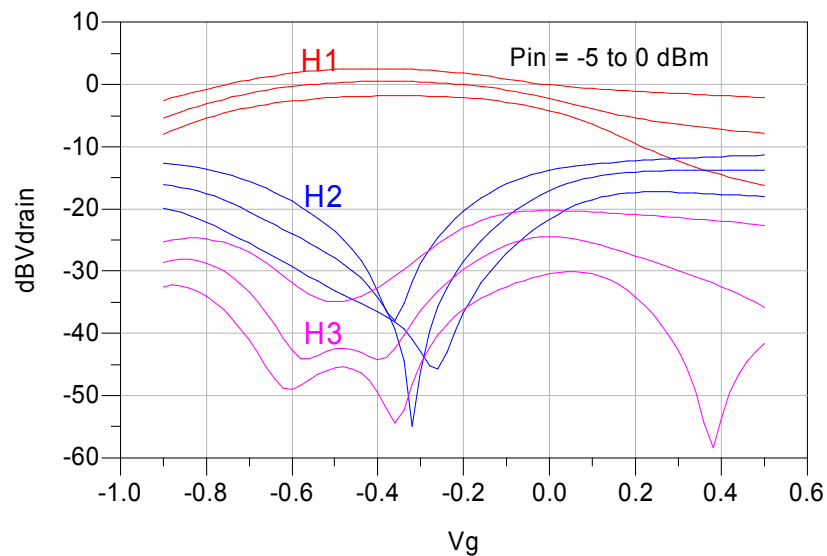**1 -Transistor bias**
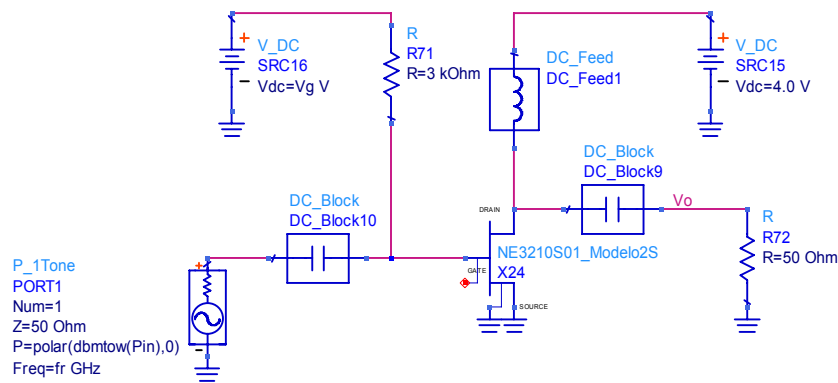
Transistor model: NE3210S01 **EE_HEMT1_Model (ADS)**.

The maximum trans-conductance of the resistive nonlinearity Ids(Vgs,Vds) for VDS = 2V takes place at VGS = -0.2V

In order to maximize the output at the second harmonic we have set the bias VGS = 0V and VDS = 4V.

The next schematic has been used to simulate the transistor behaviour:

2 – Layout

Transistor Artwork is **ARTW_NEC_mdl_S01** from the NEC ADS Design Kit, Release V.1.5, 2/10/2005, available at http://www.cel.com/static.do?command=adskit&group=4 It is installed in the folder C:/Users/Default/ NEC_mdl_kit_v1.5 library

Chip components layout downloaded from Johanson Tech.

3 – Model

The TOM Model from the NEC library component NEC_mdl_NE3210S01 is not used because it does not reproduce the saturation of the Gm trans-conductance. This model is defined in the range 0.1 to 22.5 GHz with Bias: Vds= +1/+3V and Id = 5 to 30 mA
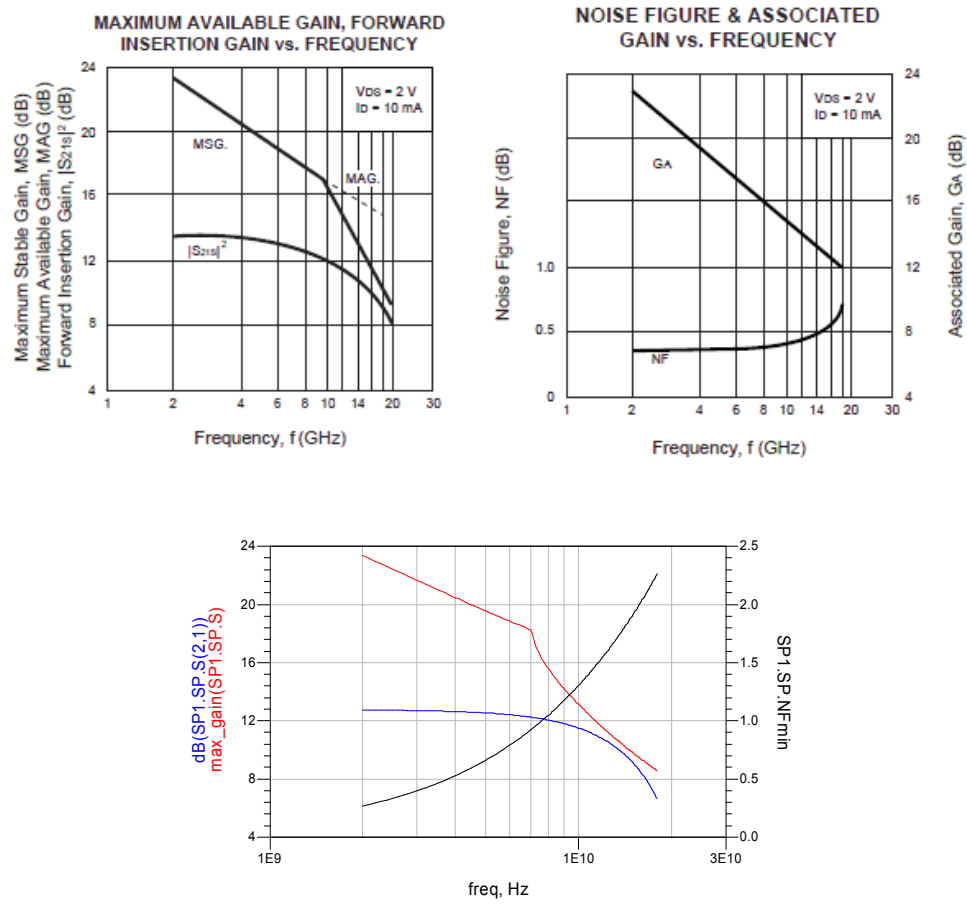
The model used is an Agilent EE_HEMT1, which was already available in the Department. Its simulated performance, as compared to the TOM model, is shown in the next plots. Information from the datasheet is also included for reference.

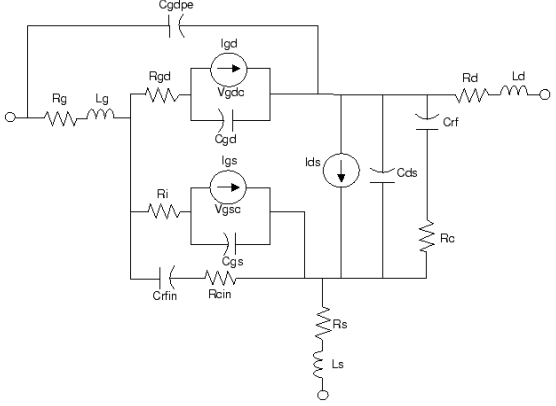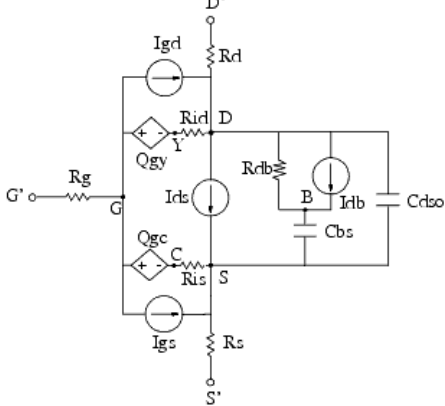Comparison of NE3210S01_Modelo2S and TOM model simulations with datasheet:
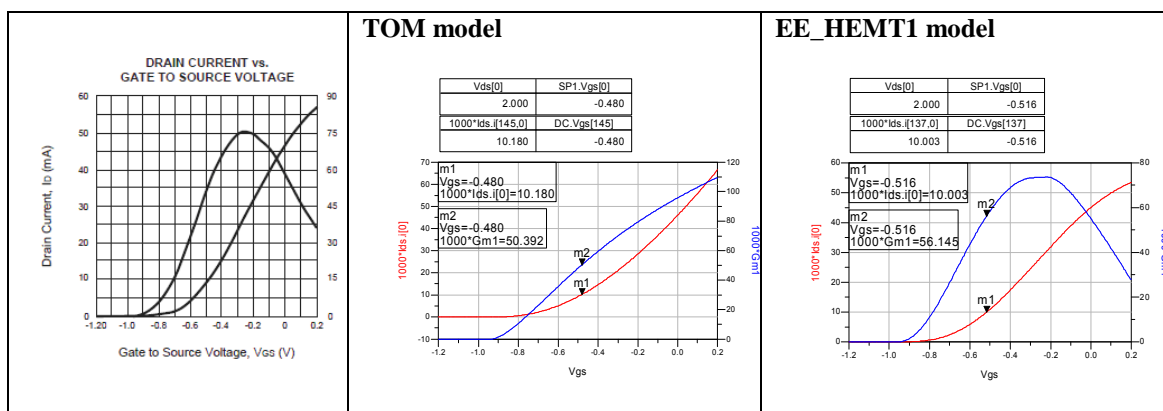
The reference datasheet is: NEC's Super Low Noise HJ FET - NE3210S01. California Eastern Laboratories, 07/01/2004

The next plots compare the simulated gain and noise factor from the EEHEMT1 model
with the datasheet information.

A III. Comparison of Device Noise Models

Angelov_Model (Angelov (Chalmers) Nonlinear GaAsFET Model)	EE_HEMT1_Model EEsof Scalable Nonlinear HEMT Model
Thermal noise of resistance Rg, Rs, Rd, Rgd: $$\frac{\langle i^2 \rangle}{\Delta f} = 4kT/R$$ Thermal noise of resistance Ri: $$\frac{\langle i^2 \rangle}{\Delta f} = 4kTg'/Ri$$ $$Tg' = Tg([1 + (1 + \tanh(\Psi)) \cdot |\tanh(\alpha V_{DS})| \cdot (1 + Lambda \cdot V_{DS})])$$ where Ψ, α, are functions calculated for the $\mathbf{I_{ds}}$ equation.	Thermal noise generated by Rg, Rs, Rd, Ris, Rid, Rdb: $$\frac{<i^2>}{\Delta f} = \frac{4kT}{R}$$
Drain and Gate noise sources, and their correlation (NoiMod=1) $$\frac{\langle i_d^2 \rangle}{\Delta f} = 4kTg_m\,NoiseP$$ $$\frac{\langle i_g^2 \rangle}{\Delta f} = 4kT\,C_{gs}^2\,\omega^2\,NoiseR/g_m$$ $$\frac{\langle i_g, i_d^* \rangle}{\Delta f} = jNoiseC4kT\,C_{gs}\,\omega\sqrt{NoiseP \cdot NoiseR}$$	Channel noise generated by the DC trans-conductance g_m : $$\frac{<i_{ds}^2>}{\Delta f} = \frac{8kTg_m}{3}$$
Ids Flicker Noise (NoiMod=1) $$\frac{\langle i_{fl}^2 \rangle}{\Delta f} = \frac{4kTg_mP \cdot Fnc}{f} + \frac{KfI_{DS}^{Af}}{f^{Ffe}}$$ Igs, Igd Shot Noise and Flicker Noise $$\frac{\langle i_{gs}^2 \rangle}{\Delta f} = 2qI_{GS} + \frac{KfI_{GS}^{Af}}{f^{Ffe}}$$ $$\frac{\langle i_{gd}^2 \rangle}{\Delta f} = 2qI_{GD} + \frac{KfI_{GD}^{Af}}{f^{Ffe}}$$	Flicker and Shot noise sources are not included. They are to be modeled by connecting bias-dependent noise sources external to the device.